Wetting and spreading

Daniel Bonn[1], Jens Eggers[2], Joseph Indekeu[3], Jacques Meunier[1], and Etienne Rolley[1]

[1]*Laboratoire de Physique Statistique, Ecole Normale Supérieure, 24, rue Lhomond, 75005 Paris, France*
[2]*School of Mathematics, University of Bristol, University Walk, Bristol BS8 1TW, United Kingdom*
[3]*Instituut voor Theoretische Fysica, Katholieke Universiteit Leuven, 3001 Leuven, Belgium*

Wetting phenomena are ubiquitous in nature and technology. A solid substrate exposed to the environment is almost invariably covered by a layer of fluid material. In this review, we first consider the surface forces that lead to wetting, and the equilibrium surface coverage of a substrate in contact with a drop of liquid. Depending on the nature of the surface forces involved, different scenarios for wetting *phase transitions* are possible; we show that recent progress allows to relate the critical exponents directly to the nature of surface forces which lead to the different wetting scenarios. Thermal fluctuation effects, which can be greatly enhanced for wetting of geometrically or chemically structured substrates, or are much stronger in colloidal suspensions, modify the adsorption singularities. Macroscopic descriptions and microscopic theories have been developed to understand and predict wetting behavior relevant to micro- and nanofluidics applications.
The second part of the paper deals with the dynamics of wetting. A drop placed on a substrate which it wets, spreads out to form a film. Conversely, a non-wetted substrate previously covered by a film dewets upon an appropriate change of system parameters. The hydrodynamics of both wetting and dewetting is influenced profoundly by the presence of the three-phase contact line separating "wet" regions from those which are either dry or covered by a microscopic film only. We review recent theoretical, experimental, and numerical progress in the description of moving contact line dynamics, and explore its relation to the thermodynamics of wetting. In addition we survey recent progress on rough surfaces. We explore in detail the anchoring of contact lines and contact angle hysteresis, resulting from surface inhomogeneities. Further, we discuss new ways to mold wetting characteristics according to technological constraints, e.g., the use of patterned surfaces, surfactants or complex fluids.

PACS numbers:

Contents

I. INTRODUCTION

A. How, What and Why?

Wetting phenomena are a playground where chemistry, physics and engineering intersect. Surface chemistry is of key importance in determining wetting behavior, and a large research effort has been put into modifying the surface chemistry of various solids in order to obtain specific wetting properties (Durian and Franck, 1987). More or less standard chemical means to do this are for instance, plasma treatment (Wu, 1982) or silanization (Brzoska *et al.*, 1992). By such treatments, one modifies the chemical properties of the surface of the materials, and hence the contact energy of the surface with liquids, vapors or other solids.

As these "chemical" interactions act over a scale of molecules, one often refers to them as short-ranged interactions. In addition to the surface chemistry, surface forces such as van der Waals or electrostatic forces are paramount for determining whether a fluid will wet a given surface or not. These forces have been studied in detail by physicists and physical chemists. As we will see below, van der Waals surface forces can still be important over distances corresponding to a few tens of molecules, because their algebraic decay is rather slow; we hence call them "long-ranged". The van der Waals forces are responsible for the equilibrium thickness of wetting films, and are believed to be important for the way fluids spread over a solid surface. Both van der Waals and electrostatic forces determine the stability of soap films (Vrij, 1966).

Indeed, wetting and spreading are of key importance for many applications. At large scales, wetting or non-wetting plays an important role in oil recovery (Bertrand, 2002), the efficient deposition of pesticides on plant leaves (Bergeron *et al.*, 2000), but also in the drainage of water from highways (Shahidzadeh *et al.*, 2003) and the cooling of industrial reactors. On a smaller scale, wetting solutions have been proposed to solve technological problems in microfluidics and nanoprinting, inkjet printing etc. (Tabeling, 2004). All these phenomena are governed by the surface and interfacial interactions, acting usually at small (a few nm for van der Waals or electrostatic interactions) or very small (molecular) distances. These length scales are now being probed with relatively new experimental techniques such as atomic force microscopy and the surface force apparatus or theoretical tools, such as molecular dynamics etc., allowing new insights into the old problems of surface forces. In addition, new concepts are being introduced to influence both the statics and dynamics of wetting, such as patterned surfaces, surfactants, non-Newtonian flow, in order to solve some of the technological problems mentioned above.

In this review, we first study the equilibrium state of liquids deposited on a solid or another liquid, and how this state is determined by both short-range and long-range molecular interactions. As a thermodynamic parameter, such as the temperature, is varied, the system may pass from one wetting state to another. These so-called wetting transitions have perhaps been the most active sub-discipline in the field of phase transitions over the past two decades. In particular, a number of recent experiments have reinvigorated interest and challenged some long-held theoretical views.

FIG. 1 Plant leaves after the rain.

Next we describe the dynamic problems involved in reaching an equilibrium state, and their relation to the surface chemistry. This is a subtle problem, as a classical hydrodynamic description breaks down at the moving contact line at the edge of a spreading droplet, and microscopic features have to be invoked. As a result, both large scale (hydrodynamic) features and short scale (molecular) dynamics are inextricably linked into a truly *multi scale* problem.

Finally, wetting is a subject in which *disorder* plays a very important role in practice, and even under idealized laboratory conditions, for both statics and dynamics. On the one hand, impurities may lead to frustration, such that the true equilibrium state is never reached: a small droplet is often observed to rest on an inclined surface, see Fig. 1. On the other hand, the resulting roughness of the contact line leads to very complicated dynamics, still poorly understood. The close connection to other dynamical problems involving many length scales, such as domain walls, imbibition fronts, or vortex lattices, have made this an extremely active field.

Some or all of the ground covered in this review has been treated in a number of previous books and articles. For older work, see the classical review by de Gennes (1985), as well as Léger and Joanny (1992) and the collection of articles in J. C. Berg (1993). More recent work has been reviewed by Voinov (2002), Blake (2006), and in the books by de Gennes *et al.* (2003) and Starov *et al.* (2007). Equilibrium phenomena are covered by Fisher (1986), Sullivan and Telo da Gama (1986), Dietrich (1988), Schick (1990), Evans (1990), Indekeu (1994), and more recently by Bonn and Ross (2001) and in the book by Safran (2003).

B. Statics

1. Basic surface thermodynamics

If we consider a liquid drop on a solid substrate, there are three different phases present, see Fig. 2. Therefore there are three surface tensions that need to be considered: solid-liquid, liquid-gas and solid-gas. Young's equation (Young, 1805) gives the relation between the equilibrium contact angle θ_{eq} the drop makes with the surface and the three surface tensions as:

$$\gamma_{SV} = \gamma_{SL} + \gamma \cos\theta_{eq}, \tag{1}$$

where throughout this review $\gamma \equiv \gamma_{LV}$ denotes the liquid-vapor surface tension. Here all the surface tensions are defined when the three phases, solid, liquid and gas, are at least in mechanical equilibrium (force balance) with each other. In addition, we consider chemical equilibrium (chemical potential matching for each component present) and thermal equilibrium (temperature matching) between liquid and gas, so that the gas is the saturated vapor of the liquid. Mechanical, chemical and thermal equilibrium together are referred to as *thermodynamic equilibrium*. As stressed by de Gennes (1985), (1) is best derived by considering a reversible change in contact line position, using global energetic arguments. Thus the nature of the contact line region, over which intermolecular forces are acting, does not enter. Accordingly, θ_{eq} is understood to be measured *macroscopically*, on a scale above that of long-ranged intermolecular forces.

If the three tensions are known, the wetting state of the fluid follows directly. If $\gamma_{SV} < \gamma_{SL} + \gamma$, a droplet with a finite contact angle minimizes the free energy of the system; we speak of partial wetting. On the other hand, if $\gamma_{SV} = \gamma_{SL} + \gamma$, the contact angle is zero. The system will consequently be in equilibrium when a macroscopic uniform liquid layer covers the whole solid surface and we speak of complete wetting.

The distinction between the different wetting states is usually made by considering the equilibrium spreading coefficient $S_{eq} \leq 0$, which represents the surface free energy γ_{SV} relative to its value for complete wetting:

$$S_{eq} \equiv \gamma_{SV} - (\gamma_{SL} + \gamma) = \gamma(\cos\theta_{eq} - 1). \tag{2}$$

Fig. 3 shows the three wetting states that may exist in any three-phase system. For a solid-liquid-vapor system, complete drying would correspond to the intrusion of a macroscopic vapor layer between the solid and the liquid. ("Drying" does not imply evaporation, see below.) From a thermodynamic point of view, the wetting and drying states are very similar, the only difference being that liquid and vapor are interchanged. In practice drying is rather rare (with mercury on for instance glass as a notable exception) since van der Waals forces tend to thin vapor layers. We will thus focus here on wetting. Partial

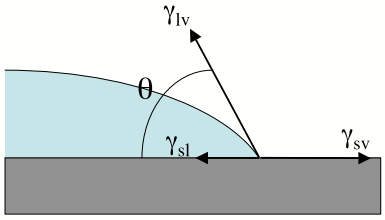

FIG. 2 Young's equation can also be interpreted as a mechanical force balance on the three-phase contact line; the surface tension is an energy per unit area, equivalent to a force per unit length acting on the contact line.

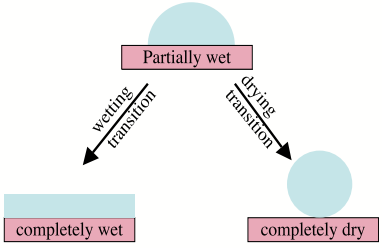

FIG. 3 The three different possible wetting states according to Young's equation.

wetting corresponds to drops, surrounded by a microscopically thin film adsorbed at the surface, and complete wetting to a macroscopically thick layer. Indeed, in a partial wetting state the surface besides the droplet is never completely dry. In thermodynamic equilibrium there will be at least some molecules adsorbed onto the substrate, since the entropy gained by the system is large in doing so. It is for this reason that we speak of a microscopic film; in experiments the average thickness of this film varies between a fraction of a molecule to several molecules, depending on the affinity of the molecules for the substrate, and the distance to the bulk critical point.

Note that for complete wetting the equilibrium spreading coefficient is zero. The solid-vapor interface then consists of a macroscopically thick wetting layer, so that its tension is equal to the sum of the solid-liquid and liquid-vapor surface tensions.

However, when a droplet is deposited on a dry substrate, it is hardly ever in equilibrium. It is important to emphasize in this context the distinction between *volatile* (Bonn *et al.*, 2001) and *non-volatile* (Brochard-Wyart *et al.*, 1991; de Gennes *et al.*, 2003) liquids. For volatile liquids thermodynamic equilibrium can be reached in a reasonable time span so that away from the droplet the substrate does not remain dry but establishes contact with the saturated vapor phase or at least some (sub)monolayer of adsorbed molecules spreads diffusively over the substrate, assuming a partial wetting configuration. Even in the complete wetting regime, for wetting layers of volatile liquids evaporating under non-equilibrium conditions theory suggests and observations confirm a two-phase state can occur in which a molecularly thin film can coexist with a macroscop-

ically thick layer (e.g. for water evaporating on clean mica)(Leizerson and Lipson, 2003; Leizerson *et al.*, 2003; Samid-Merzel *et al.*, 1998). Possibly, the thin film is stabilized by very short-ranged "polar" surface forces (exponentially decaying on a microscopic scale). For non-volatile liquids thermodynamic equilibrium cannot be reached within the experimental time window (typically days or longer). To be able to deal with both cases, an *initial* spreading coefficient can be defined (de Gennes, 1985):

$$S_i = \gamma_{S0} - (\gamma_{SL} + \gamma), \tag{3}$$

which is the pertinent quantity for the dynamics - whether a droplet will spread or not. Here γ_{S0} is the surface tension of the dry solid substrate. Note that for non-volatile liquids and for $S_i < 0$ the drop will display a finite static contact angle, say θ_i, which is not the equilibrium angle θ_{eq}, but is found by replacing γ_{SV} by γ_{S0} in (1). For non-volatile liquids and $S_i > 0$ the droplet will flatten as it attempts to spread, while preserving its volume (again, within the experimental time window). This volume constraint is essential for describing non-volatile adsorbates and leads to a "final" state which differs from an equilibrium adsorbed film. We return to this difference and quantify it in section II.A.

The equilibrium tension γ_{SV} is lower than γ_{S0} due to adsorption of molecules on the solid from the vapor phase. This follows from the Gibbs adsorption equation (Rowlinson and Widom, 1982)

$$d\gamma_{SV} = -\Gamma d\mu + \Sigma dT, \tag{4}$$

where Γ is the adsorption, Σ the surface (excess) entropy and μ the chemical potential. From (4) it follows that

$$\left(\frac{d\gamma_{SV}}{d\mu}\right)_T = -\Gamma. \tag{5}$$

If not too many molecules are adsorbed, (5), combined with $d\mu = k_B T d\ln c$, and $\Gamma \propto c$, where c is the (low) bulk concentration of the adsorbed species, implies that the surface tension is lowered by $k_B T$ per adsorbed molecule per unit area. In fact, for low adsorption (5) results in a two-dimensional ideal gas law,

$$\pi \equiv \gamma_{S0} - \gamma_{SV} = k_B T\,\Gamma, \tag{6}$$

where π is a positive "surface pressure", a force per unit length. It follows that $S_i > S_{eq}$. The initial S_i can be positive or negative, but whenever $S_i < 0$, S_{eq} is also negative and the liquid does not spread. On the other hand, if $S_i > 0$, there is no direct argument for whether S_{eq} is less than or equal to zero.

In general if S_i is large and positive, the equilibrium state is characterized by $S_{eq} = 0$. However, an exception to this empirical rule is illustrated by the example of a benzene droplet placed on a water "substrate". The droplet spreads out quite violently for short times after the deposition, but subsequently retracts into a droplet again, with a final non-zero equilibrium contact angle. This means that the initial spreading coefficient is positive, and the equilibrium spreading coefficient is negative. Since benzene is slightly soluble in water, γ_{SL} is low, thus favoring complete wetting. However, this effect is overpowered by the formation of a microscopic film of the drop phase on the substrate in equilibrium. According to (5) the benzene layer decreases γ_{SV} significantly; typical variations for light hydrocarbons such as benzene on water are on the order of 10%. Thus according to (2) S_{eq} becomes negative due to the dominant contribution of the benzene film.

The above example makes it clear that S_{eq} can in generally not be determined from the surface tensions of the *pure* substances. In the more favorable situation of a drop (L_2) wetting a liquid "substrate" L_1, for which more general equations than (1) apply (Rowlinson and Widom, 1982), care must be taken to measure the tensions γ_{L_1V} and γ_{L_2V} in the presence of the other liquid, respectively. The measurement of $\gamma_{L_1L_2}$ is standard (Ferguson, 1929). This usually works reasonably well; however, it should be kept in mind that the errors in an actual measurement of the surface tension are of the order of 1 or 2 mNm^{-1}, and that for calculating the spreading coefficient one usually subtracts two large numbers to obtain a small number.

For a solid substrate, the usual (and practically only) way of evaluating the wettability is to deposit a droplet of fluid and to measure the equilibrium contact angle (Kabza *et al.*, 2000). Zisman's original idea is that the difference $\gamma_{SV} - \gamma_{SL}$ is a property of the solid, i.e., a constant independent of the liquid used. Using a liquid with a known liquid-vapor tension, this difference can readily be evaluated by measuring the contact angle of that liquid on the solid substrate, and using (1). The data shown in Fig. 4 support Zisman's original idea. The constant is the intercept of a straight line through the data with the horizontal $\cos\theta_{eq} = 1$, which motivates the name "critical surface tension" (Fox and Zisman, 1950) for $\gamma_{SV} - \gamma_{SL}$.

However, although Zisman plots $\cos\theta_{eq}$ versus γ, (1) suggests that rather $1/\cos\theta_{eq}$ should be plotted. If this is done, a straight line (whose extrapolation passes through the origin) should be obtained. The data in Figure 4 agree remarkably well with this conjecture.

It is even more difficult to estimate the *initial* spreading coefficients for liquids on solids, which is crucial for the dynamics of spreading, see below. One possible way around this problem is to measure the adsorption isotherm of the liquid on a solid, and use Gibbs' adsorption equation to calculate the surface tension change associated with the adsorption (Ragil *et al.*, 1996a).

C. Drop spreading: basic concepts

If a drop is placed on a solid surface, it will in general be far from its equilibrium state, $S_i \neq S_{eq}$. Hence a flow is set in motion until the equilibrium contact an-

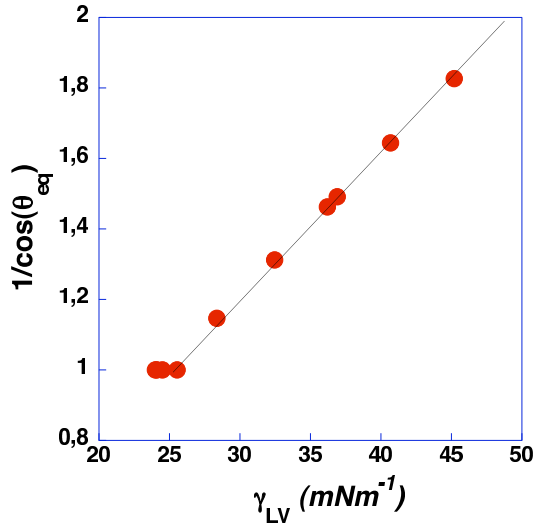

FIG. 4 Zisman plot; liquids of different liquid-vapor surface tension are deposited on a Terphene surface, and the variation of the contact angle that the liquid makes with the solid is measured, yielding the critical surface tension of the Terphene surface. A liquid with this surface tension just wets the surface completely. The liquids used here are aqueous solutions of the soluble surfactant CTAB. (D.Bonn, unpublished results). To within the experimental uncertainty, the straight line goes through the origin.

gle (1) is reached, assuming the drop is not trapped in some metastable state. The hydrodynamics of this problem has been studied extensively, both experimentally (Cazabat and Cohen-Stuart, 1986; Chen and Wada, 1989; Ehrhard, 1993; Huppert, 1982b; Kavehpour *et al.*, 2002; Levinson *et al.*, 1988; McHale *et al.*, 1995; Tanner, 1979), and theoretically (Brenner and Bertozzi, 1993; de Gennes, 1985; Greenspan, 1978; Hocking, 1983, 1992; Oron *et al.*, 1997; Tanner, 1979; Voinov, 1976). In the case of complete wetting ($\theta_{eq} = 0$) the drop spreads almost forever, presumably until it reaches a thickness set by van der Waals forces. If the static contact angle is finite but small, the initial stages are similar, followed by relaxation toward a static shape.

Let us consider the simplest case of a small viscous droplet spreading on a surface which it wets completely, see Fig. 5. By small we mean that the drop radius is smaller than the capillary length $\ell_c = \sqrt{\gamma/(\rho g)}$, so that gravity is negligible. As seen in Fig. 5 a, the drop is approximated extremely well by a spherical cap, corresponding to an equilibrium liquid-vapor surface of the drop. This is to be expected since the ratio of viscous to surface tension forces, as measured by the capillary number

$$Ca = \frac{U\eta}{\gamma}, \tag{7}$$

is very small ($Ca \approx 10^{-5} - 10^{-3}$), as is the case for most spreading experiments. Here $U = \dot{R}$ is the contact line speed and η the viscosity of the liquid. Consequently,

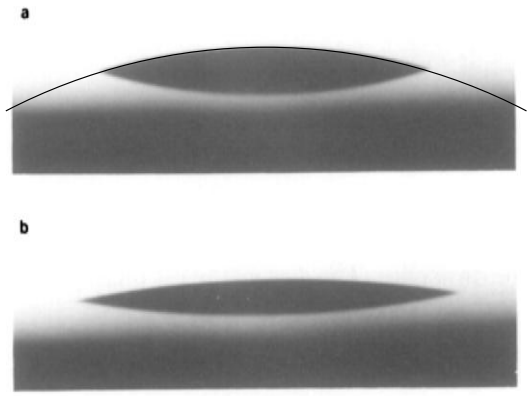

FIG. 5 Two stages of the spreading of a silicone drop on a glass substrate (Chen, 1988), which it wets completely; a: $t = 3.25s$ after deposition, b: $t = 18.25s$. Below the drop's surface one sees its reflection. The drop volume is $V = 1.7 \cdot 10^{-4}\text{cm}^3$, and $\gamma/\eta = 10.6\text{cm/s}$. Although the equilibrium contact angle is zero, the "apparent" angle is finite, and the drop is well fitted by a spherical cap.

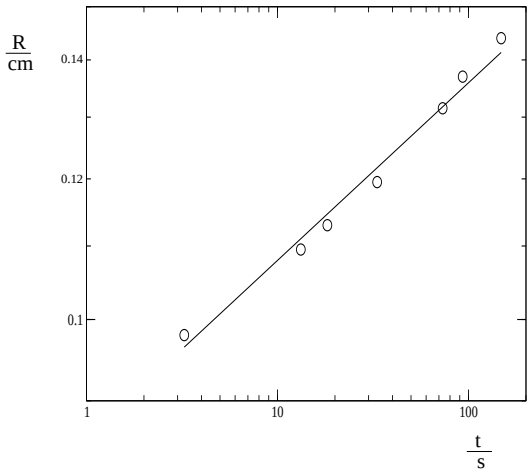

FIG. 6 The radius R of the drop of Fig. 5 as a function of time, described by Tanner's law (10).

except in a region very close to the contact line, the interface shape is not affected by viscous forces. Once the drop has become sufficiently flat ($h' \ll 1$), its thickness $h(r,t)$ is described by

$$h(r) = \frac{2V}{\pi R^2}\left[1 - \left(\frac{r}{R}\right)^2\right]. \tag{8}$$

At a given volume V, the shape of the drop is thus determined completely by the "apparent contact angle" θ_{ap} the spherical cap makes with the solid surface. For thin droplets ($-h'(R) = \tan(\theta_{ap}) \approx \theta_{ap}$) one obtains

$$\theta_{ap} = 4V/(\pi R^3), \tag{9}$$

so the apparent contact angle $\theta_{ap}(t)$ goes to zero like $1/R^3(t)$ as the drop spreads.

Fig. 6 shows a doubly logarithmic plot of the drop radius as a function of time, which is closely approximated by

$$R(t) \approx \left[\frac{10\gamma}{9B\eta}\left(\frac{4V}{\pi}\right)^3 t\right]^{1/10} \propto t^n. \qquad (10)$$

Note that, remarkably, the spreading law is *independent* of the initial spreading coefficient S_i, which is a measure of the total surface energy available to the system. The constant B (for which a theoretical estimate will be given below) is from Fig. 6 found to be close to $B^{1/10} = 1.186$. Equation (10) is universally known as "Tanner's law" (Tanner, 1979), although it was first obtained theoretically by Voinov (1976), who found it to agree with earlier experiments by Ogarev *et al.* (1974). The power $n = 1/10$ found for the viscous spreading of small droplets has been well corroborated by many other experiments (Cazabat and Cohen-Stuart, 1986; Chen and Wada, 1989; Levinson *et al.*, 1988; Tanner, 1979).

The speed of spreading is controlled by the balance of the available energy (surface or gravitational energy) and dissipation, which occurs mostly near the contact line, but also in the bulk of the drop. If the drop is small, only surface energy needs to be considered, which is

$$F_S = \frac{4V^2}{\pi R^4}\gamma - \pi S_i R^2 \qquad (11)$$

relative to the energy of the uncovered surface. The second part of (11) comes from the base area of the drop being covered by fluid, the first from the additional liquid-vapor interface that arises because the drop is curved.

From (11) one might conclude that for $S_i > 0$ spreading can be made extremely effective, since any increase in radius will lead to a decrease in surface energy proportional to $S_i R dR$. This is, however, not the case, since in practice the energy $\pi S_i R^2$ cannot be converted into *macroscopic* motion of the drop. Instead, spreading becomes a two-stage process: the macroscopic wetting front is preceeded by a thin *precursor* film of dynamical origin (of typical thickness between 100 Å (Kavehpour *et al.*, 2002) and a single molecular layer (Cazabat *et al.*, 1997)) in which all the energy corresponding to S_i is burnt (de Gennes, 1985). This dynamical structure is to be distinguished from the adsorbed film around a partially wetting drop, which exists even in equilibrium. Intuitively, moving a small number of molecules represents a more efficient pathway toward burning most of the energy than moving the whole drop at once. The structure of the precursor film can be quite complicated, and depends in detail on the interaction potentials.

Thus on the time scale on which the macroscopic drop spreads, the effective spreading coefficient has already been reduced to its equilibrium value $S_{eq} = 0$; an increase in the surface energy available for spreading does not enhance the spreading rate. For vanishing S_i the decrease of F_S becomes very small if R is large, which explains why spreading becomes exceedingly slow, as is reflected by the very small exponent $n = 1/10$ in (10). To compute the power n, the rate of energy dissipation has to be calculated as well, which at low capillary numbers is concentrated in a region close to the contact line. In fact, the rate of viscous energy dissipation increases so sharply near the drop that the total dissipation formally *diverges*. This poses a fundamental difficulty for the hydrodynamic treatment of spreading, and determines the structure of most problems involving a moving contact line.

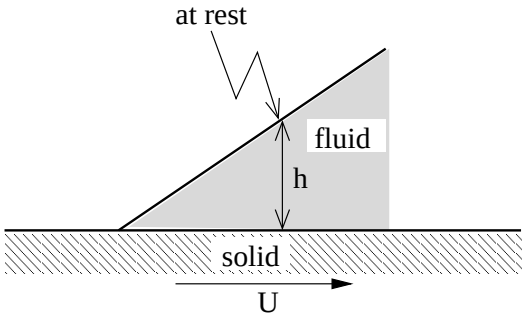

FIG. 7 A cartoon of an advancing contact line. In a frame of reference in which the contact line is stationary the solid *moves* with velocity U to the right.

1. Huh and Scriven's paradox

It was first pointed out by Huh and Scriven (1971), that applying the no-slip condition to a flow close to a contact line leads to an energy dissipation that is logarithmically *diverging*. This can be seen from a local description of the contact line, for which it is most convenient to choose a frame of reference where the contact line is stationary and the solid is moving, see Fig. 7. We assume that the interface meets the solid boundary at some finite angle θ. Owing to the no-slip condition the fluid at the bottom moves with constant velocity U to the right, while the flux through the cross section is zero. By mass conservation, the fluid at the top is moving to the left. Thus at a distance x from the contact line, the typical vertical velocity gradient is $\dot{u} \equiv du_x/dz = U/h(x)$, where $h(x) \approx \theta x$ for small θ. The rate of viscous dissipation per unit volume in a fluid of viscosity η is $\epsilon \approx \eta \dot{u}^2$ (Landau and Lifshitz, 1984). Integrating $(U/h)^2$ over the wedge, one arrives at an estimate of the dissipation per unit time and unit length of the contact line

$$D_{visc} \simeq \eta \int_L^{L_{out}} (U/h)^2 h\, dx = (\eta U^2/\theta) \ln(L_{out}/L), \qquad (12)$$

where L_{out} is an appropriate outer length scale like the radius of the spreading droplet. In addition, we were forced to introduce some small cut-off length L to make the integral finite. Thus, assuming standard continuum hydrodynamics with no slip, where L were set to zero, "not even Herakles could sink a solid", in Huh and

mechanism	reference
mesoscopic precursor film	Hervet and de Gennes (1984)
molecular film	Eres *et al.* (2000)
Navier slip	Huh and Scriven (1971)
nonlinear slip	Thompson and Troian (1997)
surface roughness	Hocking (1976)
shear thinning	Weidner and Schwartz (1993)
evaporation/condensation	Wayner (1993)
diffuse interface	Seppecher (1996)
normal stresses	Boudaoud (2007)

TABLE I A list of mechanisms that have been proposed to relieve the dynamical singularity near the contact line, along with representative references.

Scriven's apt phrase.

To account for the experimental observation that contact lines *do* in fact move, some microscopic features have to be built into the hydrodynamic description. As a result, macroscopic features of the flow must depend to some degree on those microscopic details, and the usual universality of hydrodynamics is lost. In Table I we give a list of different mechanisms that have been proposed to relieve the contact line singularity. Unfortunately, only very limited experimental information exists that would pinpoint one or the other mechanism. Namely, as is to be expected from (12), the dependence on microscopic parameters is only logarithmic, so it is very difficult to extract accurate information on their values.

Based on the above estimates for the dissipation near the contact line, we are now in a position to derive the spreading law (10) by equating the rate of change of the surface energy with the energy dissipation: $\dot{F}_S = 2\pi R D_{visc}$. To that end we take the angle θ in (12) as an approximation for the apparent contact angle, and find that $D_{visc} \propto R\dot{R}^2/\theta_{ap} \propto \dot{R}^2 R^4$. Using $\dot{F}_S \propto \dot{R}/R^5$, one arrives at $dR^{10}/dt = 10\dot{R}R^9 \propto const$, and thus at Tanner's law (10). This estimate neglects the logarithmic factor appearing in (12), which may be a time-dependent quantity in itself. Only a more involved hydrodynamic calculation, to which we return below, is able to predict the exact form of the logarithmic corrections.

2. Apparent and "microscopic" contact angles

The concept of a contact angle becomes much more problematic in the out-of-equilibrium situation of a moving contact line, where the thermodynamic arguments leading to (1) no longer apply. Namely, the local angle the interface makes with the substrate depends strongly on scale, i.e., on the distance from the contact line. On hydrodynamic scales, the strong divergence of viscous forces (Huh and Scriven, 1971) results in an interface slope that varies *logarithmically* with the distance from the contact line, as confirmed experimentally (Chen and Wada, 1989; Kavehpour *et al.*, 2003; Marsh *et al.*, 1993). We will refer to this local angle, measured macroscopically at a specified distance from the contact line, as the "dynamic contact angle" θ_d.

As one approaches the contact line, the angle will also be affected by long-ranged forces. If finally the angle is determined on a molecular scale, the interface position is no longer determined uniquely owing to thermal fluctuations and the diffusiveness of the interface itself. The concept of a "microscopic" or "actual" (Dussan V., 1979) contact angle θ_m, determined directly at the contact line, thus has to applied with care. It requires averaging over microscopic data (e.g., from molecular simulations (Thompson and Robbins, 1989)), or the application of well-defined theoretical models, taking into account the diffusiveness of the interface (Qian *et al.*, 2003).

The only uniquely defined *macroscopic* angle is the "apparent" contact angle (9), introduced in the context of drop spreading. Unfortunately, its definition is contingent on the fact that the interface shape sufficiently far away from the contact line is quasistatic, and thus speed-independent. In many cases, and in particular if the capillary number is no longer small, the surface is strongly deformed by viscous forces and a general formula for the interface shape can no longer be given. This makes it difficult to define a unique apparent angle.

The situation is summarized in Fig. 8, which shows a drop of partially wetting fluid spreading on a solid substrate. Roughly speaking, the problem can be split up into three distinct regions. Firstly, the macroscopic flow in the drop on the scale of its radius R, often referred to as the "outer" region, in the language of asymptotic expansions (Cox, 1986). Secondly, a contact line region, characterized by a balance of viscous and surface tension forces, over which the interface is strongly bent, resulting in a rapid change of the interface slope. This is called the "intermediate" region, whose size is estimated as $3CaR/\theta_{ap}$, based on where the profile turns from concave to convex (see III.B below). Thirdly, an "inner" region, forming a neighborhood of the size of nanometers around the contact line, where microscopic details matter and fluctuations are felt (Thompson and Robbins, 1989).

Thus, there are two important challenges in the large-scale modeling of moving contact line phenomena:

(a) to describe the flow close to the contact line, and to understand its consequences for the flow problem on a large scale (for example, to compute θ_{ap}).

(b) to match the hydrodynamic part of the problem to a microscopic neighborhood of the contact line (of the size of a nanometer), where a molecular description needs to be adopted.

It has been proposed (Greenspan, 1978; Oron *et al.*, 1997) that an alternative way of describing moving contact line problems consists in prescribing an apparent contact angle according to some empirical law. Firstly, this approach does not remove problems associated with the singular viscous flow near the contact line. In particular, even if the drop shape is assumed to be an equilibrium surface, the appropriate dynamic contact angle will

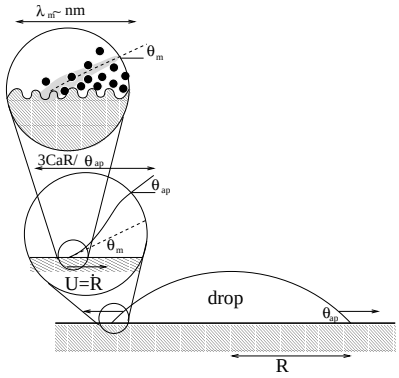

FIG. 8 A spreading drop that partially wets the solid surface, whose shape is determined by the apparent contact angle. The interface near the corner is highly curved, so θ_{ap} is larger than the angle θ_m seen on a scale of nanometers. On this scale the interface fluctuates, and the corrugation of the solid surface is seen. The size of the crossover region between microscopic and macroscopic, the "intermediate" region, is estimated based on (58) below.

still depend on the scale on which matching occurs. Secondly, little general insight is gained by imposing empirical laws. For example, an assumption of linear response, $\theta_{ap} - \theta_{eq} \propto \dot{R}$, does not suffice: applied to the spreading of a perfectly wetting fluid, with (9), it leads to $n = 1/4$, completely at odds with experimental observation.

3. Spreading laws

The above analysis of drop spreading was based on the assumption of *small* drop radius $R \ll \ell_c$ (as well as small volume, $V^{1/3} \ll \ell_c$), and the corresponding "Tanner's law" is the most easily observed case. However, as the radius grows beyond the capillary length, the drop changes towards a "pancake" shape of constant thickness, curved only at the rim, and the main driving force is now gravity. It can be balanced either against dissipation in the bulk of the drop (Lopez *et al.*, 1976) or near the contact line (Ehrhard and Davis, 1991), leading to $n = 1/8$ or $n = 1/7$, respectively.

These and similar analyses and experiments in 2D (spreading on a strip (McHale *et al.*, 1995)) are summarized in Table II. Since $n = 1/8$ corresponds to *slower* spreading for long times than $n = 1/7$, bulk dissipation dominates over contact line dissipation in the late stages of spreading. A detailed asymptotic analysis for slip laws (Hocking, 1983, 1992) and for long-ranged forces (Hocking, 1994) confirms this. A crossover between $n = 1/10$ and $n = 1/8$ was reported in the experiments of Cazabat and Cohen-Stuart (1986), while Ehrhard (1993) finds a crossover to $n = 1/7$. Available experimental data is probably not sufficiently accurate to distinguish between the two regimes.

If the drop is no longer small, neither surface tension nor the particulars of contact line dynamics will matter for such a "gravity current" (Huppert, 1982b; Lopez *et al.*, 1976). As found from a balance of gravity and bulk dissipation, the spreading exponent is again $n = 1/8$, and the shape of the drop is known from the exact solution of a similarity equation (Pattle, 1959). This of course neglects a possible "fine structure" near the contact line, where surface tension still plays a role (Hocking, 1983).

balance	n, theory	experiment
3D, s.t. - c.l.	1/10	(Cazabat and Cohen-Stuart, 1986)
2D, s.t. - c.l.	1/7	(McHale *et al.*, 1995)
3D, gr. - c.l.	1/7	(Ehrhard, 1993)
2D, gr. - c.l.	1/4	none
3D, gr. - vis.	1/8	(Huppert, 1982b)
3D, gr. - vis. (pancake)	1/8	(Cazabat and Cohen-Stuart, 1986)
2D, gr. - vis.	1/5	none

TABLE II A list of scaling exponents n, with $R \propto t^n$, corresponding to different balances in droplet spreading in 2 and 3 dimensions. Driving forces are gravity (gr.) or surface tension (s.t.), dissipation occurs either at the contact line (c.l.), or in the bulk (vis.). Listed are also experimental papers frequently cited in support of a given scaling law.

Recently, experimental studies of spreading drops at *low* viscosities have appeared (Biance *et al.*, 2003; Kavehpour *et al.*, 2002). The theoretical analysis involves a balance of inertia and surface tension, neglecting viscous dissipation. Power laws close to $n = 1/2$ for very early stages of spreading, $R \ll V^{1/3}$ (Biance *et al.*, 2003), and $n = 2/3$ for later stages (Kavehpour *et al.*, 2002) have been reported.

D. Real solid surfaces: contact line hysteresis

Most solid surfaces are not homogeneous; dust particles, roughness and chemical heterogeneity may cause the spreading coefficient S to become dependent on the position on the substrate. If the defects are sufficiently weak, one may hope that Young's relation still holds, provided that S is replaced by its mean value $\overline{S}$, i.e., its value averaged over the substrate area. This leads to the so-called Cassie-Baxter relation (Cassie, 1952)

$$\gamma(1 - \cos\theta_{CB}) = -\overline{S}, \tag{13}$$

which allows to define the contact angle of a liquid on a heterogeneous substrate. Very careful experiments with a silicone wafer grafted with two different silanes show that the cosine of the contact angle does indeed vary linearly with the surface density X of one of the components, exactly as would be expected from (13) (Silberzan *et al.*, 1991). However, (13) only makes sense if thermodynamic equilibrium can be reached. This implies that the contact angle of a liquid drop deposited on the substrate reaches a unique value θ_{eq}, independent of the way the droplet is deposited on the substrate. This only very rarely happens in experiments, since even a small heterogeneity of

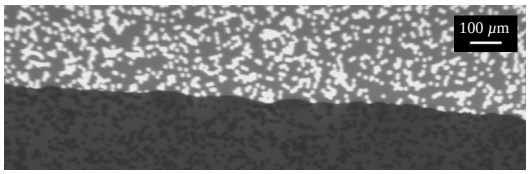

FIG. 9 The edge of a water drop receding on a disordered surface. The defects (size: 10 μm) appear as white dots.

the substrate may lead to a significant hysteresis of the contact angle.

Namely, for a drop obtained by advancing the meniscus over the substrate, θ_a (the advancing contact angle) is larger than the value θ_r (receding contact angle) for a meniscus that has been receding. Even for surfaces prepared very carefully, the hysteresis can be as large as a few degrees, and in practice it is very often of the order of several tens of degrees (Johnson and Dettre, 1993). This behavior complicates the understanding of the wetting behavior of liquids on solids tremendously, and is due to the pinning of the contact line on defects of the substrate. The size of the defects may in addition vary widely between different surfaces; when the size of the defects is macroscopic (micrometer size), the pinning can be observed directly as shown in Fig. 9. However, if the defects are microscopic (nanometric), their effect is still visible macroscopically as a hysteresis of the contact line.

A surface is considered to be relatively clean and flat if the contact angle hysteresis $\theta_a - \theta_r$ is smaller than, say, 5°. However, it is important to realize that the magnitude of the hysteresis is better described in terms of the forces that act on the three-phase contact line (recall that the dimension of surface tension is force per unit length) than in terms of the contact angle hysteresis. The important parameter is the threshold force per unit length which has to be applied to make the contact line advance or recede, which follows directly from the unbalanced Young's forces, respectively $f_c^+ = \gamma(\cos\theta_{eq} - \cos\theta_a)$ and $f_c^- = \gamma(\cos\theta_r - \cos\theta_{eq})$.

In practice, the equilibrium contact angle θ_{eq} cannot be measured, except in a gedanken experiment where the thermal fluctuations are strong enough to enable the contact line to find its minimum energy state (but then the hysteresis would disappear, too). The measurable quantity is the hysteresis force (per unit length):

$$H \equiv \gamma(\cos\theta_r - \cos\theta_a). \tag{14}$$

H can be measured directly by measuring the force exerted to a plate which is immersed and withdrawn in a liquid, as illustrated in Fig. 10. In a quasistatic experiment, the energy (per unit length) dissipated at the contact line equals the area, as one completes the loop. In the advancing part of the loop, the *rate* of energy dissipation is

$$W = U\gamma(\cos\theta_{eq} - \cos\theta_a), \tag{15}$$

with an analogous expression for the receding case.

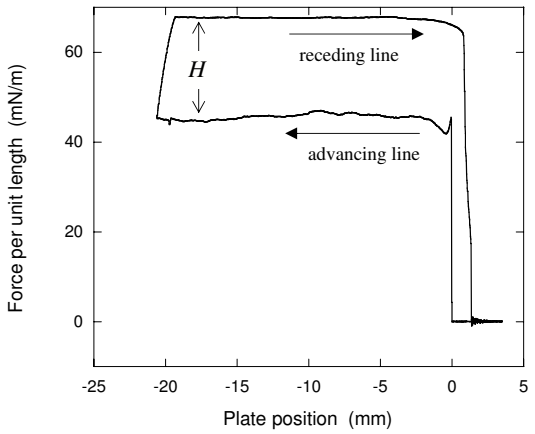

FIG. 10 Force per unit length exerted on a plate which is immersed and withdrawn in a liquid (buoyancy force has been subtracted) From (Moulinet *et al.*, 2004a).

For most systems, it turns out that $H/\gamma \gtrsim 0.1$. Using this value, it follows that the receding contact angle is zero, and consequently the contact line cannot recede, as soon as the advancing angle is smaller than about 20°. The presence of a hysteresis force (14) allows drops to be supported on an inclined plane without rolling off, until the force of gravity, projected onto the direction of the plane, equals H (Dussan V. and Chow, 1979). At the critical slope of the plane the contact angle of the front and back of the drop is θ_a and θ_r, respectively.

Because of the ubiquity of the hysteresis, the understanding of the contact line behavior on disordered solid surfaces is of great practical importance, and a variety of optical and tensiometric techniques (Johnson and Dettre, 1993) have been employed to measure the hysteresis in a large number of systems. However, in order to understand the effect of the disorder on the hysteresis, systematic studies are necessary on well-defined substrates as a function of the size, the number, and the strength of the defects. An example of the results of such a systematic study is shown in Fig. 11 : the contact angle has been measured as a function of the surface coverage X for substrates composed of patches of two different species. One may look upon the minority species as defects. As seen in Fig. 11, the advancing angle is roughly constant up to $X = 0.3$. This is consistent with the general trend that, for a non wettable substrate polluted by a few wettable defects, the advancing contact angle is close to the equilibrium contact angle on the clean non-wettable substrate. Namely, the contact line will only advance locally on the wettable patches; if the size of the defects is not too large, this will only lead to a local distortion of the contact line, which does not have a large effect on the contact angle.

Early theoretical work concentrated mainly on the calculation of the hysteresis on a substrate decorated by regular or periodic patterns (see e.g. Schwartz and Garoff (1985); more extensive references can be found in Johnson and Dettre (1993)). The hysteresis is determined

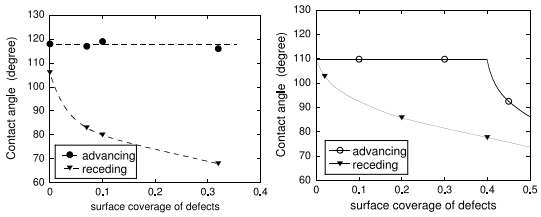

FIG. 11 Advancing and receding contact angles on a composite substrate as a function of the surface fraction of defects. Left: experimental measurements for liquid tin on $Si0_2$ partially covered by a regular array of Si defects (after de Jonghe and Chatain (1995)). Right: prediction adapted from the calculation by Schwartz and Garoff (1985).

by looking for the local minima of the total free energy for a -periodically- distorted interface. The results obtained in various approximation schemes agree qualitatively with the experimental data obtained on periodic substrates, such as those shown in Fig. 11. For the more general problem of non-periodic defects, a theoretical breakthrough occurred in the 80's when Robbins and Joanny (1987) pointed out that the dynamics of a contact line moving on a substrate with random defects was similar to the dynamics of other systems where an elastic boundary (the contact line) moves in a random medium (the disordered substrate). Examples are domain walls in ferromagnets (Lemerle *et al.*, 1998; Zapperi *et al.*, 1998), imbibition fronts (Alava *et al.*, 2004), and vortex lattices in type II superconductors (Blatter *et al.*, 1994). All these systems had been been studied for a long time, and subsequently a number of (phenomenological) models developed for these systems were used to study the behavior of the contact line. Perhaps the most interesting prediction that emanated from this work was that close to the depinning threshold ($f \gtrsim f_c^+$), the contact line undergoes a depinning transition that can be characterized by a few universal critical exponents.

This renewed theoretical interest also triggered new experiments in order to measure not only the hysteresis, but also the whole dynamical behavior of the contact line on random substrates. The qualitative features of the dynamics, such as stick-slip motion, were found to be indeed similar to the ones observed for other elastic boundaries. However, owing to the small number of controlled experiments that exist to date, it is still unclear whether quantitative agreement with current phenomenological models can be achieved.

II. EQUILIBRIUM WETTING PHENOMENA

A. Equilibrium wetting behavior in relation to the intermolecular interactions

The wetting behavior of, say, a liquid on a solid substrate is determined by the difference between the cohesive interactions holding the liquid together, and the adhesive interactions between the liquid and the solid (Israelachvili, 1992; Schick, 1990). In principle, all the equilibrium properties (such as S_{eq}) can thus be related to the molecular interaction potentials, for which the Lennard-Jones form (Israelachvili, 1992)

$$w(r) = 4\epsilon \left[(\sigma/r)^{12} - (\sigma/r)^{6}\right] \tag{16}$$

with a short-range repulsion and an algebraically decaying attraction is prototypical.

Although the algebraic $1/r^6$ tail of the Lennard-Jones form adequately applies to the London dispersion energy between non-polar molecules, the Debye energy between dipolar and non-polar molecules, as well as the Keesom energy between freely rotating dipolar molecules, there are other forces (e.g. hydrogen bonding, hydration forces, ...) which are very short-ranged and which lead to exponentially decaying forces between interfaces rather than algebraic ones. Sharma (1993) and Sharma and Jameel (1993) have referred to these short-ranged forces as "polar" and to the Lifshitz-van der Waals forces (arising from $1/r^6$ potentials) as "apolar". In a first step towards a systematic study of the effect of the interplay (or competition) between these short-ranged "polar" surface forces and the "apolar" ones, they adopt the rather severe simplifying assumption that the "apolar" spreading coefficient is simply proportional to the amplitude of the tail of the net "apolar" interaction between interfaces. Using the Young-Laplace and Navier-Stokes equations they then relate the stability properties of a thin adsorbed film to macroscopic parameters of wetting such as the contact angle.

One quantifies the net effect of the interaction potentials on the wetting behavior by considering a liquid film of thickness l on a solid substrate. If for instance the adhesive solid-liquid interactions are strong, the system can lower its free energy by increasing the distance between the two surfaces. This leads to a net repulsive force per unit area *between the solid-liquid and the liquid-vapor interfaces*, which is called the disjoining pressure $\Pi(l)$ (de Feijter, 1988; Teletzke *et al.*, 1988) and can be measured in experiment. Theoretically, it can be derived from the so-called effective interface potential $V(l)$ through

$$\Pi(l) = -dV(l)/dl, \tag{17}$$

where

$$\gamma_{SV}(l) = \gamma + \gamma_{SL} + V(l) \tag{18}$$

is the *excess* free energy per unit area of the liquid film, and $V(\infty) \equiv 0$. Surface excess free energies are well defined thermodynamically and can be calculated using statistical mechanics (Rowlinson and Widom, 1982).

The long-time static, but *non-equilibrium* behavior of non-volatile adsorbates can also be described by (18), cf. section I.B. To see this, it suffices to appreciate that the previously introduced "dry"-substrate surface tension γ_{S0} and the initial spreading coefficient S_i correspond to

taking the $\ell \to 0$ limit in (18),

$$\gamma_{S0} \equiv \gamma_{SV}(0), \text{ and } S_i \equiv V(0) \tag{19}$$

Now, in view of the volume conservation of non-volatile drops, the static film thickness after flattening, assuming $S_i > 0$, is governed not by minimizing $V(\ell)$, as would be the case for an equilibrium film, but by minimizing the surface free energy with the constraint. This leads to the modified condition (Brochard-Wyart *et al.*, 1991; de Gennes *et al.*, 2003)

$$(V(\ell) - V(0))/\ell = dV(\ell)/d\ell, \tag{20}$$

allowing the determination of the static thickness of the flattened drop through an elegant tangent rule in the plot of $V(\ell)$. Since the non-volatile drop would ideally like to spread over the entire dry substrate, but contains insufficient material to do so, the compromise is a finite "pancake", *slightly thinner* than the infinitely wide equilibrium thin film (without volume constraint, i.e. for volatile liquids).

Knowing the disjoining pressure, the equilibrium wetting state can be predicted, but a calculation based on first principles is difficult. Starting from Lennard-Jones potentials, density functional theory (DFT) (Dietrich, 1988; Evans, 1990; Schick, 1990) in principle provides a means of calculating the equilibrium wetting state. DFT is based directly on *microscopically* specified molecular interactions. Within mean-field theory, one attempts to find the free energy of the system as a functional of the density profile $\rho(\mathbf{r})$ alone. This is, however, very difficult owing to the slow decay of, e.g., the Lennard-Jones potential $w(r)$. Thus, either some simplifications have to be made, or the problem has to be solved numerically. Quantitative predictions based on numerical solutions of the full DFT that have been verified by experiment are so far limited to the wetting behavior of simple atoms or molecules (e.g., He) on simple substrates (e.g., Cs) at zero temperature (Cheng *et al.*, 1993). Considering only the $1/r^6$ van der Waals attractive tail of $w(r)$, the disjoining pressure for large distances can be calculated explicitly. If in addition the spreading coefficient is known (for instance from the phenomenological Cahn-Landau theory), the wetting behavior can be predicted.

The subtleties and strengths of an approach based on DFT are exquisitely illustrated by derivations of an effective Hamiltonian for liquid-vapor interfaces (Dietrich and Napiórkowski, 1991; Mecke and Dietrich, 1999; Napiórkowski and Dietrich, 1993). Taking into account only bulk fluctuations, first an intrinsic density profile is obtained, and in the next step undulations of the interface position are described by a statistical theory for capillary waves on all length scales. The result is a *nonlocal* and non-Gaussian functional of the interface configuration. From this the usually postulated (local) Helfrich Hamiltonian can be deduced by a gradient expansion, which, however, features divergent coefficients for all but strictly finite-range interactions. If one expands, as is usually done, the Fourier transform of the Helfrich Hamiltonian in powers of the transverse momentum q, one obtains an approximate wave-vector-dependent interfacial tension $\gamma(q)$. However, the Gaussian approximation to the nonlocal interface Hamiltonian derived by Mecke and Dietrich (1999) leads to a form for $\gamma(q)$ that is qualitatively different in the long capillary wavelength limit and agrees much better with experiments on liquids with intermolecular dispersion forces (Mora *et al.*, 2003).

1. Long-range forces: the Hamaker constant

The van der Waals interaction $w(r) \propto 1/r^6$ (cf. (16)) includes all intermolecular dipole-dipole, dipole-induced dipole and induced dipole-induced dipole interactions. Performing a volume integral over all molecules present in the two halfspaces bounding the film one finds a corresponding decay $\Pi(l) \approx A/(6\pi l^3)$ (Israelachvili, 1992), where the so-called Hamaker constant A gives the amplitude of the interaction. In the "repulsive" case, in which the layer tends to thicken, we have $A > 0$; note that Israelachvili (1992) uses a different sign convention for A.

At distances larger than the microscopic ones, (17) leads to an effective interaction energy

$$V(l) = \frac{A}{12\pi l^2}. \tag{21}$$

between the two surfaces bounding the wetting layer. Note that this is a truly long-range interface potential, and this is why van der Waals forces are considered to be of long range in the context of wetting. Assuming pairwise additivity of the interactions, Hamaker (1937) showed that A can be directly related to the amplitudes of the substrate-liquid and liquid-liquid interaction tails. Below we report a more complete calculation of A (Dzyaloshinskii *et al.*, 1961), although the numerical improvement over the original result of Hamaker (1937) is small.

To understand the effect of both long- and short-ranged interactions on the wetting behavior it is useful to consider the relation (de Feijter, 1988)

$$S_{eq} = \int_{l_{min}}^{\infty} \Pi(l) dl. \tag{22}$$

The potential minimum at l_{min} essentially contains the information about the short-ranged forces, i.e., the contributions that remain when the interaction tails are "cut off".

Partial wetting corresponds to $S_{eq} < 0$; this prohibits the formation of a wetting layer, regardless of the sign of A. If $S_{eq} = 0$ and $A > 0$, a wetting layer will form, and we speak of complete wetting. An intermediate state may occur under certain conditions if $S_{eq} \approx 0$ (it is not exactly zero but slightly negative, as will be discussed in subsection II.B.2) and $A < 0$: this intermediate wetting state

is characterized by a mesoscopic wetting film, and has been dubbed *frustrated complete wetting* (Indekeu *et al.*, 1999a,b). In this case, the interface potential has two minima such as for a first-order wetting transition (glance ahead to Fig. 13 (left)), but the second minimum occurs at a finite rather than infinite wetting film thickness.

The Hamaker constant is thus a key property for determining the *wetting* behavior, and can be calculated exactly (Dzyaloshinskii *et al.*, 1961) in terms of the dielectric properties of the three materials, which are characterized by their frequency-dependent polarizability. In addition, as will be explained below, the Hamaker constant is also important in determining the *spreading* behavior. For its calculation, one has to integrate the dipolar interactions over all frequencies, and express them as an effective interaction between the two surfaces bounding the halfspaces. A simple and usually good approximation (Israelachvili, 1992) is obtained by first considering the contribution due to dipolar interactions, given by the (zero frequency) dielectric constants of the materials:

$$A_{\nu=0} = -\frac{3}{4} k_B T \frac{(\epsilon_1 - \epsilon_3)(\epsilon_2 - \epsilon_3)}{(\epsilon_1 + \epsilon_3)(\epsilon_2 + \epsilon_3)}. \tag{23}$$

Here 1 (solid) and 2 (vapor) denote the material in the two halfspaces, and 3 (liquid) is the intermediate material. According to (23) $|A_{\nu=0}|$ can never exceed $(3/4)k_BT$, but it is usually significantly smaller. As a result, unless strongly polar molecules such as water are involved, $A_{\nu=0}$ can be neglected with respect to the finite-frequency term that accounts for the induced dipolar interactions. The only case for which the static contribution (23) is important is when at least one of the materials has a high dielectric constant (e.g., water) and the refractive index differences in the visible are small; one pertinent example of both is the wetting of light hydrocarbons on water (Ragil *et al.*, 1996b).

The main contribution to the integral comes from frequencies corresponding to visible light, and consequently $A_{\nu>0}$ is given by the refractive indices in the visible:

$$A_{\nu>0} = -\frac{3h\nu_{UV}}{16\sqrt{2(n_1^2+n_3^2)(n_2^2+n_3^2)}} \times \frac{(n_1^2-n_3^2)(n_2^2-n_3^2)}{\sqrt{(n_1^2+n_3^2)}+\sqrt{(n_2^2+n_3^2)}}. \tag{24}$$

Here h is Planck's constant and ν_{UV} ($\approx 2\times10^{16}$ Hz) is the UV frequency for which the refractive indices of the materials become identical (close to unity). The Hamaker constant is the sum of the two contributions given above.

The zero-frequency or "Keesom and/or Debye" part of the Hamaker constant preserves the $1/l^2$-dependence of $V(l)$ in (21) for all distances; however, the dispersive or "London" part $A_{\nu>0}$ is subject to retardation, as interactions due to changing dipoles only travel at the speed of light. The typical frequency ν_{UV} corresponds to distances of 15 nm; for larger distances the $1/l^2$-behavior crosses over to a $1/l^3$-decay. However, in general the correction from retardation is hardly detectable in experiment (Sabisky and Anderson, 1973).

It also follows from (24) that for a symmetrical situation (two identical materials separated by a third and different material), the net effect of the van der Waals forces is always an effective *attraction* between the two interfaces ($A < 0$). Thus if only van der Waals interactions are important, two colloid particles are attracted to each other and colloids invariably flocculate. In a wetting problem the situation is different as in general three different materials are involved. In this case, it follows from (23) and (24) that depending on the dielectric properties of the three media, A can have either sign.

For the typical case that $A_{\nu>0}$ dominates, the sign of A is given by the sign of the refractive index difference between the liquid and the solid, since the refractive index of the vapor will generally be close to unity. If the liquid has a refractive index between that of the solid and the vapor (which is usually the case), it follows that $A > 0$ and the formation of a liquid wetting layer is favored: there is an effective repulsion between the interfaces. If (and only if) in addition the equilibrium spreading coefficient is zero, complete wetting will result.

For thick equilibrium wetting films, the van der Waals interactions and a possible gravitational penalty for forming a wetting layer above its bulk reservoir have to be taken into account.This leads to (de Gennes, 1981; Deryaguin, 1940; Evans and Marini Bettolo Marconi, 1985)

$$l = \left(\frac{A}{6\pi\Delta\rho g H}\right)^{1/3}, \tag{25}$$

where H is the height of the wetting layer above its bulk phase and $\Delta\rho$ the mass density difference between the wetting layer and the phase on which it rests. Away from T_c, explicit calculation gives $A/6\pi \approx 0.5 k_B T$ and thus $l \approx 100$ Å, in general agreement with experiments on binary liquid systems (Bonn *et al.*, 1992; Findenegg and Löring, 1984; Kayser *et al.*, 1986; Law, 1991; Moldover and Cahn, 1980; Schmidt and Moldover, 1986). For low-temperature systems Sabisky and Anderson (1973) confirm that $l \propto H^{-1/3}$ as predicted by (25), where H is the height above the reservoir. More generally H can be identified as a chemical potential shift away from coexistence: $\Delta\mu \propto gH$, giving

$$l \propto |\Delta\mu|^{-1/3}. \tag{26}$$

When a substrate is brought into contact with a non-saturated vapor, $\Delta\mu = k_B T\, ln(P/P_{sat})$ and the liquid wetting layer thickness diverges as coexistence is approached (Krim *et al.*, 1984).

Closer to T_c, the bulk correlation length can become of the order of the film thickness. A recent experimental study (Fenistein *et al.*, 2002) of the binary liquid mixture cyclohexane-methanol has shown that upon approaching the bulk critical temperature, the film thickness diverges like $t^{-\hat{\beta}}$ with an apparent effective critical exponent $\hat{\beta} = 0.23 \pm 0.06$.

2. Short-range forces: the phenomenological Cahn-Landau theory of wetting

The classical theory of Cahn (1977), combined with a Landau expansion, is an explicit way to calculate the spreading coefficient. In addition it does quite well in predicting generic wetting behavior, in spite of the fact that the van der Waals tails of the intermolecular forces are not included. For a detailed discussion of Cahn-Landau theory, see, e.g., Bonn and Ross (2001). It can be used to predict first-order and short-range critical wetting transitions, and can be adapted when the tails of the van der Waals forces control the wetting behavior, as is observed for long-range critical wetting (Indekeu *et al.*, 1999a).

Cahn (1977) considered the surface free energy functional in a squared-gradient approximation, with the addition of a surface term in order to account for the interactions with the wall:

$$F_s = \Phi(m_s) + \int_0^\infty \{(c^2/4)(dm/dz)^2 + \omega(m)\}dz, \quad (27)$$

where ω is the bulk free energy density, $m(z)$ the order parameter profile as a function of the distance z from the wall, and $m_s \equiv m(0)$ its value at the substrate. For a typical adsorbed fluid m is proportional to the density minus the critical density, $\rho - \rho_c$. The term in the integral is the classical van der Waals form for a liquid-vapor interface. It leads to an interface whose density profile is a hyperbolic tangent, and whose thickness is that of the bulk correlation length ξ (Rowlinson and Widom, 1982). Cahn (1977) included a solid surface by adding the contact energy $\Phi(m_s)$ to (27) which only depends on m_s. It is usually expanded to second order (Nakanishi and Fisher, 1982):

$$\Phi(m_s) = -h_1 m_s - g m_s^2/2, \quad (28)$$

where the parameters h_1 and g are referred to as the short-range surface field and the surface enhancement, respectively. The field h_1 describes the preference of the substrate for either the liquid or the vapor, and is a measure of the difference between the substrate-liquid and substrate-vapor surface tensions (Ross *et al.*, 2001a); consequently if $h_1 > 0$, the liquid is preferred at the wall, whereas for $h_1 < 0$ the vapor is preferred. The surface enhancement g allows for the missing interactions due to the fact that a particle near a wall has a smaller number of like neighbors than a particle in bulk. It is usually negative (Bonn and Ross, 2001).

The phase diagram that follows from Cahn-Landau theory is illustrated in Fig. 12. Let us focus first on the plane $h = 0$, which corresponds to the coexistence between liquid and vapor, e.g., a drop sitting on a substrate. In fact, $h \equiv (\mu - \mu_0)/k_B T$ measures the distance in bulk chemical potential from two-phase coexistence. The remaining axes are the reduced temperature $t = (T - T_c)/T_c$ and the surface field h_1. In agreement with Cahn's expectation, upon increasing the temperature toward T_c one always leaves the hatched area

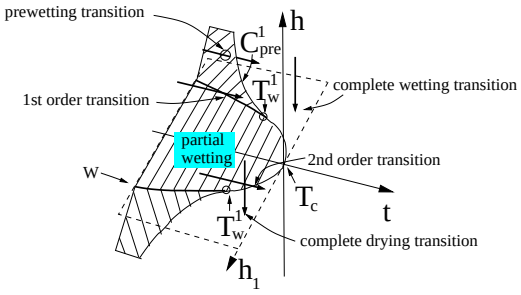

FIG. 12 The wetting phase diagram calculated by Nakanishi and Fisher (1982), where $t = (T - T_c)/T_c$ is the reduced temperature, h_1 is the surface field, and h the bulk field. The wetting line W (which is a parabola in mean field) has the critical temperature T_c at its apex. At T_w^1 there is a tricritical point which separates first-order from second-order wetting transitions. The surface of prewetting transitions is bounded by a line of critical points C_{pre}^1, called the critical prewetting line, which merges into the wetting line at T_w^1.

bounded by the so-called *wetting line*, and a wetting transition occurs. If h_1 is large, the transition is of first order. However, as one crosses the *tricritical* point at T_w^1 the transition becomes second-order or *critical*.

One of the interesting predictions of the Cahn-Landau theory (see also Ebner and Saam (1977)) is that a first-order wetting transition at coexistence should persist in regions of the phase diagram off of coexistence $h \neq 0$. As seen in Fig. 12, this *prewetting* transition is an extension of the wetting transition in the one-phase region of the bulk phase diagram. It manifests itself, e.g., by the formation of a thick (but not macroscopic) liquid film on the substrate at pressures below the saturated vapor pressure.

As one moves away from the wetting line, the line of prewetting transitions ends in a surface critical point, called the *prewetting critical point*. Upon approach of the surface tricritical point T_w^1, the prewetting line shrinks progressively away; for critical wetting there is no prewetting line (cf. Fig. 12). As one approaches coexistence for $T > T_W$, the wetting temperature, one observes complete wetting, characterized by a wetting film whose thickness diverges. All these transitions, including the prewetting line and its critical point, have been observed experimentally. Thus, although phenomenological and without direct link to the intermolecular interactions, the Cahn-Landau theory is an excellent starting point for understanding wetting transitions, and is often used as a tool in engineering applications to predict wetting behavior (Carey *et al.*, 1978).

However, Ebner and Saam (1987); de Gennes (1983) and others have shown that, generically, van der Waals forces eliminate the possibility of critical wetting. A concise discussion can be found in Indekeu *et al.* (1999a). Below (see section II.B.2) we will indicate how this can be reconciled with experiment. When van der Waals forces oppose wetting, a first-order thin-thick transition may still persist, but a macroscopic wetting layer cannot

form. Instead, at the first-order transition, a mesoscopic film forms (typically 50-100 Å in experiments) (Bertrand *et al.*, 2002; Ragil *et al.*, 1996b; Shahidzadeh *et al.*, 1998). Remarkably, in this "frustrated complete wetting" state a droplet placed on a substrate displays a tiny but finite contact angle and coexists with a mesoscopic film.

B. Real systems: three scenarios for wetting transitions

Much of the progress in the study of wetting transitions over the past decade has been experimental, using two key systems: low temperature liquid-vapor systems and room temperature binary liquid systems. Both have provided almost identical results - highlighting the robustness of the phenomena of wetting transitions over orders of magnitude of temperature and interaction strengths. This is less surprising than it may appear at first sight, since the temperature also sets the scale of the surface tension; wetting occurs at comparable values of the bulk correlation length ξ (and thus of reduced temperature), and $\gamma\xi^2/k_BT$ is nearly constant (≈ 0.1). Thus γ/T is actually similar for all the systems under study.

For solid-liquid systems, work on the low-temperature systems was motivated by the prediction (Cheng *et al.*, 1991) that liquid helium would not wet surfaces of the heavier alkali metals at very low temperatures, and therefore, according to the Cahn argument (see II.C.1 below), that wetting transitions should be observed in these systems. This prediction, and the subsequent experimental verification of the partial wetting of helium on cesium (Nacher and Dupont-Roc, 1991) at low temperatures initiated a large amount of wetting research with quantum liquids on weak-binding alkali metal substrates; for recent detailed reviews, see Bonn and Ross (2001); Bruch *et al.* (1997); Cheng *et al.* (1993).

This increased activity resulted, among other things, in the first experimental verification of the prediction (Cahn, 1977; Ebner and Saam, 1977) of the prewetting line by Rutledge and Taborek (1992). An advantage of the low-temperature systems is the simplicity of the interaction potentials, so that detailed comparisons with DFT (Cheng *et al.*, 1993) are possible. The main disadvantage is the roughness and chemical inhomogeneity of the alkali substrates, leading to pinning of the contact line, and to poor reproducibility (Klier *et al.*, 1995; Rolley and Guthmann, 1997; Ross *et al.*, 1998) and rather large uncertainties for instance in the measured contact angles. The effects of disorder will be discussed in detail in section IV.

A schematic interface potential $V(l)$ for a first-order (discontinuous) transition and for a second-order (continuous or critical) transition is shown in Fig. 13. In general, complete wetting is more likely to occur at higher temperatures. For a first-order wetting transition, this corresponds to a discontinuous jump from a thin film (partial wetting) to an infinitely thick film (complete wetting): for low T the absolute minimum in $V(l)$ is the thin film,

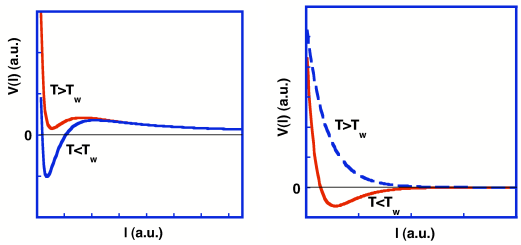

FIG. 13 Schematic effective interface potential for a first-order wetting transition (left), and for a (short-range) critical wetting transition (right).

for high T it is the infinitely thick film. At the first-order wetting temperature, the free energy of the two minima is equal. For a continuous transition, there is only one minimum, and this minimum shifts continuously to an infinitely thick film upon reaching the critical wetting temperature.

1. First-order and critical wetting

A very simple argument, due to Cahn (1977), uses Young's equation to argue that a wetting transition should always occur as the bulk critical point is approached by letting $T \to T_c$. Indeed, for the vast majority of systems studied to date a wetting transition is encountered upon increasing the temperature towards the critical point, and temperature is the most used control parameter to study wetting transitions. A beautiful demonstration of this principle of "critical-point wetting" is the transition from partial to complete wetting of the interface between the upper and lower phases by the middle phase microemulsion, when approaching either the upper or the lower critical endpoint in H_2O-octane-C_5E_2 liquid mixtures (Kahlweit *et al.*, 1993).

Note that the Cahn argument foresees only one kind of transition: a first-order wetting transition, in which the wetting layer appears on a substrate, or at an interface, in a discontinuous fashion, again in line with the vast majority of experimental observations. However, a careful analysis reveals that the Cahn argument actually breaks down for $T \to T_c$, (Bonn and Ross, 2001; Indekeu, 1991; Pandit *et al.*, 1982; Sullivan and Telo da Gama, 1986), hence the argument cannot be used too close to the bulk critical point. Experimentally, the wetting transition actually turns second order (continuous) close to the bulk critical point, as predicted by the Cahn-Landau theory.

Two (independent) critical exponents characterize the wetting transition. First, the manner in which $\cos\theta_{eq}$ approaches 1 at the wetting temperature defines the surface specific heat exponent α_s through (Dietrich, 1988; Schick, 1990)

$$(1 - \cos\theta_{eq}) \propto (T_w - T)^{2-\alpha_s}. \qquad (29)$$

For $\alpha_s = 1$, the first derivative of γ_{SV} with respect to the temperature is discontinuous at T_w ($\cos\theta_{eq} = 1$ for

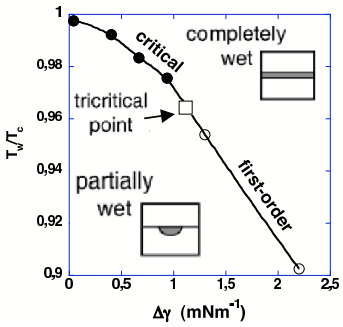

FIG. 14 Surface phase diagram measured by Ross *et al.* (2001b) for the wetting of alkanes and mixtures of alkanes of different (effective) chain lengths, corresponding to different differences $\Delta\gamma$ between surface tensions of the pure alkanes and pure methanol.

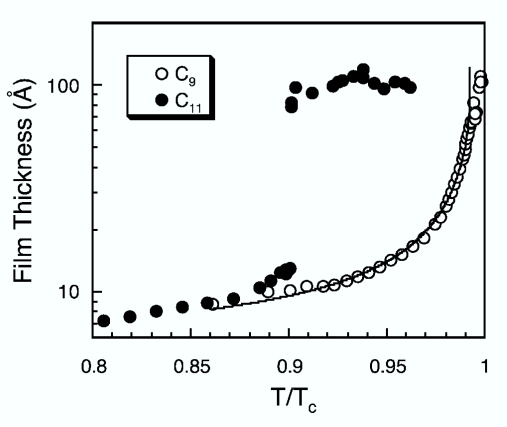

FIG. 15 The continuous divergence of the wetting layer thickness observed for the wetting of methanol on nonane (C9), compared to its behavior on undecane (C11) for which the transition is discontinuous (first order)

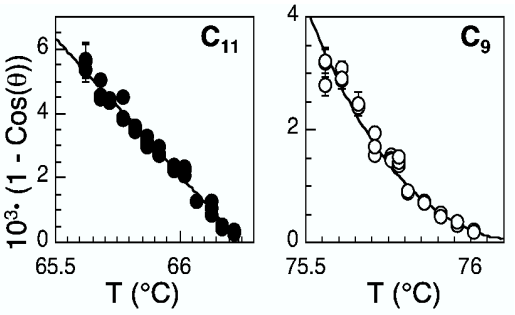

FIG. 16 Singular part of the surface free energy, as determined directly from contact angle measurements, giving the surface specific heat exponent α_s. The wetting of methanol on nonane (C9) is continuous, and so the slope of the surface free energy vanishes in a continuous fashion. For undecane, (C11) the transition is discontinuous (first order), and a discontinuity in slope is indeed apparent.

$T \geq T_w$) and so the wetting transition is of first order. For $\alpha_s < 1$, the first derivative is continuous at T_w: the transition is a continuous or critical wetting transition.

Second, the divergence of the layer thickness l is described by

$$l \propto (T_w - T)^{\beta_s}. \tag{30}$$

Note that $\beta_s \leq 0$.

Because of the difficulties of working with solid surfaces, the measurements of these critical exponents were almost all done by investigating the wetting of liquids on liquid "substrates". Studying the evolution of drops of methanol at the liquid-vapor interface of different alkanes, Ross *et al.* (1999) showed that if the wetting happens far from the critical point, it is the usual first-order transition (see Fig. 14) characterized by a discontinuous jump in the film thickness from a microscopic value to a (gravitationally limited) thickness of about 100$\mathring{A}$ (see Fig. 15). If on the other hand the wetting transition happens very close to T_c, a completely continuous and reversible critical wetting transition was observed (Fig. 14 and Fig. 15). For the latter, the divergence of the layer thickness was found to be logarithmic, in agreement with mean-field (MF) and renormalization group (RG) predictions for short-ranged forces, and implying $\beta_s = 0(log)$.

In addition, the measurement of the contact angle close to T_w (Moldover and Cahn, 1980; Ross *et al.*, 1999) yields a surface critical exponent $\alpha_s = 1.0 \pm 0.2$ compatible with a first-order wetting transition (Fig. 16). For the continuous transition close to T_c, the fit yields $\alpha_s = -0.6 \pm 0.6$, indicating critical wetting (Fig. 16). The value of this critical exponent disagrees with that predicted by RG studies, an issue which will be discussed below.

For the methanol-alkane systems, by increasing the chain length n of the alkanes, one effectively increases the preference of the "substrate" (the vapor plays the role of substrate here) for the methanol-rich phase. Thus for small $n < 8$, a drying transition is observed upon raising the temperature. For longer chains, one first crosses over to a critical wetting transition for $n = 9$, and then to a first-order wetting transition. Different (effective) chain lengths correspond to different values of the "surface field", which is proportional to the difference in surface tension of the pure alkane and pure methanol. The wetting phase diagram shown in Fig. 14 thus corresponds with (a part of) the predicted global one (Fig. 12). Critical wetting is confined to a relatively small region near the critical point: $0.97 < T_w/T_c < 1$, in very good agreement with the generic phase diagram for systems with short-ranged forces, calculated in Cahn-Landau theory.

2. Long-range critical wetting

So far, the effect on wetting scenario's of long-range van der Waals forces has not been considered. Besides first-order and critical wetting, there is a third way in

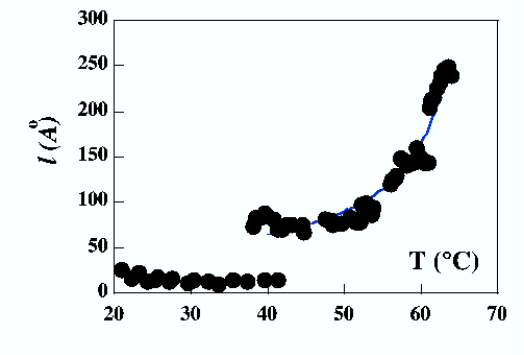

FIG. 17 Sequence of two wetting transitions for the wetting of hexane on (salt) water, salinity 1.5 mole/l NaCl, from Shahidzadeh *et al.* (1998).

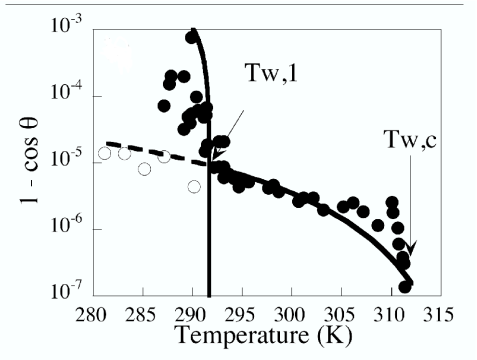

FIG. 18 Singular part of the surface free energy, 1 - cos θ_{eq} versus temperature, for hexane on brine (2.5 M) from Rafaï *et al.* (2004a). The filled circles are obtained upon increasing the temperature, and the open circles upon decreasing T: clearly a hysteresis around the first-order transition is observed. The open symbols then likely correspond to the metastable extension (undercooling) of the frustrated complete wetting state.

which a wetting transition can take place which is governed by the long-ranged forces. Bertrand *et al.* (2002); Rafaï *et al.* (2004a); Ragil *et al.* (1996b); Shahidzadeh *et al.* (1998) demonstrated a completely continuous transition between a relatively thin and a thick wetting film of liquid alkanes on water (in contact with their common vapor). This transition is associated with long-ranged forces disfavoring wetting at low temperatures, but favoring wetting at high T. For low T, $A < 0$; upon increasing the temperature, one reaches a first-order "Cahn"-like transition, but since $A < 0$ at the transition, the usual wetting transition to a macroscopically thick film cannot take place. Instead, after the first-order transition, the system is still in a partial wetting state termed "frustrated complete wetting", characterized by a mesoscopic film that is neither microscopically thin, nor macroscopically thick. As shown in Fig. 17, upon increasing T even further the film thickness diverges in a continuous fashion, which is associated with $A \to 0$: the Hamaker constant changes sign from disfavoring wetting to favoring wetting.

Fig. 18 shows the only available measurement of the singular part of the surface free energy $1-\cos\theta_{eq}$ for the same system. The change in slope at a finite but very small contact angle (about 0.25°) observed around 292 K is the signature of a discontinuity in the first derivative of the free energy, i.e., a first-order transition, in good agreement with the transition temperature of 294.5 K found for the film thickness. When increasing the temperature further, Rafaï *et al.* (2004a) observed that the contact angle vanishes in a continuous and, moreover, rather smooth fashion, signaling the critical wetting transition. Although rather noisy, a least-squares fit to the data in Fig. 18 gives $2-\alpha_s = 1.9 \pm 0.4$ (cf. (29)), demonstrating the continuous nature of the transition. Note that this is to be compared with the value $2-\alpha_s = 3$, expected for non-retarded van der Waals forces, as can be deduced by integrating the disjoining pressure from the equilibrium layer thickness ℓ_{eq} to $\ell = \infty$. The discrepancy is possibly due to the difference between the apparent value and the asymptotic value of the critical exponent (Weiss *et al.*, 2007).

To describe this transition, a higher-order term must be added to the long-ranged part of the interaction potential, since A goes to zero (Dietrich and Schick, 1985):

$$V(l) = \frac{A}{12\pi l^2} + \frac{B}{l^3}, \tag{31}$$

where $B > 0$. Physically, B is due to the fact that the film on the substrate is denser at the liquid/substrate interface than in bulk (Saam and Shenoy, 1995; Shenoy and Saam, 1995). For alkanes on water, the order of magnitude of B is given by the Hamaker constant of the alkane interacting with itself through vacuum, multiplied by a typical molecular size $a \approx 5$ Å; $B \approx 0.5 k_B T a \approx 10^{-30}$ Jm, in very reasonable agreement with the value found in experiment (Ragil *et al.*, 1996b). The free energy (31) has a minimum for

$$l = -\frac{18\pi B}{A} \propto \frac{1}{T_w - T}. \tag{32}$$

so that in the experiments a film of this thickness surrounds a droplet; with $A/6\pi \approx 0.1 k_B T$ away from T_w, this leads to $l \approx 50$ Å, in qualitative agreement with the experiments. The continuous divergence of the wetting film happens as the Hamaker constant, the only force that prevents wetting, goes to zero linearly at the wetting temperature (Dietrich and Schick, 1985; Ragil *et al.*, 1996b); this defines the critical exponent of the layer thickness $\beta_s = -1$. This prediction for the divergence was verified in experiment by Ragil *et al.* (1996b), who found $\beta_s = -0.99 \pm 0.05$, although subsequent experiments indicated a somewhat smaller value. Fig. 19 shows the excellent agreement between the measured and computed layer thicknesses using the full Lifshitz theory (Dzyaloshinskii *et al.*, 1961) for the critical wetting transition of pentane on water.

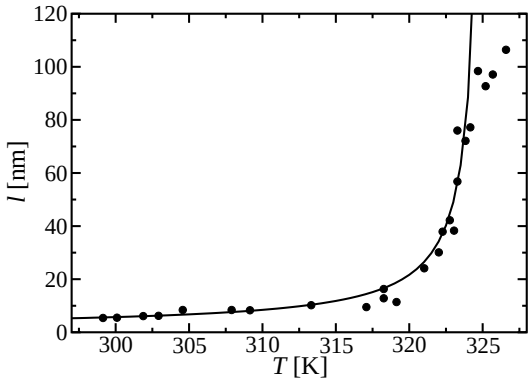

FIG. 19 Film thickness l of the mesoscopically thick film of liquid pentane on water as a function of temperature. This film is present in the frustrated complete wetting state between the first-order and the continuous transition, observed for pentane on water. The circles represent ellipsometry data of Ragil *et al.* (1996b), while the solid curve is the result of a calculation based on Lifshitz theory (Dzyaloshinskii *et al.*, 1961; Weiss *et al.*, 2007). Within this approach, the film thickness is obtained from the amplitudes of the two leading terms of the long-range interactions between adsorbate and substrate. This type of calculation requires only the macroscopic dielectric properties (static permittivities and refractive indices) of the isolated media (Bertrand *et al.*, 2001; Weiss and Indekeu, 2003).

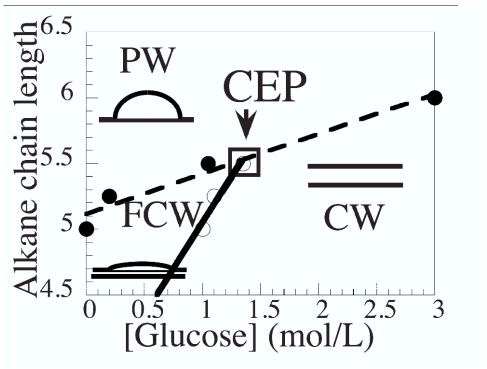

FIG. 20 Generic wetting phase diagram: alkane chain length versus glucose concentration. Filled symbols show the first-order transition (dashed line). Open symbols represent the continuous transition (solid line). The two transition lines produce three phase regions: regular partial wetting (PW), complete wetting (CW) and frustrated complete wetting (FCW). The critical end point (CEP) is the crossover between first-order and critical wetting.

By carefully tuning experimental parameters, one can achieve a system in which A changes sign *at* the first-order wetting transition (Rafaï *et al.*, 2004a). This leads to a crossover between the sequence of two wetting transitions described in this section, and the ordinary first-order wetting transition of section II.B.1 Rafaï *et al.* (2004a) provide evidence for the existence of a *critical end point*, where one crosses over from one scenario to the other, observed in a mixture of pentane and hexane, deposited on an aqueous solution of glucose. The generic wetting phase diagram obtained in these experiments is shown in Fig. 20.

In the frustrated-complete wetting state characterized by the presence of the mesoscopic film, the surface free energy is very close to that for complete wetting (Bertrand *et al.*, 2002). The difference can be estimated from the work performed against the disjoining pressure between 50 Å and an infinite film. Equation (22) then gives $S_{eq} \simeq -10^{-6}$ Nm^{-1}, much smaller than a typical surface tension. This means that the equilibrium spreading coefficient is only slightly different from zero: it is negative since the free energy of the system with an infinitely thick film is slightly higher than that of the frustrated complete wetting state.

The new state of frustrated complete wetting is different from what has previously been dubbed "pseudopartial wetting" (Brochard-Wyart *et al.*, 1991), also characterized by $A < 0$. Namely, while frustrated complete wetting is a particular case of partial wetting (allowing for a macroscopic drop having a finite contact angle), it can be distinguished from regular partial wetting by a first-order transition between two different partial wetting states. One corresponds to a minimum resulting from short-range forces, the second minimum (32) is due to the tails of the long-range forces and leads to a much thicker film. In both partial wetting states the equilibrium spreading coefficient is negative, and consequently knowing the sign of A and S_{eq} is not sufficient to distinguish them.

What are the implications of the wetting forces on the spreading? For most practical purposes spreading experiments consider the situation $S_{eq} = 0$ and $A > 0$, thereby implicitly assuming that a non-wetting situation always corresponds to $S_{eq} < 0$ and $A < 0$. However, as the studies on wetting transitions reveal, there is no fundamental reason why this should necessarily be the case. The "frustrated complete wetting state" for instance corresponds to $S_{eq} \approx 0$ and $A < 0$; the spreading behavior in this wetting state would be very interesting to study since the presence of the mesoscopic film would get rid of the singularity at the contact line, and provide us with a small-scale cutoff that is tractable. Perhaps even more interestingly, the calculation of the Hamaker constant shows that there is no fundamental reason why one could not have a situation with $S_i > 0$ and $A < 0$. From the above considerations, it follows that it is sufficient to find a substance that has a lower surface tension than the critical surface tension of the substrate (see I.B.1), and a higher refractive index (see II.A.1). In practice, refractive indices of liquids are generally lower than those of solids; however, exceptions do exist. If such a system could be found, this might help identify the elusive short-wavelength cut-off in spreading theory, and assess the importance of the precursor film, etc.

C. Fluctuation effects and short-range critical wetting

The short-range critical wetting (SRCW) transition in three dimensions ($d = 3$) has received a tremendous amount of theoretical attention, because the critical behavior may include effects beyond mean-field (MF) theory (Boulter, 1997; Brézin *et al.*, 1983a,b; Dietrich, 1988; Fisher and Huse, 1985; Halpin-Healy and Brézin, 1987; Lipowsky *et al.*, 1983; Parry, 1996; Parry *et al.*, 2004).

Fluctuations may be neglected if the (bulk) dimension d is above an upper critical dimension d^* (Hohenberg and Halperin, 1977). A typical interfacial height fluctuation has an energy of order k_BT, and a size parallel to the wall of the order of the correlation length $\xi_{||}$, with $\xi_{||} \propto (T_w - T)^{-\nu_{||}}$. In MF theory $\nu_{||} = 1$ (Dietrich, 1988; Schick, 1990; Sullivan and Telo da Gama, 1986). This results in an entropic fluctuation contribution to the surface free energy

$$\Delta\gamma_{SV} \propto k_BT/\xi_{||}^{(d-1)} \propto (T_w - T)^{(d-1)\nu_{||}} \qquad (33)$$

Since $\alpha_s = 0$ in MF theory, for $d > 3$ the critical part (29) of γ_{SV} dominates over (33), giving $d^* = 3$ (Lipowsky, 1984). Incidentally, for thermal fluctuations the gradient-squared interfacial bending energy scales like the entropic repulsion energy, corroborating $d^* = 3$. For $d \leq 3$, the hyperscaling ansatz links α_s to $\nu_{||}$ through

$$2 - \alpha_s = (d-1)\nu_{||} \qquad (34)$$

Within MF (Cahn-Landau) theory one can also calculate the effective interface potential of a film, to estimate both the film thickness l and its fluctuations. Owing to the exponential decay of the density profile, in the limit of large l, $V(l)$ can be expanded as (Brézin *et al.*, 1983a,b; Schick, 1990):

$$V(l) = ae^{-l/\xi} + be^{-2l/\xi} + \ldots, \qquad (35)$$

where ξ is the bulk correlation length. The amplitudes a, b, ..., can be calculated. Depending on whether (35) has a single minimum or two minima, the wetting transition is discontinuous or continuous, in agreement with Nakanishi and Fisher (1982). For critical wetting retaining only two terms suffices and minimizing (35) with respect to l leads to an equilibrium film thickness, for $a \to 0^-$,

$$l = \xi\, ln(2b/|a|). \qquad (36)$$

Close to T_w, $a \propto T - T_w$, leading to a logarithmic divergence of the film thickness. Thus within MF theory $\beta_s = 0(log)$, cf. (30).

In the experimentally relevant case $d = 3$, fluctuations must be included. For a long time there was no systematic analysis based on the full Landau-Ginzburg-Wilson (LGW) Hamiltonian, which is a functional akin to (27) but the fluctuating order parameter is the full three-dimensional $m(x, y, z)$ (Lipowsky and Fisher, 1987; Parry, 1996); instead, RG analyses (Brézin *et al.*, 1983a,b; Lipowsky *et al.*, 1983) started from the phenomenological "capillary wave" model (Dietrich, 1988; Schick, 1990)

$$F_s = \int d^{d-1}\mathbf{r}_{||} \left[\frac{\gamma}{2}(\nabla l)^2 + V(l)\right], \qquad (37)$$

using the effective potential (35). The critical behavior of (37) is controlled by the so-called *wetting parameter*

$$\omega \equiv k_BT_w/4\pi\gamma\xi^2, \qquad (38)$$

which depends on the wetting transition temperature. Near the bulk critical point both γ and ξ become singular, and ω approaches a finite universal value (Moldover, 1985) of $\omega_c \approx 0.8$ (Parry, 1996). The critical exponent $\nu_{||}$ depends explicitly on ω and hence on temperature, and is calculated according to (Fisher and Huse, 1985)

$$\nu_{||} = 1/(\sqrt{2} - \sqrt{\omega})^2, \qquad (39)$$

in the most relevant case of $1/2 < \omega < 2$. The layer thickness diverges logarithmically in this regime, so $\beta_s = 0(log)$ independently of ω. Furthermore, hyperscaling is found to hold. For $\omega = \omega_c$ this leads to the prediction $\alpha_s = -5.4$ for critical wetting close to T_c, implying a strong departure from the MF value $\alpha_s = 0$.

The results of the RG analysis have been confirmed by a number of groups (Dietrich, 1988), and are moreover supported by direct simulations of the capillary wave model (37) (Gompper and Kroll, 1988a,b). However, there appears to be strong disagreement both with Monte Carlo simulations of an Ising model (Binder and Landau, 1988; Binder *et al.*, 1986, 1989) and with the experiment (Ross *et al.*, 1999) using a two-fluid system. The results of simulation and experiment are consistent with MF predictions! The experiment, already discussed in II.C.1, provides a comparison of both 1st and 2nd order transitions by varying the chain length of alkanes (Trejo *et al.*, 1988): for methanol on nonane (C9) $T_w \approx 0.99\,T_c$ (2nd order), for methanol on undecane (C11) $T_w \approx 0.90\,T_c$ (1st order). Data for the contact angles are shown in Fig. 16. For undecane (C11), the best fit to the data yields $\alpha_s = 1.0 \pm 0.2$ compatible with a first-order wetting transition. For C9, the fit yields $\alpha_s = -0.6 \pm 0.6$, indicating a critical wetting transition, but consistent with $\alpha_s^{MF} = 0$, and very much inconsistent with $\alpha_s^{RG} = -5.4$.

The discrepancy between RG predictions on one hand, and the mean-field results of simulations and experiment on the other, has provoked much debate and has been discussed in detail in Dietrich (1988) or Parry (1996). In particular, the possibility that (37) does not adequately describe fluctuations near the wall and the interface contained in the full Hamiltonian, is analyzed in Fisher and Jin (1992); Parry (1996). Fisher and Jin derived a refinement of (37) in which the interfacial tension γ is replaced by a *position-dependent* stiffness $\Sigma(l)$ and discovered a stiffness instability mechanism through which the SRCW transition is driven *first order* for physical values

of $\omega \approx \omega_c$. Ten years of controversy followed since now the very existence of critical wetting was under threat.

Major relief was brought to the theoretical forum by the necessary development of a more general *non-local* interfacial Hamiltonian for short-range wetting in $d = 3$ by Parry and co-workers (Parry *et al.*, 2006, 2004), which has been discussed in the context of the history of wetting transitions by Henderson (2006). The new theory shows that when reducing the LGW functional to an interfacial Hamiltonian one must be careful to preserve the non-local character of the binding potential functional $W[l, \psi]$, which for a planar wall, $\psi(\mathbf{r}_{||}) = \text{const.}$, and a planar interface, $l(\mathbf{r}_{||}) = \text{const.}$, reduces to the interface potential $V(l)$ times the area. The binding potential functional is given by

$$W[l, \psi] = -a\Omega_1^1 + b_1\Omega_1^2 + b_2\Omega_2^1 + ..., \qquad (40)$$

where a, b_1 and b_2 are geometry-independent coefficients and the functionals $\Omega_m^n[l, \psi]$ are multiple integrals over bulk Ornstein-Zernike correlation functions connecting m points on the wall to n points in the interface. A diagrammatic expansion is obtained which provides a picture, for $d = 3$, in which the interaction is mediated by straight tube-like fluctuations connecting interface and wall, as found also in Ising model simulations, rather than by long-wavelength capillary wave fluctuations as in the wall-interface collision picture.

Interestingly, despite the fact that there is no explicit position-dependent stiffness in the non-local model, the Fisher-Jin mechanism is recovered perturbatively in the limit of a nearly planar interface (i.e., small $|\nabla l|$). However, the non-local theory allows to recognize the limits of validity of the stiffness instability mechanism, and it turns out that the SRCW transition is *not* driven first order, but rather is salvaged by non-perturbative effects arising in the RG flow equations.

Moreover, whilst the non-local theory confirms the asymptotic validity of all the results of the very simplest capillary-wave model, there are no significant deviations from mean-field like behavior for surface quantities, until the wetting layer is rather thick and the wall area is very large. This agrees with Monte Carlo simulations and is compatible with the reported experiments.

The experimental systems (Ross *et al.*, 1999) bring the added complication that long-ranged interactions are present, and thus SRCW should not be possible, at least not asymptotically (Ebner and Saam, 1987; Indekeu *et al.*, 1999a). Namely, if we naively suppose that the interactions are additive, the van der Waals forces add a term (21) to the effective interface potential, with $A > 0$ for van der Waals forces favoring wetting. Because of its slow algebraic decay, the tail of (21) dominates the interaction potential (35) for large l so that there is always a local minimum of the surface free energy at macroscopic layer thickness. For $T < T_w$, this minimum is separated from the minimum given by the Cahn theory by a maximum, and consequently any wetting transition is necessarily of first order.

Why nevertheless a SRCW transition is observed in a system with van der Waals interactions is not completely clear. Ross *et al.* (1999, 2001a) show that it is likely that the entropic repulsion due to the surface fluctuations (Bertrand *et al.*, 2001; Helfrich, 1973) dominates the van der Waals interactions for all layer thicknesses attained in the experiment; therefore the transition is effectively a SRCW transition within the experimental window. Although plausible, it is hard to demonstrate this firmly since the key problem is the estimation of the effective interactions due to the fluctuations.

D. Hot topics

Necessarily a small selection has to be made among various current "hot topics". Among those that we don't discuss here, such as wetting by liquid crystals and other complex fluids, surface melting, wetting in porous media, etc., there are two that we would have wished to cover and for which we provide at least some key references. The first is the theoretical and experimental study of the critical Casimir effect and its interplay with wetting (Balibar and Ishiguro, 2005; Fukuto *et al.*, 2005; Garcia and Chan, 1999, 2002; Hertlein *et al.*, 2008; Kardar and Golestanian, 1999; Krech, 1994; Krech and Dietrich, 1991; Rafaï *et al.*, 2007). This topic is so vast that it merits a review of its own. The second is the statistical mechanics of the three-phase contact line and its line tension, especially near wetting transitions, of which only some ingredients are reviewed here. The reader will find a profound conceptual discussion and an outstandingly complete bibliography in the recent work of Schimmele *et al.* (2007).

1. Wetting in colloid-polymer mixtures

The phase behavior of colloid-polymer mixtures is a rapidly developing field (see Brader *et al.* (2003); Poon (2002); Tuinier *et al.* (2003) for recent reviews), based on a simple idea: when (hard-sphere) colloids and (ideal) non-adsorbing polymers are brought together in a common solvent, the number of conformational degrees of freedom of the polymers will be hindered by the presence of the colloids: there is an entropy cost for adding colloids to a solution of polymers (Asakura and Oosawa, 1954, 1958; Joanny *et al.*, 1979; Vrij, 1976). This entropy cost competes with the entropy of mixing and, when dominant, leads to the remarkable effect of demixing into a phase rich in colloids and a phase rich in polymers (Lekkerkerker *et al.*, 1992). This demixing is (at least in theory) completely entropic in origin, and leads to a phase diagram with a critical point, analogous to what is found for usual gas/liquid systems.

The depletion of polymer between neighbouring colloidal particles induces an effective attraction between them when their separation is less than the polymer "di-

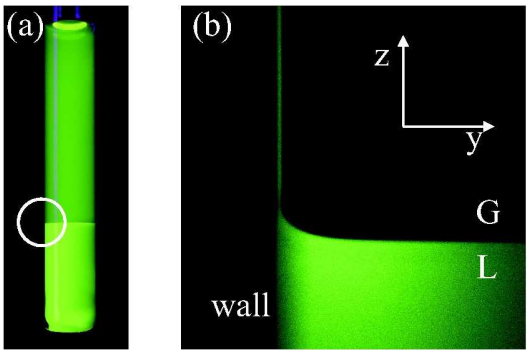

FIG. 21 (a) Photograph of a phase-separated mixture of fluorescently labeled PMMA colloids and polystyrene polymer in decalin taken under UV light. (b) A "blow-up" of the encircled region of (a) by means of Laser Scanning Confocal Microscopy (dimensions 350 μm by 350 μm). The interfacial profile is accurately described by the balance between the Laplace and hydrostatic pressure. However, the wetting layer is unexpectedly thick in this picture (Aarts, 2005; Aarts and Lekkerkerker, 2004)

ameter". This purely entropy-driven attraction is described by the so-called depletion potential which can be calculated employing DFT (Götzelmann *et al.*, 1998, 1999; Roth *et al.*, 2000) or virial expansion (Mao *et al.*, 1995). Depletion forces in bulk or in the vicinity of planar walls have also been investigated with simulations of molecular dynamics (Biben *et al.*, 1996), Monte Carlo (Dickman *et al.*, 1997) or "direct" type (Dijkstra *et al.*, 1999). Recently, the effect of polymer polydispersity on the range an the depth of the depletion potential between two plates was calculated (Yang *et al.*, 2007).

To a good approximation, the colloid-colloid forces we focus on here are short-ranged. Indeed, due to refractive index matching (for the relevant frequency range) and static dielectric constant matching of colloid and solvent, the dynamic (dispersion) and static contributions to the Van der Waals forces are practically absent (Israelachvili, 1992). Thus, all adsorbate-adsorbate and adsorbate-substrate interactions at the level of the colloidal particles are of finite range (of the order of the colloid radius augmented with the effective polymer radius). This circumstance renders the physical description in terms of the Ising model in $d = 3$ adequate for the system at hand.

In analogy with liquid/vapor systems, a (modified) Cahn argument should also apply for colloid/polymer mixtures and, upon approaching the critical point, a wetting transition should occur. Indeed, model calculations (Brader *et al.*, 2003; Dijkstra and van Roij, 2002; Wessels *et al.*, 2004) show that a layer of the heavier colloid-rich ("liquid") phase intrudes between the polymer-rich ("gas") phase and the wall at a certain distance from the critical point. Experimentally, Aarts *et al.* (2003); Wijting *et al.* (2003a,b) found the colloid phase to be favored by the wall. Contact angles and wetting behavior have been explored in Aarts (2005); Aarts and Lekkerkerker (2004), and (Hennequin *et al.*, 2008) using Confocal Microscopy to determine the interfacial profile. Fig. 21 shows such an interfacial profile including a wetting layer (Aarts and Lekkerkerker, 2004), which is visible against the wall since the colloids are fluorescent. Here, however, the wetting layer is surprisingly thick and it is unclear whether the system is fully equilibrated. Subsequent experiments, allowing a long time for equilibrium to be achieved (Hennequin *et al.*, 2008), have shown that indeed very thick films can form, typically 3 μm at 1 mm above the bulk phase. This is two orders of magnitude thicker than typical wetting films of simple liquids or in binary liquid systems, and suggests therefore that a different force stabilizes the wetting layer.

The entropic repulsion between a fluctuating interface and a wall can provide a supplementary repulsive force that can stabilize a wetting film, with a range of the order of the roughness $\xi_\perp$ of the fluctuating interface. Since the interfacial tension between the colloidal "liquid" and "gas" phases is ultralow, the rms roughness of the interface can become on the order of 1 μm, and is consequently similar to the wetting film thickness ℓ. However, the prediction $\xi_\perp \propto \ell$, valid in general in the thermal fluctuation regime(s) (Fisher and Huse, 1985), is modified in an interesting way in the pertinent case of short-range complete wetting in $d = 3$.

Identifying the interface displacement fluctuation about its average position ℓ with the roughness $\xi_\perp$, the equipartition theorem leads to the relation (Helfrich, 1973, 1978; Helfrich and Servuss, 1984)

$$\xi_\perp^2 = \frac{k_B T}{2\pi\gamma} \log(\frac{\xi_{||}}{R_c}), \qquad (41)$$

which depends on a microscopic cut-off scale R_c, the colloid radius, and a mesoscopic scale $\xi_{||}$. The parallel correlation length $\xi_{||}$ is now limited by the typical distance between wall-interface collisions. Clearly, the thermal reference length scale for our problem is $\sqrt{k_B T/\gamma}$.

On the other hand, renormalization group theory for short-range complete wetting transitions in $d = 3$ has predicted that $\xi_{||}$ and ℓ are related through (Fisher and Huse, 1985)

$$\ell/\xi \approx (2+\omega)\log(\xi_{||}/\xi), \text{ for } 0 < \omega < 2, \qquad (42)$$

where ξ is the bulk correlation length in the colloidal liquid phase and ω the wetting parameter, which takes a value of about 0.8 for the Ising model in $d = 3$, near bulk criticality.

Combining (41) and (42) we obtain

$$\xi_\perp^2 = \Big((\omega/\pi)^{1/2}/(2+\omega)\Big)\, \ell\sqrt{k_B T/\gamma}, \qquad (43)$$

hence RG theory predicts a peculiar dependence $\xi_\perp \propto \ell^{1/2}$. The exponent as well as the amplitude have been tested experimentally, as we outline below.

A first observation of a (quasi-linear) increase of interfacial width with film thickness was made in a phase-separated binary mixture of random copolymers (Kerle

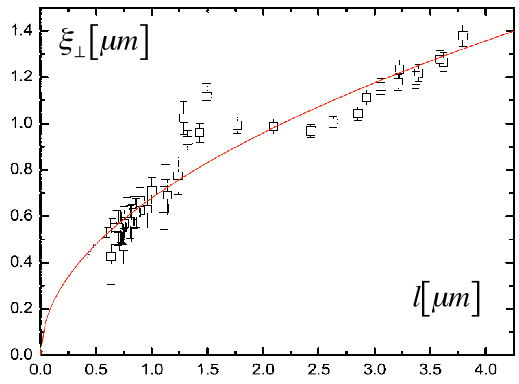

FIG. 22 Interface width as a function of the wetting layer thickness. The dashed line is $\xi_\perp^2 = 0.29\mu m\,\ell$, while $\xi_\perp^2 = 0.23\mu m\,\ell$ is the theoretical prediction obtained for wetting parameter $\omega = 0.8$ using the independently measured surface tension (Hennequin *et al.*, 2008)

et al., 1996). The data were compared with 3d Ising model simulations which showed a clear square-root dependence of w on ℓ (Kerle *et al.*, 1996). In the experimental system the possible presence of long-range (van der Waals) forces, for which a logarithmic dependence of w on ℓ is predicted, along with surface tension effects imposed by the confining surfaces, was invoked to explain the differences between the observations and the pure square-root dependence predicted for short-range forces (Kerle *et al.*, 1999). Monte Carlo simulations with van der Waals wall potentials confirm that the capillary-wave broadening of the interface is reduced, but a simple logarithmic dependence was not sufficient for describing the data quantitatively (Werner *et al.*, 1999).

Hennequin *et al.* (2008) have shown by a simultaneous measurement of the film thickness and the surface roughness that the interface excursions are indeed inhibited in a finite wetting film, and Fig. 24 demonstrates that their dependence is in good agreement with (43). This appears to be a unique case in which thermal fluctuation effects on wetting are observable in planar geometry in $d = 3$. This is perhaps not so surprising given that direct visual observation of thermal capillary waves on the free interface is possible in this system (Aarts *et al.*, 2004b).

Further, equilibrating the fluctuation repulsion resulting from the confinement of the interface fluctuations to the gravitational energy cost of having the wetting fluid at a certain height above its bulk phase then leads to a calculated wetting film thickness of 2 μm, at a height of 1 mm above the bulk phase, in fair agreement with the experimentally measured value of 3 μm. Residual differences are likely to be due to a still incomplete equilibration, or electrostatic effects due to charges on the colloids that have not been taken into account (Hennequin *et al.*, 2008).

These first observations of the wetting behavior in ultralow interfacial tension systems pose a number of challenging problems concerning the order of the possible wetting transition, the (fluctuation) interactions stabilizing the wetting layers, and consequently the critical exponents that are associated with the transition. In addition, in practice colloid-polymer systems are hardly ideal, and much of the current research is focusing on describing the non-ideality in order to account for their behavior; see (Fuchs and Schweizer, 2002; Likos, 2001; Poon, 2002; Tuinier *et al.*, 2003). This also affects the surface behavior, as shown in Aarts *et al.* (2004a). An interesting result is that the common Asakura-Oosawa approximation modeling the polymer coils as hard spheres turns out to fail completely for small colloidal particles (small enough for the polymer chains to be able to wrap around them), as was shown using field-theoretic methods by Hanke *et al.* (1999). Further, measurements and calculations have shown that wall-colloid depletion forces contain repulsive and attractive parts which are not purely entropic but governed by dispersion forces (Bechinger *et al.*, 1999).

As a precursor to the next two hot topics we draw attention to an accurate DFT study of depletion potentials between a hard-sphere colloid and a geometrically structured substrate in the form of a wedge or an edge (Bryk *et al.*, 2003b). This geometry leads to an enhanced attraction (wedge) or to a repulsion (edge) of the colloidal particle.

2. Wetting on structured surfaces

Surface structure can change wetting properties in an important way. If the surface structure is not too small (above 100 nm, say), macroscopic laws can still be applied locally and in the bulk, and surface and line contributions can be resolved as separate entities. If on the other hand structures are on the nanoscale, the fine details of the spatial variation of inter-molecular forces and the effects of thermal fluctuations such as interfacial capillary waves become important. For a review, see Dietrich *et al.* (2005). For example, three-phase contact lines can cross microchannel boundaries, but such events lose sharpness and thus meaning for nanochannels or nanostrips. We will first consider surfaces patterned on the micron scale.

One way of changing surface properties is microtexturing; see Quéré (2005) for a recent review. Studies undertaken so far have focused on two main ways to alter the surfaces: patterned surfaces, for which the wetting properties vary spatially in a controlled way, and structured surfaces, in which the geometry of the surface is controlled but its chemical structure is the same everywhere. For rough or patterned surfaces, minimization of the free energy leads to an equilibrium effective contact angle θ_W, that accounts for the extra area of the drop that is in contact with the solid (Borgs *et al.*, 1995; De Coninck *et al.*, 2002; Swain and Lipowsky, 1998; Wenzel, 1936):

$$\cos\theta_W = r\cos\theta_{eq}. \tag{44}$$

Here r is the ratio of the real to the projected area covered by the drop. Note that roughness ($r > 1$) reinforces the wetting properties of the smooth substrate, in agreement with experiments (Bico *et al.*, 2001; Shibuichi *et al.*, 1996). If $\theta_{eq} > \pi/2$, θ_W becomes even larger, in the opposite case it decreases. On the other hand, if only chemical heterogeneity is present such that the spreading coefficient varies locally, the contact angle is given by the average value of the spreading coefficient as given by the Cassie-Baxter equation (13).

The combined effects of roughness and heterogeneity can lead to superhydrophobicity: as shown in Fig. 23, a water droplet attains a contact angle of almost 180° (Bico *et al.*, 1999; Onda *et al.*, 1996; Quéré, 2005). Superhydrophobicity arises when air is trapped between protrusions that are present on the surface, the so-called "fakir"-effect in which the droplet reposes on the extremities of the protrusions. The droplet then feels an effective spreading coefficient of -2γ, corresponding to perfect drying, on the surface fraction $1 - f$ in between the posts. Application of (13) then gives

$$\cos\theta_{CB} = f\cos\theta_{eq} - 1 + f, \tag{45}$$

where θ_{eq} is the contact angle on the material of the posts. If f goes to zero, θ_{CB} can get close to 180°, as seen in Fig. 23.

Superhydrophobicity therefore demands very few, very hydrophobic protrusions. This can be achieved (Quéré, 2005) for instance by depositing particles (Nakajami *et al.*, 2000), by photolithography (Fig. 23), or by chemically growing carbon nanotubes onto the surfaces (Nakajami *et al.*, 2000). The latter two methods usually need to be followed by a chemical treatment enhancing the hydrophobicity of the protrusions; otherwise the liquid imbibes the space between them. A second condition for the stability of the "fakir" state is that the protrusions should be sufficiently dense and high so that the meniscus between two protrusions does not touch the surface on which they lie; for a detailed discussion of the stability, see Bartolo *et al.* (2006).

Superhydrophobic surfaces show remarkable properties: droplets of water bounce off them, and gently deposited droplets rest on the surface like pearls and role off. The water-repellent properties of these surfaces make them ideally suited for a large number of applications (Blossey, 2003), ranging from self-cleaning surfaces through water-repellent clothing and shoes to highly lubricated flows of water through superhydrophobic (micro-) channels (Cottin-Bizonne *et al.*, 2003).

The study of patterned - but not superhydrophobic - surfaces revealed the occurrence of "morphological (de-)wetting transitions". Depending on the pattern imprinted on the substrate, the wetting phase usually chooses to minimize its energy by taking different shapes: droplets, channels or films. The morphological transitions between those different states have been studied in detail (Brinkmann and Lipowsky, 2002; Gau *et al.*, 1999; Lenz and Lipowsky, 1998; Lipowsky, 2001; Seemann *et al.*, 2005a). From a theoretical point of view however, a theoretical description of these phenomena is difficult, due to the contact angle hysteresis that is inherent in the use of patterned substrates (Kusumaatmaja and Yeomans, 2007). Due to large energy barriers, it is not evident that the systems will actually be able to minimize their free energy (Ishino *et al.*, 2004).

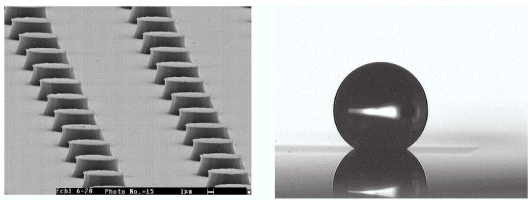

FIG. 23 Left: patterned surface. Right: water droplet posed on the patterned surface. Superhydrophobic behavior results from the fact that due to the patterning the droplet is mainly in contact with air (F. Bouamirene, unpublished).

The wetting morphologies display an important scale dependence when zooming in from the micro- to the nanoregime (Lipowsky *et al.*, 2000). Further, wetting phenomena in which the wetting phase is confined in a slab between two parallel chemically patterned planes involve bridges, channels and sequences of morphological transitions (Swain and Lipowsky, 2000). Soft matter (liquids, membranes, vesicles) undergoing shape transitions has been reviewed from a unified perspective by Lipowsky *et al.* (2005a,b).

Experimentally, non-contact mode atomic force microscopy (AFM) permits to image static liquid structures condensed from a vapor onto chemical nanopatterns, with a lateral resolution better than 10nm. With this technique Checco *et al.* (2006) studied wetting of ethanol and octane on a geometry composed of alternating wettable/non-wettable nanostripes. Morphological wetting transitions could thus be investigated at the nanoscale (for octane) by delicately adjusting temperature, through which the amount of condensed liquid can be controlled. Also more precise determinations of the three-phase contact line tension are possible with this approach. The understanding of the stability of such contact lines of sessile ridges and drops has recently been refined (Mechkov *et al.*, 2007).

As reviewed by Dietrich (1999), static wetting properties can to a great extent be captured using an effective interface potential derived from DFT. This applies to the vicinity of three-phase contact lines, to wetting on curved surfaces (for which spheres or cylinders are the paradigms), on chemical steps, and in wedge-shaped geometry. The so-called nonlocal theory, featuring a nonlocal integral equation for the interface profile, was compared with the (usual) local approximation, obtained after a gradient expansion. Although at first the differences between the interface profiles computed from local and nonlocal theories were reported to be important (Getta and Dietrich, 1998; Koch *et al.*, 1995), improved compu-

tations showed that the deviations had been greatly overestimated (Bauer and Dietrich, 1999a; Dietrich, 1999). Consequently, the widely used *local* interface displacement model is not only qualitatively trustworthy but, provided the profile curvature is sufficiently small, is also quantitatively reliable for predicting transition zone structure, line tension and morphological phase transitions (Bauer and Dietrich, 1999b, 2000; Bauer *et al.*, 1999).

A thorough review of wetting on curved surfaces was provided by Bieker and Dietrich (1998). Phenomenological models supplemented with a fully microscopic treatment, based on DFT with all forces properly taken long-ranged, were shown to be appropriate tools for describing many experimentally relevant systems. Remarkably, the essential step in our understanding of wetting in complex geometries with curved surfaces consists of scrutinizing the wetting behavior on (or in) single spheres or cylinders. The often subtle curvature dependences of surface tensions have continued to attract interest. Combining analytical expressions, exact statistical mechanical sum rules and DFT has proven powerful to obtain coherent results. Two illustrations of this are hard-sphere fluids at hard-spherical and cylindrical walls (Bryk *et al.*, 2003a), and van der Waals fluids confined in a hard-spherical cavity (Stewart and Evans, 2005). The complication of orientational ordering near geometrically structured substrates has been investigated using DFT for colloidal hard rods (Harnau *et al.*, 2004). Sprenger *et al.* (2005) addressed the different complication of being near bulk criticality, by studying critical adsorption of binary liquid mixtures at chemical steps or stripes.

Studies of complete wetting of geometrically structured substrates, based on an effective interface Hamiltonian derived from microscopic DFT, have revealed that as long as one is not too close to saturation, the filling of a cavity does not depend on whether it stands alone or is part of an array (Tasinkevych and Dietrich, 2006, 2007). For small undersaturation, however, the wetting layer thickness is determined by the array as a whole. Experimental x-ray scattering studies of the filling by simple hydrocarbon liquids of an array of nanocavities patterned on silicon (Gang *et al.*, 2005) suggest that finite-size effects significantly shift the measured adsorption exponent from the value that it would have for infinitely deep cavities towards the value for a planar substrate. However, a reanalysis of the data by Tasinkevych and Dietrich (2006, 2007) indicates that the results are actually closer to the deep-cavity predictions. Thus, to understand the (early) filling regime of a substrate with pits and grooves, adsorption in individual wedges and cones has to be considered first. As the next subsection will attempt to convey, this also sheds new light on the fundamental problem of fluctuation effects on wetting transitions.

3. Wedge filling transitions

If a solid wedge is subjected to adsorption from a gas, a liquid phase may form abruptly by capillary condensation provided the wedge opening angle is small. For large wedge angles, a continuous increase of the wetting film is expected when the pressure is increased, as is generally observed for planar substrates in the complete wetting regime. The basic question of the competition between continuous filling and capillary condensation has been addressed very successfully by considering a substrate wedge geometry which interpolates between a planar substrate and a capillary slit (Rascón and Parry, 2000b). In this model the substrate height varies as a power law $|x|^\gamma$, where x runs perpendicular to the wedge. For $\gamma = 1$ the familiar linear wedge is obtained, for which a fairly large body of surprising preliminary results were obtained prior to 2000 by Cheng and Cole (1990); Napiórkowski *et al.* (1992); Pomeau (1986) and especially Hauge (1992). Hauge observed that the wetting transition in a wedge is shifted downwards in temperature to the point where the contact angle equals the tilt angle. He then discussed the continuous (or first-order) character of the transition away from bulk two-phase coexistence (or at coexistence) using macroscopic arguments. Since this work, wedge wetting has become interesting, not only as a tool to study wetting on structured surfaces, but also as a problem in itself. Before going into individual results, we stress the correspondence between interface statistical mechanics and geometry that governs wedge filling, as elucidated by Henderson (2004a,b). This has provided a set of exact sum rules linking fluid structure and surface free energy, of direct relevance to computer simulations and significant to the filling transitions discussed here.

If we focus for a moment on realistic systems with van der Waals forces, Rascón and Parry (2000a,b) established that the approach to complete wetting in a wedge is characterized by novel critical exponents which are geometry-dependent for $\gamma > 1/2$, while for $\gamma < 1/2$ wedge filling is controlled by the singularities pertaining to complete wetting on a planar substrate. Interestingly, in the geometry-dominated regime, which includes the usual linear wedge, the critical exponents are universal with respect to the exponent associated with the range of the intermolecular forces. Several of these predictions have been verified experimentally. Bruschi *et al.* (2001, 2002, 2003a) measured the adsorption of mainly liquid Ar (but also Kr) on an array of linear wedges and observed the theoretically predicted cross-over in the critical exponent of the excess adsorbed mass from planar to geometry-dominated behavior. In addition, it was checked that geometrical disorder in the wedge array spoils the clear cross-over and leads to an effective exponent closer to but still quite different from that of planar rough (including self-affine) geometry (Bruschi *et al.*, 2003b).

This work was extended to Ar adsorption measurements on arrays of nonlinear cusps and of semicircular channels, corresponding to $\gamma \approx 1/2$ and $\gamma \approx 3.3$, respec-

tively (Bruschi *et al.*, 2006). For the nonlinear cusps the observed cross-over is distinctly different from that in a linear wedge and the exponent agrees with the prediction of Parry *et al.* For the convex channels a very steep increase in the excess mass is observed close to saturation, qualitatively consistent with the predicted coalescence of two menisci on both sides of the channel into one meniscus, predicted for $\gamma > 2$ (Rascón and Parry, 2000b).

We now move from the complete wetting regime to the transition from partial to complete wetting itself, first considered quantitatively by Rejmer *et al.* (1999) for the linear wedge. Using an effective interface model, these authors mapped out a phase diagram of continuous and discontinuous filling transitions, together with their "prefilling" extensions off coexistence. This approach constituted a compromise between a prohibitively difficult full microscopic treatment and the earlier macroscopic theory, which only yields qualitative result. It permits to discuss mean-field results, and how these can be affected by fluctuation effects important in reduced dimensionality. In addition, the thermodynamic behavior of the line tension and the shape of the meniscus were accessible through this method.

A refinement of (Rejmer *et al.*, 1999) was proposed by Parry *et al.* (2000), who found that *continuous* filling transitions at $T = T_F$ are possible in linear wedges not only when the planar substrate displays critical wetting, but also when it shows a *first-order* wetting transition, at $T = T_w > T_F$. This significantly increases the experimental opportunities for observing critical filling. Moreover, interfacial fluctuation effects at critical filling (in $d = 3$) are predicted to be surprisingly strong and remarkably universal (Parry *et al.*, 2000). They give rise to more dramatic effects than the subtle short-range critical wetting (SRCW) singularities discussed in Section II.C. For example, $\beta_s = 0(log)$ can shift to $\beta_s = 1/4$ for forces of sufficiently short range. Moreover, in a linear wedge in $d = 3$ the interface displacement fluctuation is predicted to obey the universal power-law divergence $\xi_\perp \propto (T_F - T)^{-1/4}$, independently of the range of the intermolecular forces.

Another breakthrough was achieved when it was realized that the singularities associated with critical filling transitions can mimic those belonging to the strong fluctuation regime of planar critical wetting (Parry *et al.*, 2001b). For instance, in the case of a *cone geometry* in $d = 3$, the filling height and interface roughness show the same singularities as those of SRCW in $d = 3$ and for large wetting parameter $\omega > 2$. A similar correspondence was proposed (Parry *et al.*, 2001b) and supported by transfer matrix calculations (Parry *et al.*, 2001a) in $d = 2$. This correspondence, in $d = 2$, leading to universal critical exponents and scaling functions that depend only on the interface roughness (or "wandering") exponent ζ, was found to emanate from a deeper symmetry, called *wedge covariance* (Parry *et al.*, 2002). For example, the following covariance relation was found between the $d = 2$ excess wedge (or "corner") free energy f_w and the strong-fluctuation regime critical wetting $d = 2$ line (or "point") tension τ,

$$f_w(\theta, \alpha) = \tau(\theta) - \tau(\theta - \alpha), \tag{46}$$

with θ the thermodynamic contact angle and α the geometrical tilt angle. Such $d = 2$ covariance relations are valid near filling ($\theta \to \alpha$) and hold not only for shallow but also for acute wedges and for orientation-dependent interfacial tension (Abraham *et al.*, 2002a).

A partial answer to the possible extension of wedge covariance to $d = 3$ was provided by Greenall *et al.* (2004) who showed that the $d = 2$ covariance relations have analogues at mean-field level that apply to higher-dimensional systems. Further, two types of continuous wedge filling transitions in $d = 3$ were identified, critical and tricritical (Romero-Enrique and Parry, 2005).

While covariance of wedge filling and fluctuation-dominated planar critical wetting in $d = 3$ is restricted to the mean-field regime, a new general covariance for complete filling in *wedge and cone* geometries was demonstrated in Rascón and Parry (2005) at the level of the interfacial heights at the geometrical midpoints. Interestingly, this symmetry identifies both leading and subleading critical exponents and amplitudes, which are accessible experimentally.

Another step in uncovering hidden symmetries was the finding that complete wetting at an apex (inverted wedge) mimics precisely planar critical wetting, the apex angle playing the role of the contact angle (Parry *et al.*, 2003). This naturally adds geometrical ways of studying critical wetting singularities experimentally. In fact, Ar adsorption was already investigated on arrays of wedges *and* apexes (Bruschi *et al.*, 2001).

The verification of wedge filling theories involves not only experiments, but also exactly solved models and high-precision computer simulations. Exact solutions in the $d = 2$ Ising model with a corner have established the existence and location of the filling transition, both on the square (Abraham and Maciolek, 2002) and on the triangular lattice (Abraham *et al.*, 2003). Monte Carlo simulations (MCS) of corner wetting in the $d = 2$ Ising model (Albano *et al.*, 2003) strongly support the detailed theoretical predictions. For $d = 3$ extensive MCS were carried out in the wedge geometry by Milchev *et al.* (2003a,b), to test the predictions of Parry *et al.* and to clarify finite-size effects on wedge filling in a double-wedge pore geometry, with opposing surface fields on opposite wedges. Unlike the situation for SRCW in $d = 3$ on planar substrates, for which simulations could not detect the rather subtle effects of thermal fluctuations, the simulations for the wedge geometry now confirm the critical exponent values predicted for short-range forces. Moreover, the MCS reveal that critical wedge filling underlies a new universality class of transitions in a double wedge, characterized by strong fluctuations and anisotropic scaling, and with bulk critical exponents $\alpha = 3/4$, $\beta = 0$ (order parameter discontinuity), and $\gamma = 5/4$ (Milchev *et al.*, 2003a). This unusual critical

behavior is related to the strong fluctuation effects of filling of a single wedge. These findings are compared, by Müller and Binder (2005), with the phase behavior of thin films bounded by parallel planar walls with opposing surface fields, which is controlled by planar wetting phenomena. In sum, the wedge geometry turns out to be a more promising arena for observing the strong fluctuation regime of critical wetting than the standard planar one.

4. Incomplete wetting by crystalline phases

Generically, a solid film wets a solid substrate only incompletely due to elastic effects. The lattice parameter in the wetting film usually suffers from a mismatch with that of the substrate. In the first few adsorbed layers various defects may alleviate most of the induced stresses, but after that the lattice parameter of the film relaxes slowly towards the lattice parameter of the wetting phase in bulk. The elastic free energy cost of this weakly strained film contributes a negative (attractive) term to the interface potential $V(l)$ which decays as slowly as $1/l$. Thus a long range force comes into play which inhibits complete wetting. Huse (1984) and Gittes and Schick (1984) pioneered the theoretical understanding of this effect and offered a qualitative explanation of various experimental results.

More recently, it has been realized that in many systems of experimental relevance, *surface roughness* is yet another and much more important factor in preventing complete wetting by crystalline layers (Esztermann and Löwen, 2005; Sohaili *et al.*, 2005). Even for a weak surface modulation with a wavelength large compared to interatomic distances, the adsorbed film thickness is strongly reduced as compared to the already limited thickness predicted by the Huse-Gittes-Schick theory. Surface roughness contributes a term proportional to l^3 to $V(l)$, which is even stronger than the effect of driving the wetting phase unstable in bulk, i.e., away from bulk two-phase coexistence, which would be achieved by a contribution linear in l. The theory, including surface roughness, was able to describe quantitatively the adsorption data for H_2 on Au (Esztermann *et al.*, 2002).

It would seem that purely strain-induced incomplete wetting cannot be observed in real systems, because perfectly flat substrates exist only in theory. However, experiments on a binary alloy (CuAu) close to a bulk order-disorder transition have revealed incomplete wetting by the ordered phase, which in this case consists of a layered Cu/Au structure (Schweika *et al.*, 2004). In this case the substrate is a gas phase and the surface of the solid is microscopically smooth and clean for the bulk disordered phase, and rough for the bulk ordered phase. Assuming that the surface remains flat when the wetting film of the ordered phase develops, the observed incomplete wetting must be due to strain effects alone.

Elastic effects are not the only considerations when discussing factors that influence wetting or non-wetting of solids by solids. The question of *critical-point wetting for solids* has been addressed from various angles in a paper by Cahn (2000). One intriguing conclusion of this work is that interfaces between macroscopic phases with lattices that are not fully coherent, must show a non-zero contact angle with the sample surface.

5. Electrowetting

The spreading of a drop is determined by the equilibrium contact angle, which is set by intermolecular forces. However, the drop can be made to spread by the application of an electric field (Lippmann, 1875). Some of the applications of this effect, called electrowetting, in microfluidics or optics are discussed by Quilliet and Berge (2001) and by Mugele *et al.* (2005). A review, including many applications, is offered in Mugele and Baret (2005).

Typically, one considers a conducting liquid on an insulating substrate of thickness d, having a dielectric constant ϵ_r. A potential difference U_{el} is applied between the liquid and a conducting layer below the dielectric, so the system forms a capacitor whose electric energy is proportional to the surface covered by the drop. If one approximates the electric energy by that of a parallel capacitor, the total energy becomes

$$E = \gamma S_{drop} - \pi R^2 \left(\gamma \cos\theta_{eq} + \frac{\epsilon_0 \epsilon_r U_{el}^2}{2\gamma d} \right), \qquad (47)$$

where S_{drop} is the surface area of the drop. For finite U_{el}, it thus becomes advantages for R to increase, i.e. the drop spreads. It is popular to write the term in brackets as (Quilliet and Berge, 2001)

$$\cos\theta_{el} = \cos\theta_{eq} + \epsilon_0 \epsilon_r U_{el}^2/(2\gamma d), \qquad (48)$$

in which case the energy (47) formally looks like that of a drop with an *effective* contact angle θ_{el}. However, on a sufficiently small scale the contact angle remains θ_e, which follows from considering the diverging surface charge σ at the edge of the drop, which is that of a conducting wedge (Jackson, 1975). From the surface force balance $\gamma\kappa - \sigma^2/(2\epsilon_0) = -p_0$ it follows that the curvature κ only has an integrable singularity at the edge, the boundary condition for the slope thus remains unchanged (Fontelos and Kindelán, 2008; Mugele and Buehrle, 2007).

If however the insulator thickness d is very small, the electric field away from the edges becomes uniform, and electric forces are small. The surface shape thus becomes a spherical cap, with an apparent angle θ_{el} (48) measured on a scale larger than d (Bienia *et al.*, 2006). Typical measurements of (θ_{el}) are shown in Fig. 24, and compare well with experimental data up to a critical voltage. Note that most experiments are performed with AC voltage, to avoid charge accumulation at the solid-liquid interface. Furthermore, ion adsorption gives rise to a small

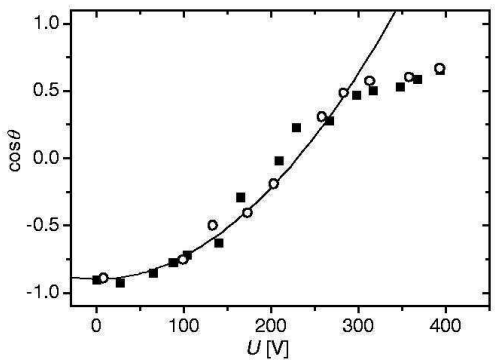

FIG. 24 The apparent contact angle as function of the root mean squared amplitude of the applied voltage (AC field) for a drop of oil, taken from (Mugele and Baret, 2005). The filled squares are for increasing field (advancing contact line), the open circles for decreasing field (receding contact line). The solid line is the theoretical curve (48).

shift of the maximum contact angle away from zero applied voltage, to the potential of zero charge (Seyrat and Hayes, 2001). The saturation of the angle is not understood (Mugele and Baret, 2005; Quilliet and Berge, 2001). An explanation that has as yet not been pursued is the possibility that the approximation of a spherical cap away from the contact line is no longer a good approximation (Fontelos and Kindelán, 2008), and nonaxisymmetric shapes are energetically favorable with respect to axisymmetric shapes.

High electric fields are also accompanied by an instability of the contact line (Mugele *et al.*, 2005; Quilliet and Berge, 2001), which lead to the expulsion of small droplets. A qualitative explanation consists in the observation that the charge density becomes very large near the contact line (Mugele *et al.*, 2005). Thus in analogy with the instability of small charged drops (Duft *et al.*, 2003), Coulomb repulsion may become too strong to be overcome by surface tension forces.

In closing, we draw attention to a combination of wetting of structured substrates and high electric fields. Arscott *et al.* (2006) studied theoretically and experimentally the spontaneous filling of a microfluidic capillary slot for the purpose of designing more controlled miniaturization of electrospray ionization sources, to be used in mass spectroscopy of large biomolecules.

III. DYNAMICS

We organize the description of contact line dynamics according to the microscopic, intermediate, and outer regions introduced above, beginning with advancing contact lines. In III.A we describe the intermediate region, characterized by a balance of viscous and surface tension forces. Using drop spreading as an example, in III.B we then show how it can be matched to an outer region, where other forces come into play. In the light of this hydrodynamic description, we review the experimental situation in III.C, treating perfectly and partially wetting fluids separately. In the former case, the macroscopic drop is usually preceded by a mesoscopic precursor film, which greatly simplifies the hydrodynamic description. To describe the effect of the contact line itself, we use two different approaches: in III.D, the effect of the contact line is captured through the dissipation it generates. Alternatively, one can attempt to match to the contact line by including some microscopic parameters, as described in III.E. Finally, in III.F we describe findings based on a truly microscopic description using molecular dynamics.

In III.G we show that the maximum speed at which a *receding* contact lines can move is limited by a hydrodynamic mechanism. Receding fronts also come into play for the dewetting dynamics of a liquid film, see III.H. In III.I and III.J.1 the contact line is no longer considered straight, subject to linear and nonlinear instabilities. The remaining hot topics are complex fluids and evaporation. Useful reviews of the hydrodynamics of moving contact lines are to be found in Ramé (2002) and Voinov (2002).

A. Contact line region

Most of the analytical descriptions to be reported below relies on a number of simplifying assumptions:

(i) The capillary number is small, $Ca \lesssim 0.1$.

(ii) Inertial effects can be neglected, meaning that the viscous length scale $\ell_\nu = \eta^2/(\rho\gamma)$ is larger than other length scales relevant for the contact line motion.

(iii) The surfaces are perfect (no heterogeneity), so there is no contact angle hysteresis.

Not much is known if (i) or (ii) are violated; departures from (iii) will be the subject of the next section. We proceed by first solving the coupled interface-viscous flow problem at distances from the contact line where microscopic effects are negligible. This solution then has to be matched to the small-scale behavior near the contact line. Almost all our analysis is going to be concerned with the two-dimensional flow problem where the contact line moves perpendicular to itself. This carries over to situations where the contact line is not too strongly curved (Rio *et al.*, 2005; Snoeijer *et al.*, 2005), such that the curvature perpendicular to the contact line always remains much larger.

The calculation becomes much more transparent if we limit ourselves to the so-called lubrication approximation, characterized by the assumption that the flow profile is nearly parabolic, see Fig. 25. The parabolic approximation is valid in the presence of only a *single* fluid, for small contact angles, and assuming that the forces driving the flow do not change too quickly. Near the contact line, the dominant driving force is capillarity, and the rate of change of curvature is proportional to

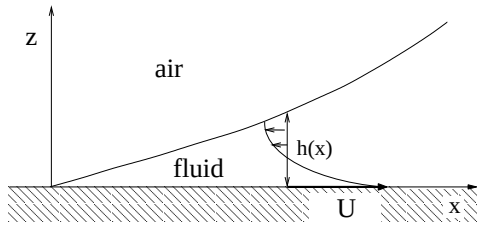

FIG. 25 Parabolic flow in a wedge near an advancing contact angle. The substrate moves with speed U to the right.

the capillary number (7). Thus in a systematic expansion in $Ca^{1/3}$ (Benney, 1966; Oron *et al.*, 1997; Snoeijer, 2006), and moving with the speed U of the contact line, such that the profile is stationary, one obtains to leading order

$$\frac{3Ca}{h^2} = -h'''. \tag{49}$$

This equation represents a balance of viscous (left) and capillary forces (right), where a prime denotes differentiation with respect to x. The crucial simplification of (49) lies in the fact that the velocity field has been eliminated, and everything is expressed through the interface shape $h(x)$ alone. Note that as expected, viscous forces *diverge* as the contact line is approached ($h \to 0$), so body forces such as gravity (which adds a constant to (49)), or any imposed shear will not affect the solution near the contact line. Equation (49) is scale invariant, solutions being of the form

$$h(x) = LH(x/L), \tag{50}$$

where L is as yet unspecified. A characteristic length L must be set by microscopic effects like slip, long-ranged forces, or a diffuse interface. We adopt the sign convention that Ca is positive if the contact line is *advancing*, which is the case we are now focusing on. Changing the sign in (49) (receding contact line) has important consequences, which will be elaborated later.

Two of the boundary conditions necessary to find a solution of (49) come from specifying the values of h and of the slope h' near the contact line. The missing third condition can be derived from the requirement that the local solution must match onto the macroscopic behavior of the solution away from the contact line. This "outer" solution $h_{out}(x)$ will depend on the precise geometry of the problem and the forcing the liquid is subjected to. However, if the typical scale of the outer solution and the microscopic scale L are well separated, the "intermediate" solution, which connects the contact line with the outer solution, becomes universal: Namely, for the solution (50) to be compatible with the outer solution, the curvatures of the two solutions must agree some small distance Δx away from the contact line: $h''_{out}(\Delta x) = H''(\Delta x/L)/L$. But in the limit of very small L this means that $H''(\infty) = 0$, which, together with the boundary conditions at the contact line, uniquely fixes a solution.

The behavior of the solution characterized by a vanishing slope at infinity was given by Voinov (1976). For sufficiently large arguments x/L, relevant to the matching to the macroscopic problem, this asymptotic solution of (49) is

$$h'^3(x) = \theta_m^3 + 9Ca\ln(x/L). \tag{51}$$

Equation (51), or some variation of it, is usually referred to as the "Cox-Voinov law". As discussed in section I.C.2, the microscopic properties of the contact line are represented by a "microscopic" contact angle θ_m, and the corresponding length scale L. Both parameters need to be determined by matching to an appropriate microscopic model of the contact line, to which we return below. Three points should be noted:

(a) The slope varies logarithmically with the distance from the contact line. Thus it is impossible to assign a unique "dynamical contact angle", to a moving contact line moving at a given speed.

(b) The local profile (51) depends only very weakly on the microscopic parameter L. It is much more important to find estimates for the microscopic angle θ_m.

(c) The speed dependence in the Cox-Voinov law follows from the fact that Ca can be eliminated from (49) by the transformation $h \to Ca^{1/3}h$. It is thus not a perturbative result for small Ca.

The equivalent of (51), but without resorting to the assumption of small slopes, was also given by Voinov (1976). The same result is found from a generalized form of the lubrication equation (49), valid for arbitrary slopes (Snoeijer, 2006). A further extension to two fluids with viscosity ratio $M = \eta_{out}/\eta$ was derived by Cox (1986), which reads

$$g(\theta(x), M) - g(\theta_m, M) = Ca\ln(x/L), \tag{52}$$

where $\tan(\theta(x)) = h'(x)$. In the absence of an outer, dynamically active fluid, $g(\theta, 0)$ reduces to $g(\theta)$, defined by

$$g(\theta) = \int_0^\theta \frac{x - \sin x\cos x}{2\sin x}dx, \tag{53}$$

which cannot be integrated in elementary terms. The advantage of (52),(53) is its validity for arbitrary slopes. However, the difference between g and $\theta^3/9$ remains smaller than 1% if $\theta < 3\pi/4$, or 135°, so (51) is a very good approximation even for moderately large angles.

Having found the interface profile (51) for intermediate scales, we now have to understand its relation to the microscopic physics at the contact line on one hand, and to the macroscopic hydrodynamics away from the contact line on the other hand. We first turn to the latter, and show how (51) serves as the effective boundary condition for the macroscopic hydrodynamic problem. Since

the slope is varying with the distance from the contact line, this is not a straightforward boundary condition that could be applied at a point. This feature mirrors, of course, the difficulty of measuring a dynamic contact angle by simply recording the slope near the contact line.

B. Matching to a macroscopic flow

To explain the hydrodynamic treatment of a moving contact line, we describe how (51) is matched to the surface of a small spreading drop, a problem already considered qualitatively in section I.C on the basis of energy conservation. This hydrodynamic calculation permits one to compute the constant B in Tanner's law (10) in terms of microscopic parameters of the contact line. Effectively, we have to compute how the apparent contact angle $\theta_{ap} = \theta_{ap}(\dot{R}, L, \theta_m)$ depends on the contact line speed $\dot{R}$, so using (9) one obtains an equation of motion for the drop radius.

Many researchers (de Gennes, 1985) simply identify θ_{ap} with the slope (51) near the contact line, but evaluated at a length scale characterizing the outer problem, such as the drop radius R. This is obviously only approximate, since the logarithmic dependence of (51) is incompatible with the outer solution (8). However, we now show that the correct matching equation is

$$\theta_{ap}^3 = \theta_m^3 + 9\dot{R}\eta/\gamma \ln(Rc/L), \tag{54}$$

which is almost the result of the naive "patching" procedure, but with a constant c which depends on the outer solution.

To set up the problem, we begin with the *dynamical* lubrication equation for a film $h(\mathbf{x}, t)$ moving over a two-dimensional substrate (Oron *et al.*, 1997):

$$3\eta \frac{\partial h}{\partial t} = \nabla \cdot [m(h) \nabla p], \tag{55}$$

where

$$m(h) = h^3 + 3\lambda h^2 \tag{56}$$

is called the *mobility* and λ is the Navier slip length (Lauga *et al.*, 2008; Navier, 1827). If long-ranged forces as well as gravity are neglected for the moment, the pressure in the film is

$$p = -\gamma \triangle h. \tag{57}$$

For $\lambda = 0$ and in the frame of reference of the contact line, one spatial integration yields the stationary equation (49). Progress on rigorous mathematical existence theorems for (55) is summarized in Becker and Grün (2005); Grün (2004). Curiously, it remains an open problem to show rigorously that the contact line cannot move if $m(h)$ vanishes like h^3 at the contact line position, while this is obvious from the Huh-Scriven argument (Huh and Scriven, 1971).

To perform the matching between (51) and the static (outer) drop shape (8), speed dependent terms have to be added to the outer solution to make it match to the logarithmic dependence (51). To this end one solves (55) for a radially symmetric profile with no-slip boundary conditions $\lambda = 0$, since any microscopic scale is effectively zero on the scale of the outer solution. In accordance with (12), the solution of (55) will have a logarithmic singularity corresponding to (51) as one approaches the contact line. The spherical cap (8) is the solution in the limit of zero speed, to which a contribution at the linear order in Ca has to be added:

$$h_{out}(r, t) = h_0(x) + Ca h_1(x) + O(Ca^2), \tag{58}$$

where $x = R - r$. The curvature of h_0 is negative, while $h_1''(x)$ is positive; the point x where both curvatures become comparable leads to the estimate $3CaR/\theta_{ap}$ for the size of the intermediate region, quoted in Fig. 8. The transformation to x absorbs the leading-order time dependence, which comes from R, so solutions remain locally quasi-steady. To compare (58) to the local solution (51), the slope h'_{out} has to be raised to the third power. Namely, from (51) we then know that $-(h'_{out}(r))^3 \approx (h_0'(x))^3 + 3Ca(h_0'(x))^2 h_1'(x)$ has the logarithmic singularity $9Ca \ln(x)$ as $x \to 0$. Note that by comparing the third power of the slope, the logarithmic coefficient contains a known universal constant, making a consistent matching possible. Comparing the prefactors and using $\theta_{ap} = h_0'(0)$ and (54), one arrives directly at

$$\ln(Rc) = -\lim_{x \to 0} \left[h_0'^2(0) h_1'(x)/3 \right] + \ln(x). \tag{59}$$

Inserting the expansion (58) into (55), one finds after one integration

$$-\frac{3}{h_0^3(R-x)} \int_0^x h_0'(s)(R-s) ds = (h_1'' + h_1'/r)', \tag{60}$$

subject to the boundary conditions

$$h_1'(R) = 0, \quad h_1(0) = 0, \quad \int_0^R (R-x) h_1(x) dx = 0. \tag{61}$$

The boundary conditions come from the requirement that the drop is symmetric around $r = 0$, and that h vanishes at the contact line $r = R$. The final condition fixes the volume at V. Having found h_1 from (60) and (61), it is straightforward to find $c = 1/(2e^2)$ from (59), where $e = 2.718281\ldots$. For bigger drops, gravity must also be taken into account, and h_0 becomes more complicated. As a result, some integrals have to be calculated numerically (Hocking, 1983).

In the case of a perfectly wetting fluid, $\theta_m = 0$ and the drop will continue to spread forever. Thus (54) becomes, using equation (9) for the apparent contact angle,

$$\left(\frac{4V}{\pi R^3} \right)^3 = 9(\eta/\gamma) \dot{R} \ln(R/(2e^2 L)), \tag{62}$$

which must be integrated to deduce the time dependence of R. If logarithmic dependencies are ignored and the logarithm is approximated by a constant, one finds that $R^9\dot{R} \propto C$, and hence $R \propto t^{1/10}$, in agreement with (10). Essentially the same result, using a different set of approximations, was obtained in Voinov (1976, 2000b). Note that L is the only specific feature of the contact line which appears in (62), entering only logarithmically. This explains the remarkable robustness of Tanner's law. Below we will calculate L explicitly for the case of a precursor film.

Similar calculations have been done (Hocking, 1992, 1994; Voinov, 1976, 2000b) for spreading drops, two-dimensional drops (Hocking, 1981; Lacey, 1982), and capillary tubes (Hocking, 1977; Kafka and Dussan, 1979; Voinov, 1976, 1995, 2000a). Indeed, many dynamic contact angle measurements (Fermigier and Jenffer, 1991b; Hoffman, 1975) have been performed by pushing fluid through a capillary tube of radius R_c, and measuring the radius of curvature R of the resulting meniscus. The apparent contact angle is then given geometrically as $\cos(\theta_{ap}) = R_c/R$. By matching the static meniscus to (51), one obtains (Voinov, 1976, 2000a), in complete analogy to the above calculation,

$$\theta_{ap}^3 = \theta_m^3 + Ca \ln(0.16R/(\theta_{ap}L)). \tag{63}$$

In Cox (1986) the same matching as that described above is studied without reference to a specific geometry, to give the general structure of the expression for the apparent contact angle. Some of the earlier calculations (Dussan V., 1979; Hocking, 1977; Kafka and Dussan, 1979) did not recognize the need for an intermediate region (51), and obtained results valid only for small interface deformations: $\theta_m \approx \theta_{ap}$. In Voinov (2000a,b), various "inverse relations" are given, which permit one to calculate the microscopic parameters from the apparent contact angle, defined unequivocally by the macroscopic interface shape.

The results and ideas underlying the intermediate region (52),(53) as well as its matching to the outer problem have been carefully tested in a series of experimental papers (Chen *et al.*, 1995, 1997, 2004; Marsh *et al.*, 1993), dipping a solid cylinder into a fluid at various angles of inclination α. A solution combining (52),(53) and the outer meniscus was fitted to experiment treating either L or the apparent contact angle as a free parameter. As shown in Fig. 26, agreement with theoretical interface profiles is excellent for different angles α and small capillary number. The same is true for the entire flow profile (Chen *et al.*, 1997). Small Ca asymptotics however starts to fail for $Ca \gtrsim 0.1$ (Chen *et al.*, 1995). In Chen *et al.* (2004) the emergence of the intermediate region (52) is tracked as the ratio between inner (contact line) scales and the outer scale becomes more disparate. This is achieved by preparing the substrate with liquid films of different thicknesses, which effectively provide the inner length scale L.

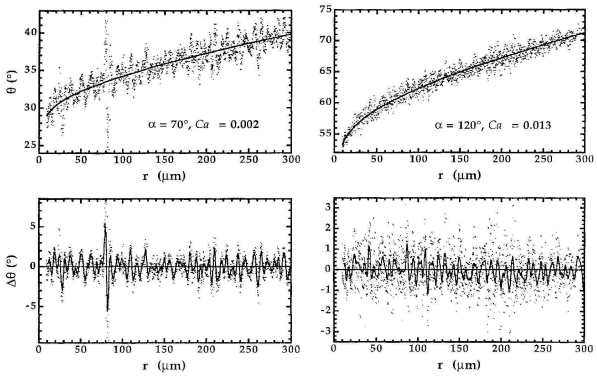

FIG. 26 The dependence of the interface slope on the distance from the contact line (Marsh *et al.*, 1993). The solid curve is based on (52),(53) with L treated as an adjustable parameter (Dussan V. *et al.*, 1991). Also plotted in the lower two frames are deviations $\Delta\theta$ from theory, the solid curve showing a running average over $5\mu m$.

1. Numerical simulations

The asymptotic matching described above is possible by analytical means only in the simplest of cases, essentially when the outer solution is described by a static equilibrium. In general, the outer part of the solution is itself a complicated problem and can only be solved by numerical simulation. In principle, one can attempt to resolve the full problem down to a microscopic neighborhood of the contact line at considerable numerical cost. This has been done using a variety of methods (Renardy *et al.*, 2001; Spelt, 2005), but only for unrealistically large slip lengths. Fully resolved calculations will require strong refinement in the neighborhood of the contact line. More fundamentally still, microscopic features of the contact line such as the microscopic contact angle are beyond a continuum description.

There has been a considerable activity trying to account for microscopic features near the contact line. In particular, "diffuse interface models", to be discussed in more detail in section III.E.2 below, describe contact line motion without the introduction of any slip. Such models have been implemented in a variety of ways (Briant *et al.*, 2004; Jacqmin, 2000; Qian *et al.*, 2003), and allow to investigate the effect of surface thermodynamics on contact line motion (Qian *et al.*, 2006). Lattice-Boltzmann models (Benzi *et al.*, 2006; Briant *et al.*, 2004) describe two phases using a simlified dynamics on a mesoscopic scale. Their main advantage lies in their flexibility, so they are implemented easily even in complex geometries (Biferale *et al.*, 2007; Kusumaatmaja and Yeomans, 2007).

On the other hand, microscopic features can also be incorporated into a contact line model, which needs to be matched to the macroscopic flow. We very briefly describe the principles of such a matching; a review of numerical work is given in Ramé (2002). Following Somalinga and Bose (2000), we illustrate the numerical modeling of contact line flow in Fig. 27. The shaded region

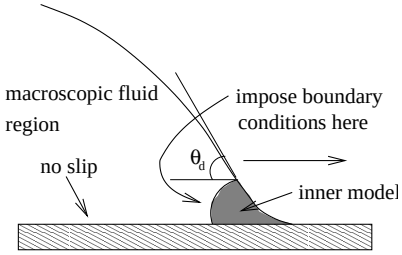

FIG. 27 Schematic of the procedure for continuum modeling.

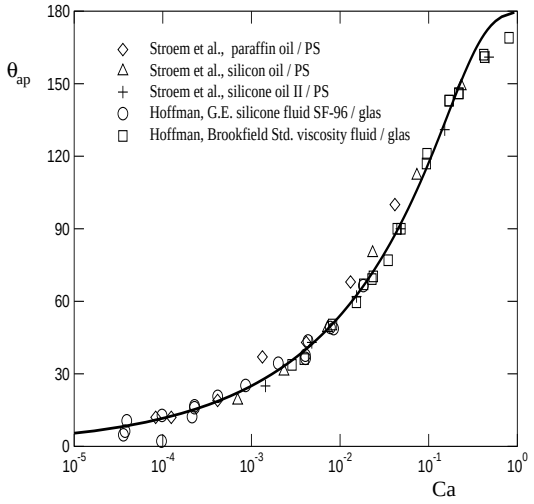

FIG. 28 Apparent dynamic contact angles of perfectly wetting fluids measured in a capillary (Hoffman, 1975) and for a plunging plate (Ström *et al.*, 1990b). Each symbol corresponds to a different fluid and/or substrate. The solid line is (52),(53) with $\theta_m = 0$ and $x/L = 10^4$.

around the contact line is cut out from the flow to avoid the contact line singularity. Its size ℓ_{in} corresponds to the resolution of the computational grid. Since ℓ_{in} is much larger than the microscopic scale, the stress field is smooth at the edges of the shaded region. On the other hand, ℓ_{in} should be small enough for the local contact line solution to be valid, which can be tested by changing ℓ_{in}.

The local solution (51) or its fully two-dimensional counterpart (52) give the interface angle $\theta_d(\ell_{in})$ at the edge of the computational domain. Of course, this local solution is also associated with a velocity field, which supplies the boundary conditions at the edge of the shaded region. Away from the contact line, this velocity field is consistent with the no-slip boundary conditions on the solid surface. Hence standard boundary conditions can be applied everywhere, without encountering any singularities.

Earlier numerical work has tested the consistency of various slip models (Bazhlekov and Chesters, 1996; Finlow *et al.*, 1996), by resolving the flow field down to the microscopic scale. Somalinga and Bose (2000) adopt the procedure described above, and compare the results to numerical simulations which resolve the microscopic scale. The agreement is very good for capillary numbers $Ca < 0.1$, but deteriorates for larger capillary numbers, which is consistent with experimental observation (Chen *et al.*, 1995).

Many more problems require further study in this area. If the contact angle is *receding*, a local solution of the type (51) can only be applied at very small capillary number. As shown in Eggers (2004a), there is in general no unique local solution, but rather a one-parameter family of solutions. Which solution is selected is determined only by matching to the outer flow problem (Eggers, 2005b; Pismen and Thiele, 2006). Finally, no established description of the contact line flow exists for low-viscosity fluids, for which inertia is expected to enter the description (Cox, 1998).

C. Experiment

We now review experimental tests of the hydrodynamic description given above. The difficulty with (54) or (63) is that no accurate information on θ_m is available. The best theoretical understanding exists for the case of $\theta_{eq} = 0$, and in particular for positive Hamaker constant $A > 0$. As we explain in more detail below, in that case the contact line is preceeded by a thin fluid precursor film, to which the profile has to match, which fixes $\theta_m = 0$ in (51) or (52),(53). Thus we first turn to the particular case $\theta_{eq} = 0$.

1. Zero equilibrium contact angle

There exists a wealth of experimental data supporting the capillary dependence of (51) or (52),(53) for $\theta_m = 0$. Typical configurations are fluid displacement in a capillary tube (Fermigier and Jenffer, 1991a,b; Hansen and Toong, 1971; Hoffman, 1975), between parallel glass plates (Shen and Ruth, 1998), or drops spreading on a surface (Chen, 1988; Chen and Wada, 1989; Kavehpour *et al.*, 2003; Tanner, 1979). Also, researchers have considered flow on cylinders (Chen *et al.*, 1995; Inverarity, 1969a,b; Marsh *et al.*, 1993; Petrov *et al.*, 2003a,b; Seebergh and Berg, 1992), plates (Gutoff and Kendrick, 1982; Ström *et al.*, 1990a,b), or tapes (Burley and Kennedy, 1976a,b, 1978; Gutoff and Kendrick, 1982; Prevost *et al.*, 1999) plunging into a fluid. The data have earlier been reviewed by Kistler (1993).

The cleanest test of theory is possible if measured *apparent* contact angles are compared directly to (54) or (63), or entire profiles are recorded (Kavehpour *et al.*, 2003; Marsh *et al.*, 1993). In most cases however, experiments simply report the value of a dynamic angle recorded at some scale x on the order of the optical resolution of the experiment ($\approx 1/10$ *mm*). Fig. 28 shows data from two different experimental setups and for a variety of different fluids and substrates in the per-

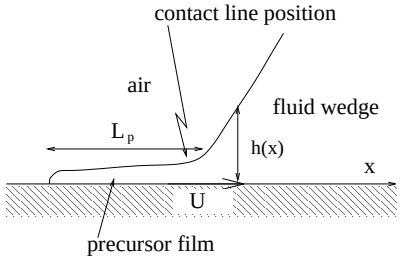

FIG. 29 Schematic of a moving contact line for $S_i > 0, A > 0$. Ahead of the apparent contact line one finds a precursor "foot" driven by van der Waals forces.

fectly wetting case. The solid line is the theoretical prediction (52) with only one adjustable parameter, set to $\ln(x/L) = \ln(10^4)$ to give the best fit. In particular, there is ample support for universality near the contact line, namely that the contact line behavior is independent (apart from small logarithmic corrections) of the particular system *and* of the flow geometry.

To understand the remarkable universality of perfectly wetting fluids, one has to appreciate the existence of a precursor film (Hardy, 1919). By a precursor film we will always understand the *dynamical* film structure that preceeds a spreading drop, to be distinguished from films that exist in equilibrium. Such a film exists even if the fluid is non-volatile "dry spreading" (Cazabat *et al.*, 1997), so that the film was established by flow from the main droplet. This feature was confirmed using ellipsometry (Bascom *et al.*, 1964; Beaglehole, 1989), interference patterns (Bascom *et al.*, 1964), polarized reflection microscopy (Aussere *et al.*, 1986), or phase-modulated interference microscopy (Kavehpour *et al.*, 2003).

Away from the liquid drop, the thickness of the precursor film is typically just a single molecular layer, but it has long been suspected from theoretical arguments (Hervet and de Gennes, 1984; Joanny and de Gennes, 1984; Voinov, 1977) that there is a small region around the drop where the film is thicker, making it amenable to a hydrodynamic treatment. The reason is that for $A > 0$ the long-ranged part of the disjoining pressure (17) tends to *thicken* the film. Using $p = -\gamma h'' - \Pi(h) \approx -\gamma h'' - A/6\pi h^3$, the analog of (49) becomes

$$\frac{3Ca}{h^2} = -h''' + 3a^2 \frac{h'}{h^4}, \tag{64}$$

with the microscopic length scale

$$a = \sqrt{\frac{A}{6\pi\gamma}}, \tag{65}$$

which is typically 1Å.

In equilibrium, and subject to the constraint of fixed volume, van der Waals forces produce a thin fluid film of thickness (de Gennes, 1985)

$$\ell = a(3\gamma/(2S_i))^{1/2}, \tag{66}$$

as determined from (20). In a dynamical situation, depicted in Fig. 29, the advancing macroscopic front has to be treated together with the precursor film. An analysis of the thin-film equations (64) reveals (Hervet and de Gennes, 1984) the physically intuitive result that the precursor film ends when the profile reaches the thickness set by (66). Thus a particularly simple limit is that of vanishing ℓ (infinite spreading coefficient), for which the precursor film formally extends to infinity.

The precursor film, whose thickness is 10-100 nm (Kavehpour *et al.*, 2003), means a tremendous conceptual simplification as it removes the singularity at the macroscopic contact line. A solution to equation (64), which matches onto the thin precursor film, has the similarity form

$$h(x) = \frac{a}{Ca^{1/3}} \phi_{vdw}((Ca)^{2/3} x/a). \tag{67}$$

The similarity function ϕ_{vdw} depends on the variable $\xi = a^{-1}Ca^{2/3}x$, and satisfies the equation

$$\frac{3}{\phi_{vdw}^2} = -\phi_{vdw}''' + 3\frac{\phi_{vdw}'}{\phi_{vdw}^4}. \tag{68}$$

Equation (68) has to be solved subject to the asymptotic boundary condition $\phi_{vdw} \approx -1/\xi$ as $\xi \to -\infty$, which corresponds to the precursor film. By solving (68) numerically, the length scale L in (51) is found to be (Eggers and Stone, 2004; Hervet and de Gennes, 1984)

$$L = 0.69a/(Ca)^{2/3}. \tag{69}$$

Note that L can become mesoscopic if Ca is small. For example, in the drop spreading experiment of Fig. 6 $R \approx 1$ mm and $Ca \approx 4 \cdot 10^{-5}$, giving $L \approx 120$ nm if one uses $a \approx 2$Å(Valignat *et al.*, 1993). If one inserts (69) into (62), one obtains the ultimate spreading law for a small drop in the presence of a precursor film. Comparing to (10) we find $B = \ln(R/(2e^2L)$ and thus $B^{1/10} = 1.19$, in very good agreement with the experimental value of $B^{1/10} = 1.186$, cf. section I.C. Of course, we recover the result that the spreading rate *does not* depend on the spreading coefficient S_i. As we stressed before, this is consistent with energy conservation, since all the excess energy is dissipated in the film. We will demonstrate this result explicitely in the section on contact line dissipation below.

From the condition that the precursor film ends where it reaches the thickness (66), one finds that its total length L_p decreases with speed (de Gennes, 1985; Voinov, 1977) like

$$L_p \approx a(S_i/\gamma)^{1/2} Ca^{-1}. \tag{70}$$

Thus even for $Ca = 10^{-5}$, L_p is typically just 100 μm (Kavehpour *et al.*, 2003)), so most experimental techniques lack the lateral resolution to observe the precursor film directly. Detailed measurements of L_p were recently performed by Kavehpour *et al.* (2003) with much improved lateral resolution, finding remarkable agreement

with (70). The vertical resolution however was not sufficient to confirm the predicted inverse fall-off of the film thickness with distance from the contact line. Earlier experimental work is also not conclusive: Beaglehole (1989) finds the precursor film thickness to fall off too rapidly, Léger *et al.* (1988) observe the theoretically predicted profile, but find inconsistencies in the amplitude.

Most of the existing experimental work (see Cazabat *et al.* (1997) for a brief review) is on the monomolecular *diffuse* film that precedes the mesoscopic film described above. Its radius advances like $t^{1/2}$ (Abraham *et al.*, 2002b; Cazabat *et al.*, 1997; Heslot *et al.*, 1989a), but may also be sub-diffusive for polymeric liquids (Albrecht and Leiderer, 1992). Various theoretical models for the diffusive motion of molecules have been proposed (Abraham *et al.*, 2002b; Ala-Nissila *et al.*, 1996; Burlatsky *et al.*, 1996; Hjelt *et al.*, 1998; Popescu and Dietrich, 2004), which reproduce the diffusive spreading law,(Abraham *et al.*, 2002b), and produce profiles in agreement with experimental data (Ala-Nissila *et al.*, 1996; Hjelt *et al.*, 1998).

Another important variant of single layer spreading is *terraced* spreading (Heslot *et al.*, 1989b). In this case the monolayer joins the drop in a sequence of steps, the radius of each of which grow like a square root in time (de Gennes and Cazabat, 1990). However, the problem with continuum models such as that of de Gennes and Cazabat (1990) is that its applicability to layers of single molecules is suspect (Cazabat *et al.*, 1997). Instead, there are a number of microscopic simulations using SOS models (De Coninck *et al.*, 1993) or MD simulations with effective Lennard-Jones potentials between polymer molecules (Bekink *et al.*, 1996) which show terracing, with the expected scaling behavior.

Thus the variety of different precursor film behaviors is enormous. It is however unlikely that precursor structure has an important impact on the spreading of the macroscopic droplet, since it simply implies a different route to the burning of excess energy, see section III.D below. A counterexample is however proposed in Webb III *et al.* (2003), based on MD simulations of Pb on Cu. The reason is that the film alloys with the substrate, slowing it down so much that the spreading is controlled by the slow spreading of the precursor.

2. Finite equilibrium contact angle

In the absence of a mesoscopic precursor film it is much harder to calculate the parameters L and θ_m appearing in (51) based on first principles. Owing to Huh and Scriven's paradox, there is no self-contained hydrodynamic description, but microscopic effects need to be included near the contact line, of which Table I gives a brief overview. Since L only appears logarithmically, for practical purposes it suffices to recognize that it is a microscopic length, of the order of a nanometer. It is much more difficult to estimate θ_m, which out of equilibrium will in general not be equal to θ_{eq}.

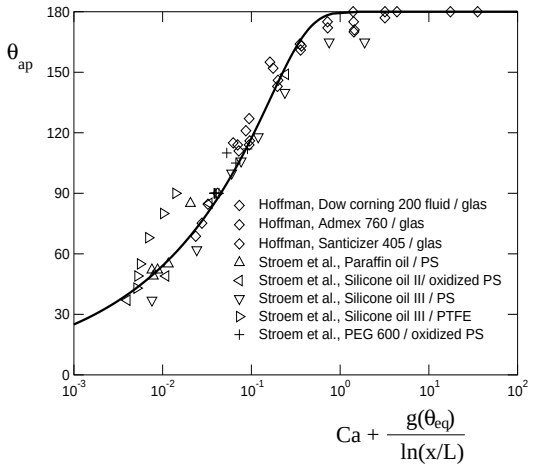

FIG. 30 Apparent dynamic contact angle data from Hoffman (1975) and (Ström *et al.*, 1990b) for partially wetting fluids. The value of $g(\theta_{eq})/\ln(x/L)$, with $x/L = 10^4$, is added to the abscissa to make the theoretical curve the same as in Fig. 28. Again each symbol corresponds to a different experiment, the equilibrium contact angle is taken from experiment. Those data sets from Ström *et al.* (1990b) that showed evident contact angle hysteresis were not included.

Nevertheless, as discussed in detail in the next section, if viscous dissipation is large compared to local dissipation at the contact line, the departure of the interface angle from θ_{eq} is mostly due to viscous bending, and one can put $\theta_m \approx \theta_{eq}$ in (51). This assumption is confirmed in Fig. 30, which shows data analogous to Fig. 28, setting $x/L = 10^4$. Apart from some experimental scatter, the data is well described by (52), which is remarkable in view of the fact that there is essentially no adjustable parameter. However, the same type of description no longer works if the viscosity is small, as demonstrated in a recent set of experiments (Petrov *et al.*, 2003a,b). This may in part be due to inertia, but more crucially the assumption $\theta_m \approx \theta_{eq}$ only works if viscous dissipation dominates, which will no longer be the case for small viscosity.

Indeed, the results for the extreme case of liquid helium being dragged across a cesium substrate at very low temperatures show that viscous bending becomes altogether negligible (Prevost *et al.*, 1999). Rather, as shown in Fig. 31, there is an *exponential* dependence of the contact line speed on the force necessary to move the interface. This suggests that the contact line motion can be described by a thermally activated process (Blake and Haynes, 1969), which takes place close to the contact line. The slopes shown in Fig. 31 scale like $1/T$, as expected for thermal activation. By considering the total dissipation in a suitable region around the contact line, we are able to unify both the viscous and the thermally activated contributions to the contact line motion, as outlined in section III.D below.

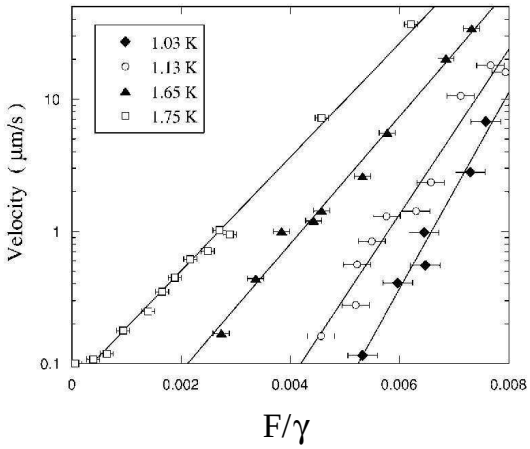

FIG. 31 Plot of the contact line velocity as function of the applied force per unit length for various temperatures (Prevost *et al.*, 1999). Solid lines are exponential fits to the experimental data.

D. Contact line dissipation and microscopic contact angles

1. Free energy balance

No continuum theory of the immediate neighborhood of a contact line will be able to capture molecular processes responsible for contact line motion. Instead, to compute the parameters θ_m and L that appear in (51), hydrodynamics has to be combined with a microscopic description, which may cover a variety of different features, such as fluid slip, diffusiveness of the interface, or evaporation of one fluid into the surrounding gas. Even for one particular effect, this is a demanding proposition, but made even more difficult by the possibility of several effects working in parallel. By considering the total energy dissipated in a macroscopic contact line region, and equating it to the energy pumped into the system (Brochard-Wyart and de Gennes, 1992; de Gennes, 1985; Voinov, 1976), it is possible to disentangle some of the disparate mechanisms at work. Namely, energy is additive, so there is a unique prescription for combining different effects by adding the contribution to the energy dissipation they produce.

To compute the rate of energy input W, consider the *macroscopic* angle $\theta_d(x) = \tan^{-1}(h'(x))$ at some distance x from the contact line. Upon some shift in the contact angle position δx, the work done on the system is

$$\delta W = (f_{cl} + ph(x))\delta x, \quad f_{cl} = \gamma(\cos\theta_{eq} - \cos\theta_d), \quad (71)$$

where f_{cl} is the force per unit length on the contact line and $ph(x)$ the work of the pressure forces on the fluid cross section at x [1]. In a steady state, the change in free energy $\mathcal{F}$ per unit length of the system (we are considering a situation of constant temperature) must be zero: $0 = \dot{\mathcal{F}} = W - T\dot{S}$, and we obtain

$$(f_{cl} + ph)U = W = T\dot{S}. \quad (72)$$

Here $T\dot{S}$ corresponds to all dissipative processes occurring in the wedge of fluid up to x, including the contact line itself. Firstly, the viscous dissipation in the fluid is (Landau and Lifshitz, 1984)

$$T\dot{S} = \frac{\eta}{2}\int_V \left(\frac{\partial u_i}{\partial x_j} + \frac{\partial u_j}{\partial x_i}\right)^2 dxdy \approx 3U^2\eta\int_L^x \frac{1}{h}dx, \quad (73)$$

where the integral is over the volume of fluid from some microscopic cut-off scale L up to a hypothetical boundary at x. It is easily confirmed that the energy *flux* across the fluid boundary of V is small compared to (73). The approximation on the right-hand side of (73) is based on the lubrication approximation, assuming a parabolic velocity profile. Using the corresponding approximations $\tan^{-1}(h') \approx h'$ and $p \approx -\gamma h''$,we find

$$U\gamma(h'^2 - \theta_{eq}^2 - 2h''h) = 6\eta U^2\int_L^x \frac{1}{h}dx + 2W_m(U)U. \quad (74)$$

All additional dissipative processes which occur near the contact line, below some microscopic scale L, have been subsumed into a rate of dissipation $W_m(U)U$ per unit length of contact line.

To solve (74) for the profile $h(x)$, it is most convenient to differentiate once (Eggers, 2004b), from which one recovers (51) exactly. The crucial advance however is that we are able to associate the microscopic contact angle θ_m with the total dissipation W_mU that takes place *below* the microscopic scale L. As a result, θ_m becomes *speed dependent*:

$$\theta_m^2(U) = \theta_{eq}^2 + \frac{2W_m(U)}{\gamma}, \quad (75)$$

as already remarked by Voinov (1976). The equation for the macroscopic slope away from the contact line is

$$h'^3(x) = \left[\theta_{eq}^2 + \frac{2W_m(U)}{\gamma}\right]^{3/2} + \frac{9\eta U}{\gamma}\ln(x/L), \quad (76)$$

restoring the definition of the capillary number. For sufficiently large viscosities, one expects the second, viscous contribution to dominate over any speed dependence of W_m.

Note that a constant $W_m = W/U$, as implied by (15) for a contact line with hysteresis, simply leads to a shift in the angle measured at vanishing speed. This means that for an advancing contact line, combining (76) and (15) in the small-angle approximation, the angle θ_m is to be replaced by θ_a in the Cox-Voinov law (51) (and correspondingly by θ_r for a receding contact line). This generalization of the Cox-Voinov law has been confirmed in (Le Grand *et al.*, 2005) with experiments on sliding drops. In section IV below we will give estimates of the contact line dissipation in terms of defect properties.

[1] We are grateful to Laurent Limat for pointing out the contribution of the pressure forces

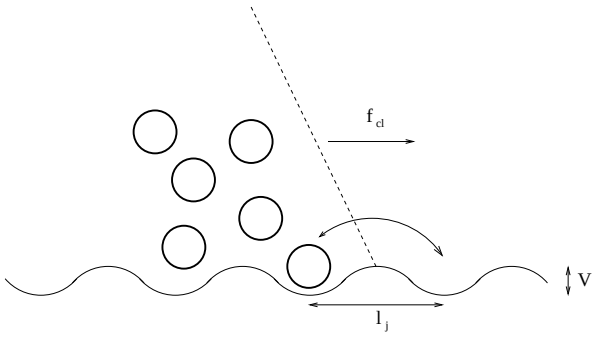

FIG. 32 A schematic of the theory by Blake and Haynes (1969), associating contact line motion with the hopping of molecules between the potential wells provided by the substrate.

2. Sources of dissipation

Blake and Haynes (1969) have developed a theory of contact line motion, based on activated processes (Eyring, 1941). This theory is often referred to as "molecular kinetic theory", although it is found to hold for activation events on scales much larger than the molecular scale, as we are going to see below. Following Brochard-Wyart and de Gennes (1992) and de Gennes *et al.* (2003), we estimate W_m as associated with molecular jump processes, so θ_m can be computed from (75).

The idea, as illustrated in Fig. 32, is that for the contact line to move under a force f_{cl} at the contact line, individual molecules jump over a corrugations of wavelength ℓ_j and potential depth V. The same ideas apply if potential wells are in fact somewhat above the molecular scale, linked for example to mesoscopic pinning sites or roughness of the surface (Prevost *et al.*, 1999). In equilibrium, backward and forward jumps are equally likely and balance each other out. The applied force per molecule $f_{cl}\ell_j$ deforms the potential landscape to make forward steps more likely:

$$\frac{1}{\tau} = \frac{2}{\tau_0}\exp\left(-\frac{V}{k_BT}\right)\sinh\left(\frac{f_{cl}\ell_j^2}{2k_BT}\right), \qquad (77)$$

so τ is the *average* time for a forward step, where τ_0 is a microscopic time for a single "attempt".

Since the contact line speed is $U = \ell_j/\tau$, and using (71) we thus obtain

$$U = \frac{2\ell_j e^{-V/(k_BT)}}{\tau_0}\sinh\left(\frac{\gamma\ell_j^2}{(2k_BT}(\cos_{eq} - \cos_d)\right), \quad (78)$$

which gives the exponential dependence of Fig. 31, for sufficiently large forcing $f_{cl}\ell_j^2/(k_BT) \gg 1$. The relationship (78) between speed and θ_d is the main result of molecular kinetic theory. Since both f_{cl} and k_BT are known experimentally, the fits of Fig.31 determine the activation length ℓ_j. For the helium on cesium system under study, $\ell_j = 10nm$ is found, which is significantly larger than any atomic distance. Since $W_mU = f_{cl}U$ we obtain from (75) that

$$\theta_m^2 = \theta_{eq}^2 + \frac{2k_BT}{\gamma\ell_j^2}\text{arcsinh}\left[\frac{U\tau_0}{2\ell_j}e^{V/k_BT}\right]. \qquad (79)$$

Any microscopic speed ℓ_j/τ_0 will be quite high, much greater than a typical contact line speed of mm/s. Hence the speed dependence described by (79) would be negligible if it were not for the exponential factor. Pomeau (2000) has proposed that V be estimated as the heat of evaporation per molecule, which would lead to $e^{V/(k_BT)} \approx \rho_{liq}/\rho_{gas} \approx 10^3$, significantly enhancing the speed dependence of the microscopic contact angle. However, these are order-of-magnitude estimates, so effectively one has to treat $e^{V/(k_BT)}\tau_0/\ell_j$ as an adjustable parameter, fitting macroscopic measurements of the interface slope to (74), to infer the microscopic angle θ_m.

This approach has been followed in Petrov *et al.* (2003b) and Petrov *et al.* (2003a), to obtain V and ℓ_j for a range of low-viscosity alcohols on an amorphous substrate. Remarkably, the length ℓ_j is found to be of the order of 5nm, in qualitative agreement with the activation length extracted from Fig. 31. This result once again points to a process limiting the contact line speed that takes place on scales much larger than a molecular length. It has been suggested by Prevost *et al.* (1999) that ℓ_j is to be identified with the density of pinning sites, at least for the systems mentioned above. As we will discuss in more detail in subsection IV.D, this observation points to a new interpretation of the potential V in terms of the contact angle hysteresis of the system.

3. Precursor films

If the fluid is perfectly wetting, we have seen that van der Waals forces lead to the formation of a precursor film in front of the contact line. The initial spreading coefficient S_i is now positive, and the work per unit length done on the contact line is $U(S_i + \gamma(1 - \cos\theta_d))$. The free energy balance (74) becomes

$$US_i + U\gamma h'^2(x) = 6\eta U^2\int_{-L_p}^{x}\frac{1}{h}dx, \qquad (80)$$

where the integration starts at the tip of the precursor film, rather than at the position of the macroscopic contact line $x = 0$.

It was shown by Hervet and de Gennes (1984) that the integral in (80) can be split into two parts: one from the tip of the precursor film $-L_p$ to the macroscopic contact line at $x = 0$, and one covering the bulk fluid from 0 to x. The crucial observation is that the viscous dissipation in the film exactly cancels the "extra" work US_i, to make (80) consistent with (51), where $\theta_m = 0$. In particular, this means it is very difficult to accelerate the spreading of liquids. The only known way to achieve that is by adding "superspreaders", to which we come back in subsection III.J.2 below.

E. Matching to the contact line

The free energy arguments of the previous section give a good phenomenological description, yet the dependence on microscopic parameters is never explicit unless a detailed matching to the contact line is performed. The necessary framework for such a matching is one in which the fluid flow equations are coupled to the thermodynamics of the liquid-vapor (liquid-liquid in the case of two-fluid systems) and solid-liquid interface, ensuring a consistent description of both statics and dynamics. A recent article (Qian *et al.*, 2006) summarizes such efforts, which are built on the Cahn model, cf. section II.A.2. As part of such a thermodynamic description, the interface has finite thickness, introducing another length scale into the problem, which can take over the role of the slip length if the interface is sufficiently diffuse. However let us begin by briefly reviewing the literature on interfaces of zero thickness, only taking into account fluid-wall interactions.

1. Sharp interface

In the simplest case, the contact line singularity is regularized by a slip length (Eggers, 2004a; Hocking, 1983, 1992), using the Navier-Stokes equation throughout. In many cases involving the flow between two solids (Cottin-Bizonne *et al.*, 2005; Israelachvili, 1986) this gives a good description of experimental data, adjusting λ to $\approx 1nm$ for wetting fluids. A generalization of (56) is $m(h) = h^3 + 3\lambda^{2-\alpha}h^{1+\alpha}$ (Eggers, 2004a), $\alpha = 1$ being the classical Navier condition. Now (55) can be solved up to the contact line, imposing a microscopic angle $h'(0) = \theta_m$. Using an expansion in the capillary number (Eggers, 2004b; Hocking, 1983) one finds

$$L = 3\lambda/(e\theta_m) + O(Ca\lambda), \tag{81}$$

where only the $O(Ca)$ correction depends on α. For $\theta_m \to 0$ the expansion breaks down (Cox, 1986), indicating a new type of asymptotics in that limit.

Indeed, using a similarity solution in the spirit of (67) to solve (55) with the slip law (56), the length L now depends on Ca like a power law (Eggers and Stone, 2004; Hocking, 1992):

$$L = 0.54\lambda Ca^{-1/3}. \tag{82}$$

Interestingly, the power in (82) is different from the power $Ca^{-2/3}$ observed for a precursor film (cf. (69)). Thus (82) could be the correct description for a system with $A < 0$ and $S_i > 0$, in which case there is no mesoscopic precursor film. Recent MD simulations of a propane film spreading on gold (Moseler, 2007), as well as DPD models (Hoogerbrugge and Koelman, 1992), but with the long-ranged interaction truncated, are indeed consistent with (82). In Marsh *et al.* (1993), the speed dependence of L was found experimentally by fitting the *macroscopic* profile shape to (51). The result seems to favor (69) over (82) (Eggers and Stone, 2004), as indeed $A > 0$ for the system under study. Another important consideration is one of time scales (Moseler, 2007), since on the nanoscale there is not necessarily enough time for a mesoscopic precursor film to develop. Thus if one considers the impregnation of a nanoscale pore (Henrich *et al.*, 2008), the correct description might be closer to (82).

To build in the equilibrium properties of the fluid more systematically, one can take the disjoining pressure into account, cf. (17). The first such calculation was performed by de Gennes *et al.* (1990), but only including the long-ranged part of $\Pi(h)$, giving $L = a/(2\theta_{eq}^2)$. Hocking (1993) expanded on this calculation by including both slip and treating the van der Waals attraction beyond the lubrication limit. This allowed him to perform the matching to the contact line $h(0) = 0$ explicitly. Assuming that the minimum h^* of the interface potential produces a thin equilibrium film even in the partially wetting case (Becker *et al.*, 2003; Seemann *et al.*, 2001b), the contact line singularity is formally avoided since $h > 0$ everywhere. Of course, h^* is a molecular thickness at best, so hydrodynamics is not strictly applicable. As shown in Eggers (2005a); Pismen and Pomeau (2004), the calculation gives $L = 4h^*/(e\theta_{eq})$ for a $1/h^4$ repulsive potential; the prefactor depends only weakly on the form of the repulsion.

2. Diffuse interface

Considerable work has recently been devoted to diffuse interface models, either in the guise the Cahn-Landau model for partially miscible fluids (Briant and Yeomans, 2004; Chen *et al.*, 2000; Jacqmin, 2000; Qian *et al.*, 2003, 2006; Seppecher, 1996), or the van der Waals model for a liquid-vapor interface (Briant *et al.*, 2004; Pismen and Pomeau, 2000; Pomeau, 2002). We focus on the variational formulation of Qian *et al.* (2006), who combine the fluid equations, including slip, with the Cahn-Landau free energy (27),(28) including wall interactions. The order parameter profile m is now of course allowed to vary in three dimensions, hence F_s is to be integrated parallel to the wall. In addition, m obeys a convection-diffusion equation

$$\frac{\partial m}{\partial t} + \mathbf{u}\cdot\nabla m = M\triangle m, \tag{83}$$

where M is a mobility coefficient. A similar equation appears for order-parameter relaxation at the wall, with Γ the corresponding surface mobility.

In this description, the Navier slip law is generalized to

$$\frac{u^{slip}}{\lambda} = -\frac{\partial u}{\partial z} + \frac{L(m_s)}{\eta}\frac{\partial m_s}{\partial x}, \tag{84}$$

where x is a direction parallel to the wall and

$$L(m) = \frac{c^2}{2}\frac{\partial m}{\partial z} + \frac{\partial \Phi}{\partial m_s}. \tag{85}$$

The last term on the right hand side of (84) is the "uncompensated Young stress", representing the tangential stress the fluid-fluid interface exerts on the fluid. In equilibrium, its integral across the interface must give zero. Qian *et al.* (2003, 2006) find, and confirm by numerical simulations, that the uncompensated Young stress is in fact the dominant contribution to fluid slip near the contact line.

Let us now consider the limit of small interfacial thickness, such that the interface is centered closely around a plane that makes an angle θ_m with the solid. Then the integral over the uncompensated Young stress is precisely the contact line force f_{cl}, cf. (71). Neglecting the viscous contribution in (84) relative to the sharply peaked interfacial contribution, one obtains an expression for the slip velocity which, integrated over the interface, gives the contact line speed U. In terms of the description of section III.D.1, this amounts to a dissipation $W_m = \xi\eta U/\lambda$ in (75), where ξ is the thickness of the interface, or

$$\theta_m^2 = \theta_{eq}^2 + 2\frac{\xi Ca}{\lambda}. \tag{86}$$

Curiously, the dynamic contact angle is controlled by the capillary speed, with a functional form that is quite different from that produced by viscous bending.

Thus the bottom line of the analysis of the sharp interface limit is that the classical description in terms of a Navier slip condition, which leads to (81), is in fact valid. Namely, the capillary forces on the right hand side of (84) are highly concentrated inside the interface, and the classical Navier law remains outside of the interfacial region. The effect of the force balance *inside* the interfacial region leads to the speed dependence of the microscopic contact angle (86). Ren and E (2007) focus on this effective model in the limit of zero interfacial thickness, and confirm its validity by extensive comparisons to MD simulations (see below).

In the opposite limit of a very diffuse interface, the contact line can move by virtue of order parameter diffusion or evaporation-condensation alone (Briant *et al.*, 2004; Chen *et al.*, 2000; Pomeau, 2002), even if there is no slip. In the case of a fluid-vapor interface, evaporation-condensation is the relevant mechanism (Briant *et al.*, 2004). Intuitively, the fluid evaporates in response to the interface trying to relax back to its equilibrium shape, which in turn is driven out of equilibrium by the singular flow. The fluid then condenses in front of the contact line, making it move. In the case a liquid-liquid interface, on the other hand, order parameter diffusion is more relevant. This process sets an effective length scale, which in the case of a fluid-fluid system was estimated using two simultaneous balances (Briant and Yeomans, 2004): first a force balance across the interface, and second the equality of convection and diffusion in (83). The result is

$$L_{diff} = \left(\frac{\eta M \xi^2}{(\Delta m)^2}\right)^{1/4}, \tag{87}$$

where Δm is the jump of the order parameter across the interface. This relation was tested by comparison with a lattice Boltzmann model (Briant and Yeomans, 2004), for which the interface can be made very diffuse. The diffusive length L_{diff} is expected to assume the role of L in the contact angle law (51), but a consistent calculation of L as well as of θ_m still needs to be performed in the diffuse limit.

A slightly different approach was taken in Pismen and Pomeau (2000). Starting from diffuse interface theory, an effective equation for a sharp interface is derived within the lubrication approximation, but with a disjoining pressure that differs from the conventional version in that it remains finite in the limit $h = 0$. The existence of a minimum in $\Pi(h)$ guarantees that the solid is covered by a thin film, which cuts off the viscous singularity.

Although the results on diffuse interface models represent a significant conceptional advance, one has to keep in mind the extreme simplicity of the system, characterized, for example, by perfect solid surfaces. In reality, there is always some contact angle hysteresis in the system, to which we turn in the next section. In addition, no long-ranged forces have been included in the analysis. This avoids more nonlocal interactions in the interface region, as well as a more complex precursor film structure. Any application to real systems will likely involve a more complex interplay of different physical effects. Nevertheless, in view of nanoscale applications of contact lines (Gogotsi *et al.*, 2001; Iwamoto and Tanaka, 2002), the interest in a quantitative description of the immediate neighborhood of the contact line will undoubtedly become more pronounced.

Note that the influence of fluctuations on contact line motion has been neglected completely in the analyses of diffuse interface models. The success of mean-field descriptions under defined conditions indicates that the neglect of fluctuations is perhaps a reasonable assumption, in particular if the interface is sharp. As a result, capillary forces are very strong and highly concentrated, reducing the relative importance of fluctuations. However, under certain geometrical constraints on the geometry of the initial drop, a recent study (Davidovitch *et al.*, 2005) based on a stochastic thin film equation (see also (Mecke and Rauscher, 2005; Moseler and Landman, 2000)) predicts enhanced spreading in the presence of noise. Namely, in close analogy to a result found previously for the break-up of a nanoscale jet (Eggers, 2002; Moseler and Landman, 2000), the spreading exponent for a two-dimensional ridge can change from $n = 1/7$ (cf. table II) to $n = 1/4$. Similar enhancement has been found for dewetting of thin films (Grün *et al.*, 2006), to be discussed below, cf. section III.H.

F. Molecular dynamics

Computer simulations of fluids consisting of individual molecules with more or less realistic interactions be-

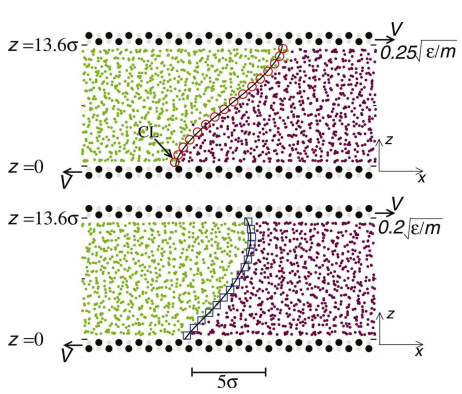

FIG. 33 MD simulation of a Couette flow with a moving contact line (Qian *et al.*, 2003). The colored dots are the instantaneous molecular positions of the two fluids, projected on the xz-plane. The black (gray) circles denote the wall molecules. The upper panel shows the symmetric case, $\theta^s_{eq} = 90^\circ$, the lower the asymmetric case, $\theta^a_{eq} = 64^\circ$.

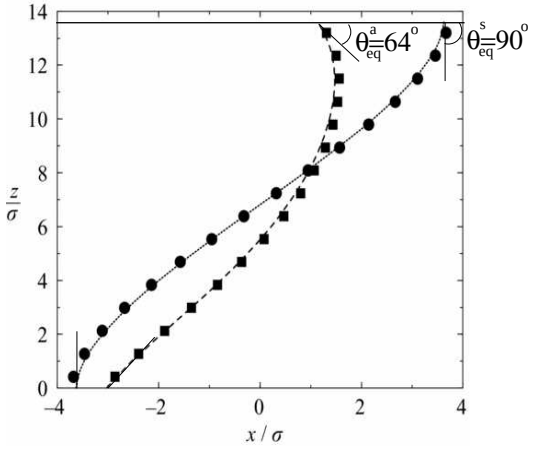

FIG. 34 Comparison of the MD (symbols) and continuum (lines) interface profiles for the symmetric and asymmetric potentials shown in Fig. 33 (Qian *et al.*, 2006). The MD results were obtained by averaging over at least 10^5 atomic time scales, the continuum calculation is based on the diffuse interface theory described in the previous section, with parameters determined from the MD simulation.

tween them are an extremely promising avenue to understand microscopic features of fluid flow. A typical molecular dynamics (MD) study of a Couette flow is shown in Fig. 33, where molecules are treated as point particles, with Lennard-Jones interactions (short-range repulsive and long-range attractive) between them (Allen and Tildesley, 1987). Molecular interactions are typically cut off at 2-3 times the interaction distance, hence the effect of long-ranged forces is not captured by most of the present simulations.

By tuning the interaction parameters between the molecules, particular wetting properties of the fluids can be chosen (Cho *et al.*, 2004). One particular focus of such studies has been the slip condition near solid walls (Cho *et al.*, 2004; Koplik *et al.*, 1989; Thompson and Troian, 1997). Contact lines have been studied by simulating the Couette flow between two sheared walls (Qian *et al.*, 2003, 2004; Ren and E, 2007; Thompson and Robbins, 1989), or spreading drops (Hadjiconstantinou, 2003; Ruijter *et al.*, 1999). The fluid-wall interactions are modeled by Leonard-Jones interactions as well. No attempt has yet been made to model a specific fluid-fluid-solid or fluid-gas-solid system, with view to a direct comparison with experiment.

Existing MD simulations of moving contact lines confirm the main theoretical ideas behind the continuum description of moving contact lines (Qian *et al.*, 2003; Ren and E, 2007; Thompson and Robbins, 1989), in particular if the interface is described by a Cahn-Landau model (Qian *et al.*, 2006). The impressive agreement that is achievable is illustrated in Fig. 34, which compares the interface as found from averaging MD data to the results of the Cahn-Landau model. The same degree of agreement is found for the averaged velocity profile. Slip of the velocity is concentrated almost exclusively inside the interface region, in agreement with earlier observations (Thompson and Robbins, 1989). The angle θ_m at which the (averaged) interface intersects with the wall is seen to deviate slightly from the equilibrium angles, included in Fig. 34.

The small departures of θ_m from θ_{eq} found in Fig. 34 agree well with the continuum modeling, and the corresponding analytical result (86). Similar tests were performed in Ren and E (2007), but for conditions under which the departure $\theta_m - \theta_{eq}$ is much larger. Results are once more consistent with (86). If driven even harder into the non-linear regime (Ren and E, 2007), results are consistent with the functional from of (79), predicted by molecular kinetic theory. In addition, the intermediate region of the profile, where viscous bending becomes important, was included in the analysis as well. The results compare well with (52) for the viscosity ratio $M = 1$, appropriate for the simulation by Ren and E (2007).

It is evident that MD simulations are not well suited to study macroscopic systems, the most recent simulations of contact line flow comprising about 10^6 particles (Ren and E, 2007). On the other hand, a hypothetical MD simulation of a bulk material would not contribute much additional information: the relative size of fluctuations will be quite small. The moving contact line is thus an ideal problem for hybrid numerical schemes (Hadjiconstantinou, 1999a,b; Hadjiconstantinou and Patera, 1997; O'Connell and Thompson, 1995), in which a small region around the contact line is treated by an atomistic method, the remaining fluid domain is described by the Navier-Stokes equation. Information between the two domains is exchanged through an overlap region. In Hadjiconstantinou (1999a,b) the method was shown to work for contact line flows, albeit in systems which are still quite small.

G. Receding contact line

We have been careful to point out that the asymptotic solution (51) only applies to an advancing contact line, which is easily seen from the expression itself. Namely, a receding contact line corresponds to $Ca < 0$, hence (51) does not make sense for $x/L \to \infty$, since $h'(x)$ becomes negative for $\ln(x/L) >= -\theta_m^3/(9Ca)$. This means that h would eventually become negative, and a completely different description of receding contact lines is necessary. The properties of the interface profile for $Ca < 0$ are best inferred from an exact solution (Duffy and Wilson, 1997) of the thin film equation (49), expressed in terms of Airy functions (Abramowitz and Stegun, 1968). In the spirit of section III.E, this solution must be matched to the contact line (Eggers, 2005b).

In the case of an advancing contact line, the solution is determined uniquely by the condition that the curvature must vanish at infinity for it to match to an outer solution. Instead, all solutions of (49) with $Ca < 0$ (receding contact line) have strictly positive curvature at infinity. For large x/L one finds (Eggers, 2005b)

$$h'(x) = \kappa_\infty x + \frac{3|Ca|2^{2/3}Ai'(s_1)}{Ai(s_1)} + O(L/x), \qquad (88)$$

where

$$\kappa_\infty = -\frac{3|Ca|\exp(-\theta_m^3/(9|Ca|))}{2^{1/3}Ai^2(s_1)L} > 0 \qquad (89)$$

is the curvature at infinity. It is clear from (88) that it does not make sense to speak of a dynamic contact angle $h'(x)$, since the slope is varying *linearly* with x, except at very small capillary numbers, for which there exists a region $\ln(x/L) \lesssim -\theta_m^3/(9Ca)$, over which $h'(x)$ is still described by (51).

With increasing contact line speed, the curvature κ_{cr} becomes so large that it becomes impossible to match to an outer solution, leading to a maximum speed Ca_{cr} at which the contact line can move relative to a plate (Eggers, 2004a, 2005b). Experimentally, this is seen for example by withdrawing a plate from a bath of liquid that does not wet the plate, cf. Fig. 35. Above a maximum speed of Ca_{cr}, no more stationary solutions exist, so the contact line must move up the plate and a macroscopic film is deposited. Strictly speaking, the data shown in Fig. 35 was taken from a non-stationary experiment. However, the collapse for different speeds demonstrates that the contact line moves quasi-statically, and effectively represents the stationary solution.

Away from the contact line, the profile is that of a static meniscus, whose *apparent* contact angle θ_{ap} can be determined from the capillary rise x_{cl} according to Laplace's classical solution (de Laplace, 1805; Landau and Lifshitz, 1984). As shown in Fig. 35, the transition toward a film occurs very close to the maximum capillary rise $x_{cl} = \sqrt{2}\ell_c$, for which θ_{ap} goes to zero. This is in agreement with previous experimental work on fibers

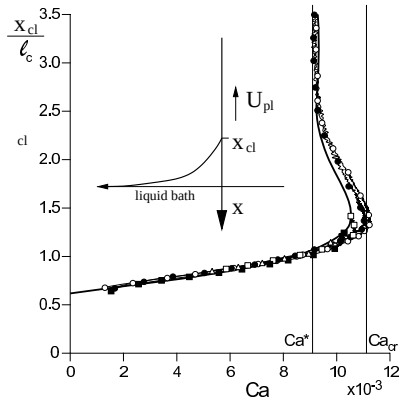

FIG. 35 A plate is being withdrawn from a bath of non-wetting liquid at speed U_{pl}, which forms a contact line at height z_{cl} (Delon *et al.*, 2007). The capillary numbers based on the plate speed U_{pl} are $Ca_{pl} = 9.7 \times 10^{-3}(\triangle)$, $Ca_{pl} = 10.2\times10^{-3}(\blacksquare)$, $Ca_{pl} = 10.7\times10^{-3}(\square)$, $Ca_{pl} = 11.2\times10^{-3}(\bullet)$, $Ca_{pl} = 11.5 \times 10^{-3}(\circ)$. These values are all above the critical capillary number Ca_{cr}, so the contact line moves up very slowly, and each curve is traced out in a time-dependent fashion for each experiment. The full line is found from the thin film equation (55), (56), including gravity.

(Sedev and Petrov, 1991), and confirms the classical phenomenological argument by Deryaguin and Levi (1964). It contradicts the approach by de Gennes (1986) to which we return below. Note that the critical capillary number for a receding contact line is quite small, while stable advancing contact lines can persist to $Ca \approx 50$ (Simpkins and Kuck, 2003) (pushing a solid into a liquid bath). This once more highlights the fundamental difference between advancing and receding contact lines.

To calculate the meniscus profile quantitatively, the "outer" meniscus solution must be matched to the contact line solution (88), which is not possible above a maximum speed Ca_{cr}, as first noticed by Voinov (2000a) and confirmed numerically by Hocking (2001). The only way to avoid this transition is to cause the contact line to incline, to which case we return in subsection III.J.1 below. The outer solution, extrapolated to the position of the contact line, has the form

$$h'_{out}(x) = \theta_{ap} + \sqrt{2 - 2\theta_{ap}}(x - x_{cl}) + O((x - x_{cl})^2), \qquad (90)$$

whose functional form must agree with (88) for matching to be possible. As shown in Eggers (2005b), θ_{ap} goes to zero at a critical capillary number

$$Ca_{cr} = \frac{\theta_m^3}{9}\left[\ln\left(\frac{Ca_{cr}^{1/3}\theta_m}{18^{1/3}\pi(Ai(s_{max}))^2\lambda\sqrt{2}}\right)\right]^{-1}, \qquad (91)$$

above which no more solution exists (matching becomes impossible), in agreement with experiment (Sedev and Petrov, 1991, 1992).

As seen in Fig. 35, the experimental values of Ca_{cr} are in good agreement with the theoretical prediction (full line). The prediction $Ca_{cr} \propto \theta_{eq}^3$ of (91) also agrees

with earlier experiments (Quéré, 1991) for a wide range of contact angles, although the prefactor is smaller. This might be due to the considerable contact angle hysteresis present for the materials used in Quéré (1991), pointing to surface roughness. This will tend to reduce the critical capillary number (Golestanian and Raphaël, 2001b, 2003). In addition, any speed dependence of the microscopic contact angle, neglected in the present description, will effectively lower θ_m and thus lead to a smaller critical capillary number.

The critical capillary number according to de Gennes (1986) has a structure similar to (91), but predicts a "first order" transition at a *finite* value of θ_{ap}, in disagreement with experiment, cf. Fig. 35. This discrepancy can be traced back to an erroneous speed-angle relationship used by de Gennes (1986), which only agrees with (51) to first order (Eggers, 2004b). As seen from both experimental and theoretical data in Fig. 35, the bifurcation is rather of a saddle-node type (Drazin, 1992). At a speed Ca^* below Ca_{cr}, a new type of solution is predicted and found experimentally (Snoeijer *et al.*, 2006), which consists of a leading capillary ridge, that can climb arbitrarily high up the plate. In fact, if experiments were conducted by slowly increasing the capillary number from below Ca^* (Snoeijer *et al.*, 2006), the solution was always found to jump to the ridge solution. The reason for this discontinuous transition observed by Snoeijer *et al.* (2006) is unknown and warrants further study. In a forthcoming publication (Ziegler *et al.*, 2007), we will investigate the relation of the ridge solution to a new type of film covering the plate, which is distinct from the classical Landau-Levich-Derjaguin film (Deryaguin, 1943; Landau and Levich, 1942).

H. Dewetting

In many recent experiments and applications a uniform liquid layer is laid down on a solid that it does not wet (Seemann *et al.*, 2001b, 2005b). For a review of multi-layer dewetting as well as dewetting of structured surfaces, see (Geoghegan and Krausch, 2003). As a consequence of the non-wetting properties, the film may destabilize to expose "dry" patches, unless it is sufficiently thick to be stabilized by gravity (de Gennes *et al.*, 2003). In many practical cases the system is perturbed by the presence of surface heterogeneities or dust particles, which form the initial nucleus for a hole: "heterogeneous nucleation". If the nucleation is driven by thermal noise, one speaks of "homogeneous nucleation". In both cases the system is separated from its true equilibrium state by an energy barrier: the opening of a small hole costs more energy than is gained by thinning the film.

However, if the film is sufficiently thin (2 - 10 nm) for long-range forces to be important, the system can become *linearly unstable*, so the growth of thermal fluctuations leads to spontaneous destabilization. This scenario has been called "spinodal dewetting", in analogy to the spontaneous decomposition of incompatible bulk phases (Mitlin, 1993).

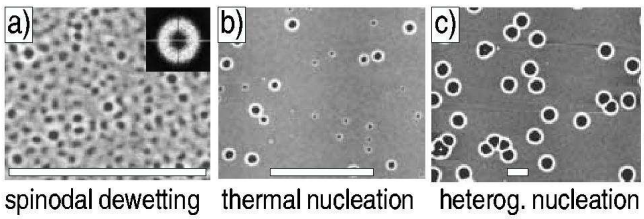

FIG. 36 Dewetting patterns as observed with the AFM. The height scale ranges from black (0nm) to white (20nm) (Seemann *et al.*, 2001a). (a) is typical for spinodal dewetting, (b) shows homogeneous (thermal) nucleation, and (c) heterogeneous nucleation.

To investigate the stability of the film, we consider small perturbations to a film of constant thickness h_0:

$$h(\mathbf{x},t) = h_0 + \epsilon e^{i(\omega t + \mathbf{kx})}. \tag{92}$$

Linearizing the thin film equation (55) in ϵ and using $p = -\gamma\Delta h - \Pi(h)$, one obtains the dispersion relation (Ruckenstain and Jain, 1974; Vrij, 1966)

$$\omega = -\frac{h_0^3\gamma}{3\eta}k^2(k^2 + K_0/\gamma), \tag{93}$$

where $K_0 = V''(h_0)$ is the curvature of the effective interface potential. From (93) one finds the *optimal* or "spinodal" wavelength λ_s, corresponding to the fastest growing mode (Sharma, 1993):

$$\lambda_s = 2\pi\sqrt{-2\gamma/K_0}. \tag{94}$$

Thus if $K_0 < 0$, long wavelength perturbations are unstable, in complete analogy with the Plateau-Rayleigh instability of fluid jets (Eggers, 1997). Given a random disturbance, one will thus observe the most unstable "spinodal" wavelength (94).

Thus in systems with long range forces (21) the film is unstable if $A < 0$, and stable for $A > 0$. In the former case the wavelength scales like $\lambda_s \propto h_0^2$, as is indeed found experimentally (Bischof *et al.*, 1996; Seemann *et al.*, 2001a). In addition, *in situ* AFM scans (Seemann *et al.*, 2001b) confirm the exponential growth (92) of the amplitude of the surface undulation. If on the other hand $A > 0$ one observes nucleation (Brochard-Wyart and Daillant, 1990; Seemann *et al.*, 2001b), where the position of holes is randomly (Poisson) distributed (Jacobs *et al.*, 1998). Fig. 36 illustrates the main mechanisms of instability discussed above.

Combining information gleaned from measuring the instability of a thin film with contact angle data, one obtains a sensitive tool to measure surface potentials (Seemann *et al.*, 2001a), as shown in Fig. 37. For example, by coating a Si substrate with a layer of silicone oxide, a fluid layer of polystyrene (PS) is linearly stable at large distances, but very thin layers are unstable.

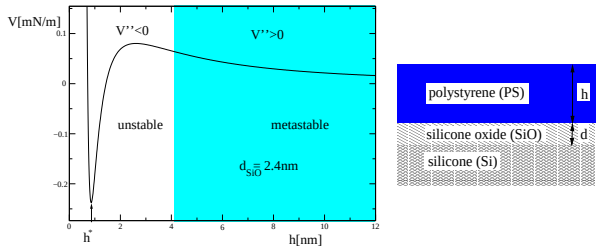

FIG. 37 Reconstructed surface potentials $V(h)$ for PS films on a silicone wafer coated with a layer of SiO of varying thickness d_{SiO} (Seemann *et al.*, 2001a). The fits are to the curve $V(h) = c_i/h^8 + A_{SiO}/(12\pi h^2) + (A_{Si} - A_{SiO})/(12\pi(h + d_{SiO})^2)$, with experimentally determined Hamaker constants. For the particular kind of wafer used, the strength of the short-range interaction is $c_i = 5.1 \times 10^{-77} Jm^6$. The arrow marks the thickness h^* of the microscopic film left behind after dewetting.

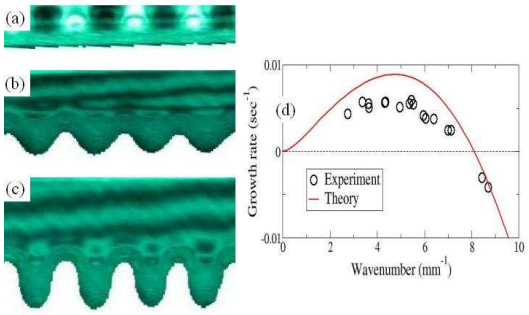

FIG. 38 The driven spreading of a thin film on a horizontal substrate (Garnier *et al.*, 2003). A small sinusoidal perturbation of wavelength $\lambda = 1.4$ mm is imposed optically, which grows into a sequence of fingers of the same wavelength. By applying perturbations of different wave numbers in a series of experiments, the dispersion relation for the instability is measured and is compared with linear stability theory (with no adjustable parameters in the stability analysis).

This is because the Hamaker constant of silicone against PS is positive ($A_{Si} = 1.3 \times 10^{-19} J$), while A_{SiO} is negative ($A_{SiO} = -2.2 \times 10^{-20} J$). The boundary between the spinodal and the metastable regime is determined by $K_0(h_{crit}) = 0$, as illustrated in Fig. 37, and leading to a phase diagram confirmed by experiment (Seemann *et al.*, 2001b).

Work concerning both the initial instability and the subsequent dynamics is reviewed in Thiele (2003). More recently, attention has focused on the non-linear dynamics that follows the initial growth of perturbations described above. In Becker *et al.* (2003) numerical simulations of (55) were compared to experimental dewetting patterns. To describe the surface potential, independently determined experimental parameters were used as described above. The temporal evolution was followed by taking temporal series of AFM scans of PS films beading off a SiO surface. For both cases of spinodal dewetting and nucleation, good qualitative agreement between theory and simulation was found, but dewetting proceeds faster than predicted by theory. This mismatch in the timescales is corrected if the effect of noise is taken into account in the thin-film equations (Grün *et al.*, 2006).

Analytical studies have focused on the growth of individual holes in the nucleation regime (de Gennes *et al.*, 2003), whose radius increases linearly in time (Redon *et al.*, 1991). The excess fluid collects in a rim, whose size is set by mass conservation. If the fluid is very viscous (as is the case for most polymer films), the dominant retarding mechanism is viscous dissipation near the contact line. By balancing this with the free energy gained, one finds (de Gennes *et al.*, 2003) $Ca_{ret} \propto \theta_{eq}^3$ for the capillary number based on the speed of retraction, where the constant can vary logarithmically based on the geometry of the rim. This is of course analogous to (91) for the maximum speed of retraction of a contact line.

A host of more recent papers have addressed the effect of non-Newtonian and visco-elastic behavior (Münch *et al.*, 2006; Rauscher *et al.*, 2005; Saulnier *et al.*, 2002b; Vilmin and Raphaël, 2005; Vilmin *et al.*, 2006), for example on the growth velocity of holes. In addition, polymer films can also exhibit strong slip (de Gennes *et al.*, 2003; Fetzer *et al.*, 2005; Münch *et al.*, 2006). As a result, the speed of the dewetting front can decrease significantly (Damman *et al.*, 2003). A considerable body of work has also been devoted to the shape of the profile near the dewetting front (Fetzer *et al.*, 2005; Herminghaus *et al.*, 2002; Münch *et al.*, 2005; Rauscher *et al.*, 2005; Saulnier *et al.*, 2002a), and in particular the question whether the film thickness decreases monotonically from the rim or whether there are oscillations. One challenge lies in the fact that most coatings are made up of polymers, and thus exhibit non-Newtonian fluid properties, no longer described by (55). Instead, a shear-dependent viscosity (Saulnier *et al.*, 2002a) or viscoelasticity (Herminghaus *et al.*, 2002) may explain the observed behavior. However, experiments by Fetzer *et al.* (2005) show a disappearance of oscillations for fixed fluid properties, but increasing slip length. Thus it appears that a difference in boundary conditions alone, but staying within the Newtonian realm, is sufficient to explain the observed morphological transitions.

I. Linear instabilities of driven contact lines

An example of the linear instability of a driven contact line is shown in Fig. 38 (left), where the contact line is driven by Marangoni forces, originating from a temperature gradient. A small initial perturbation of a given wavelength is imposed, which eventually grows into fingers. Similar instabilities are observed experimentally for contact lines driven by body forces (gravitationally (de Bruyn, 1992; Huppert, 1982a; Jerret and

de Bruyn, 1992; Silve and Dussan V., 1985) or centrifugally (Fraysse and Homsy, 1994; Melo *et al.*, 1989)), or by surface forces (Marangoni effects induced either by temperature (Cazabat *et al.*, 1991) or surface tension (Troian *et al.*, 1989a) gradients), or combinations thereof (Bertozzi *et al.*, 1998; Kataoka and Troian, 1998). The gravity and the Marangoni-driven cases are reviewed in Kondic (2003) and Grigoriev (2005), respectively. If the ridge is very narrow, either a varicose, or at higher inclination angles, a zigzag instability may be observed (Thiele and Knobloch, 2003), effectively coupling the motion of the front and back contact lines.

The crucial feature which is common to all these flows is the development of a capillary ridge near the contact line, which occurs naturally in the presence of driving: the driving forces supply an extra amount of fluid, which accumulates behind the contact line. Instability occurs if the ridge is sufficiently pronounced (Kataoka and Troian, 1997; Spaid and Homsy, 1996; Troian *et al.*, 1989b), a peculiar exception being the case of two competing driving mechanisms (Bertozzi *et al.*, 1998), for which even "fat" ridges are stable. Energy is supplied to the instability by the increased gravitational pull of thickened ridge regions (or increased Marangoni forcing in the case of the surface instability). The more massive thick regions are pulled forward, enhancing the effect and causing a finger to grow. If the wavelength in the spanwise direction is too small, too much surface is created in the spanwise direction, which provides a lower cutoff for the disturbance wavelength.

To outline the theoretical analysis it is simplest to consider flow down an incline at angle α, described by (55) with $p = -\gamma\triangle h + \rho g(\cos\alpha h - \sin\alpha x)$. The direction down the slope is measured by the coordinate x, y goes in the spanwise direction. The front of the falling film forms a traveling wave with envelope $H_0(x/\ell - ct) = h(x,t)/H_N$, where $\ell = H_N/(3Ca)^{1/3}$ (Troian *et al.*, 1989b) sets the characteristic size and H_N is the thickness of the film. A linear analysis around H_0 (Troian *et al.*, 1989b) yields $\lambda \approx 14\ell$ for the most unstable wavelength of the perturbation. To leading order in the wavenumber q, one finds for the largest eigenvalue ω_{max} of the perturbation that

$$\omega_{max} = q^2 \int_0^\infty H_0(\bar{x})(H_0(\bar{x})^2 - 1)d\bar{x} + O(q^4), \qquad (95)$$

and similar results are available for Marangoni flow (Grigoriev, 2003). This expression clearly shows that the growth rate of a long wavelength perturbation only becomes positive if there is a sufficiently pronounced ridge with $H_0 > 1$.

Comparisons of experimental base-state profiles with theory show good agreement (Bertozzi *et al.*, 1998; Garnier *et al.*, 2003; Sur *et al.*, 2003), as do experimental measurements of the most unstable wavelength both for gravitationally (Johnson *et al.*, 1999) and Marangoni driven (Kataoka and Troian, 1997) flow. However, as shown in Fig. 38 (right), there is significant disagreement between measurements of the actual growth rates as a function of wave number and theory (de Bruyn, 1992; Garnier *et al.*, 2003). In particular, there are cases where theory predicts the front to be stable, while experimentally an instability is observed (de Bruyn, 1992).

Bertozzi and Brenner (1997) proposed that the origin of the discrepancies in the gravity-driven case is to be found in the *non-normality* of the eigenvalue problem, which permits a large amount of *transient* growth to occur. Thus in principle even a linearly stable mode can become unstable owing to transient growth, if it has grown large enough for non-linear effects to kick in and to support further growth. However, there is considerable theoretical disagreement about the importance of transient growth for both gravity-driven (Bertozzi and Brenner, 1997; Davis and Troian, 2003b) and surface-tension-driven flow (Davis and Troian, 2003a). Grigoriev (2005) revisits the controversy and finds that results obtained with different models generally agree for perturbations applied *behind* the contact line. To realize the strong growth found by Bertozzi and Brenner (1997), perturbations must be applied to the precursor film *in front of* the driven contact line.

As mentioned above, a substantial capillary ridge can be consistent with a *stable* contact line if two competing forcings are of a similar magnitude (Bertozzi *et al.*, 1998). In this case the moving front acquires a special "undercompressive" shock structure, associated with a non-monotonic flux function, which is analyzed in detail in Bertozzi *et al.* (1999). This new type of base solution is much more stable against transversal perturbations than the conventional ridge, created by a single driving force.

The *nonlinear* growth of fingers has been investigated computationally in Kondic and Bertozzi (1999), Eres *et al.* (2000), and Thiele *et al.* (2002). Using a weakly non-linear analysis, Kalliadasis (2000) shows that the evolution of fingers is controlled by a Kuramoto-Sivashinsky-type equation. In Kondic and Bertozzi (1999), the question of transient growth is re-examined, showing that small precursor-film perturbations can amplify. In Eres *et al.* (2000), the growth of fingers is followed far beyond the linear regime, (cf. Fig. 38(c)), and good agreement with experiment (Cazabat *et al.*, 1992) is found.

Considerable effort has also been devoted to the spreading and the instability of surfactant-laden films and droplets (Borgas and Grotberg, 1988; Cachile *et al.*, 2002c; Jensen and Grotberg, 1992; Matar and Troian, 1999; Troian *et al.*, 1989b; Warner *et al.*, 2004), which can lead to film rupture, fingering instabilities, and fractal boundaries. A recent detailed analysis of the linear and non-linear stability of a surfactant-laden drop (Warner *et al.*, 2004) concludes that the modification of the base profile by the surfactant has to be taken into account. However, in view of the complexity of the problem, a quantitative comparison with experiment does not seem to be on the horizon.

J. Hot topics

1. Corners and air pockets

For many practical applications such as coating, it is of crucial importance to understand the maximum speed at which a plate being withdrawn or plunging into a liquid is covered exclusively by one phase. In III.H we calculated a critical speed (91) above which a *straight* receding contact line can no longer be maintained. As illustrated in Fig.39, however, a different scenario is possible if for example the contact line is pinned at the edge of the plate: in both the receding (Blake and Ruschak, 1979; Podgorski *et al.*, 2001) and the advancing (Blake and Ruschak, 1979; Burley and Kennedy, 1978) case, the contact line can incline relative to its direction of motion at a well-defined angle; contact lines inclined in opposite directions meet at a sharp corner with an opening half-angle ϕ. If the system is sufficiently wide, the contact line assumes an irregular sawtooth shape (Blake and Ruschak, 1979).

The inclination permits the contact line to remain stable at higher speeds, since the speed U_n *normal* to the contact line is decreased according to $U_n = \sin\phi U$. Above yet another critical speed U_{riv}, the corner ejects a rivulet (cf. Fig. 39(b)), so the plate can no longer be dry above U_{riv}. An analogous sequence of transitions is observed for a drop running down an inclined plane, cf. Fig. 40. Qualitatively similar structures have been seen in the simulations reported in Thiele *et al.* (2002) and Schawrtz *et al.* (2005). The formation of rivulets is remarkably similar to air entrainment from free-surface cusps (Lorenceau *et al.*, 2004, 2003), tip-streaming of air bubbles (de Bruijn, 1993; Taylor, 1934), electric jets from Taylor cones (de la Mora and Loscertales, 1994), or selective withdrawal (Cohen *et al.*, 2001; Courrech du Pont and Eggers, 2006). However, alternative mechanisms are possible, as air pockets can also nucleate at a distance away from the tip (Burley and Kennedy, 1978).

Limat and Stone (2003); Snoeijer *et al.* (2005); Stone *et al.* (2002) found that the triangular shape of a receding contact line is described by a similarity solution

$$h(x,y) = Ca^{1/3} x H(y/x) \tag{96}$$

of (55),(57) with $\lambda = 0$, where x is measured in the streamwise direction. However, Huh and Scriven's paradox implies that (96) breaks down at the contact line; it has to be matched to a contact line solution which includes the slip. Recently, such a matching was performed (Snoeijer *et al.*, 2007) making the additional simplifying assumption of small ϕ, which is valid close to the transition toward a rivulet. In this limit the profile in the transverse direction is approximately parabolic, and by averaging over cross-sections an effective one-dimensional description is obtained, with x the independent variable. The Cox-Voinov relationship (51) is used in the direction normal to the contact line. This is valid even in the receding case, since the normal speed remains significantly below the critical value Ca_{cr} (Eggers, 2005b; Snoeijer *et al.*, 2007).

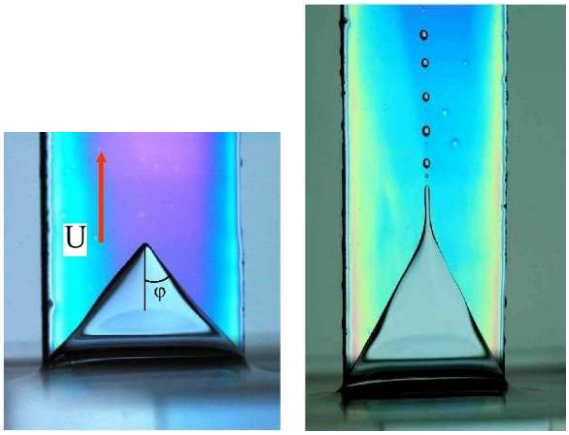

(a) (b)

FIG. 39 A plate being withdrawn from a bath of viscous liquid, with the contact line pinned at the edge of the plate (Delon, 2007). (a): below the rivulet transition the contact line forms a corner. (b): above the transition a rivulet comes out of the tip of the corner, and eventually decays into droplets.

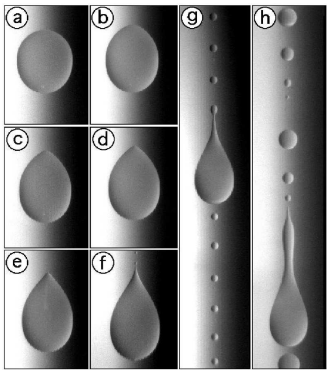

FIG. 40 Drops of silicone oil running down planes at increasing inclination (Podgorski *et al.*, 2001). As the velocity increases, a corner first forms, which becomes unstable to the ejection of drops at even higher speeds.

Using $\epsilon = 1/\sqrt{\ln(L_{out}/\lambda)} \approx 0.3$ as a small parameter, one obtains the following relationship between the speed and the opening angle:

$$Ca = \frac{2\theta_{eq}^3 \phi}{35 + 18(\phi/\epsilon)^2}, \tag{97}$$

shown as the solid line in Fig. 41. The most important feature is that there exists a *maximum* speed Ca_{riv} above which no corner solution can exist:

$$Ca_{riv} = \frac{\epsilon \theta_{eq}^3}{3\sqrt{70}}. \tag{98}$$

Above this speed, rivulets are formed. A simple argument shows (Snoeijer *et al.*, 2007) that only the branch to the right of the maximum is physical. The experimental data collapse nicely under the rescaling suggested by

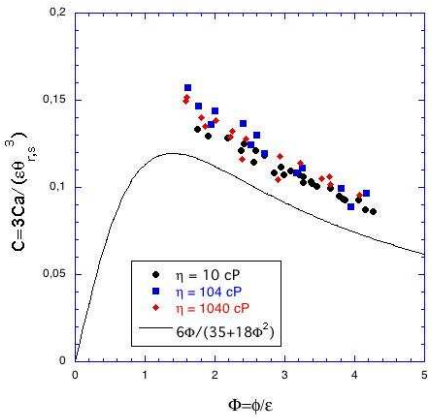

FIG. 41 The normalized speed $\mathcal{C}$ of the drop as function of the normalized opening angle Φ. Symbols represent rescaled experimental data for silicone oils with viscosities 10, 104, and 1040 cP. The data were rescaled using the receding static contact angle θ_r.

theory. The measured speeds are about 30% too high for a given angle, which is acceptable given that the asymptotic parameter ϵ is not very small. Note that (97) is different from the relationship suggested originally by Blake and Ruschak (1979) (tested experimentally in Blake and Ruschak (1979); Petrov and Sedev (1985)), based on the assumption that the speed normal to the contact line be *constant*. However, a constant normal velocity is recovered from (97) for large ϕ/ϵ.

For $Ca > Ca_{riv}$, the equation describing the contact line shape has to be solved with a boundary condition corresponding to a rivulet of constant width (Snoeijer *et al.*, 2007). Curiously, it is found that the rivulet width cannot be fixed by local parameters alone, but some external length scale is needed. In the case of the running drop treated experimentally in (Snoeijer *et al.*, 2007) (cf. Fig. 40), this length is the drop size. Good agreement with experimental measurements of the rivulet width was found, except very close to Ca_{riv}, where the width is expected to go to zero. A possible reason is that near the transition drops are ejected almost directly from the tip, while theory does not consider the secondary "pearling" instability of the rivulet.

A similar sequence of instabilities occurs if a liquid is *advancing* over a solid, but at much higher speed. Thus there is a maximum speed $U_{cr}^{(a)}$ for the motion of a straight contact line, and a maximum speed $U_{riv}^{(a)}$ at which a corner can move without ejecting a "rivulet". However, these transitions are much less understood. Proposals to increase critical speeds (some of which quite successful) are the subject of many patents (Deneka *et al.*, 1988; Jochem and van der Ligt, 1987). However, in the absence of an understanding of the forced wetting

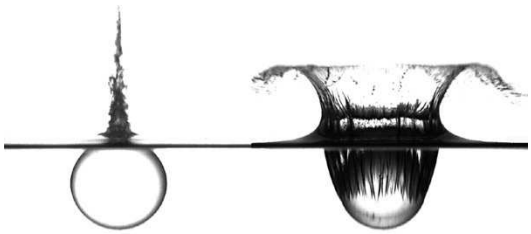

FIG. 42 The splash produced by a sphere impacting on water is caused by the contact line of the solid-air-water interface becoming unstable, so a sheet of water detaches from the solid (Duez *et al.*, 2007). On the left, no instability occurs for a static contact angle of $\theta_{eq} = 15^\circ$, while for $\theta_{eq} = 100^\circ$ a splash is produced.

process, efforts to increase critical speeds at present proceed on a trial-and-error basis. Reviews of the stability problem from an applied point of view are found in Blake (1993); Blake and Ruschak (1997); Kistler (1993).

Experimentally, $U_{cr}^{(a)}$ corresponds to $\theta_{ap} = 180^\circ$ (Burley and Kennedy, 1976a,b; Inverarity, 1969a,b) or $\theta_{ap} \gtrsim 160^\circ$ (Blake and Ruschak, 1979; Simpkins and Kuck, 2003). The former condition was used by Duez *et al.* (2007) to predict the critical impact speed at which splashing occurs when a sphere impacts on a deep pool of water. This criterion leeds to a much smaller critical speed if the wetting angle is already large, see Fig. 42. If the fluid is more viscous, there exists an analogy to the disappearance (Eggers, 2001; Lorenceau *et al.*, 2004, 2003) of cusp solutions (Jeong and Moffatt, 1992; Joseph *et al.*, 1991) on free surfaces, driven by lubrication pressure inside the cusp. Indeed, Jacqmin (2002) adds air pressure to a contact line solution appropriate for $\theta_{eq} = 180^\circ$ (Benney and Timson, 1980; Mahadevan and Pomeau, 1999), to argue that the solvability of gas in the fluid increases critical speeds. Experimentally, unusually high coating speeds have been observed using highly solvable gases (Deneka *et al.*, 1988), or by pressurizing the container (Simpkins and Kuck, 2003).

2. Spreading of complex fluids: polymers and surfactants

Efficient spreading is critical to most painting, coating, and solution delivery applications, Drop spreading can be improved by adding a surface-active agent to the liquid. However, little fundamental work has been devoted to understanding the influence of complex fluids on the *dynamics* of spreading. The main conclusion of different experiments using different types of complex fluids (mainly surfactant and polymer solutions) is the perhaps surprising robustness of Tanner's law; most deviations from it are very small, the only exception being "superspreading" surfactants discussed below.

For the important case of liquids on *hydrophobic* surfaces, one effect of surfactants is to lower γ sufficiently to

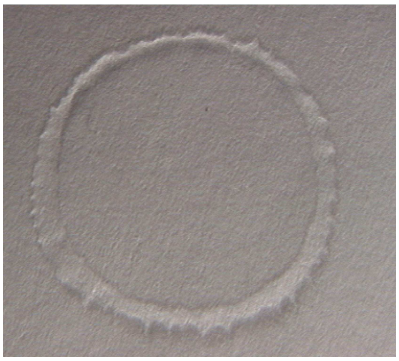

FIG. 43 Photograph of a spreading trisiloxane solution droplet at high surfactant concentration for which the radius increases linearly in time; clearly the droplet is no longer a spherical cap.

make the spreading coefficient positive; for this the surfactant concentration must typically be above the critical micellar concentration (cmc). If $S_i > 0$, the evolution of the radius can be fitted to Tanner's law (10), but the prefactor is typically 25 % smaller than a Newtonian reference system with the same viscosity and equilibrium tension (Rafaï *et al.*, 2002). Namely, when new interface is created during the spreading, surfactant needs to be transported to the interface in order to lower the tension. As the creation of new area is faster than the arrival of surfactant molecules to the interface, this can decrease the dynamic spreading coefficient and slow down the droplet spreading dynamics.

For one specific class of (trisiloxane) surfactants around the cmc concentration, however, the spreading is enhanced strongly in that the *exponent* n of the spreading law $R \propto t^n$ is increased (see Hill (1998) for a recent review). For the highest bulk concentrations, a linear relation $n = 1$ is obtained, a power one order of magnitude larger than that of Tanner's law (Rafaï *et al.*, 2002). This so-called superspreading suggests that the motor driving the spreading is different; Fig.43 shows a picture of a "superspreading" droplet that illustrates this point. Explanation of this effect poses a challenge as both dynamic surface tension effects and inertial forces can only slow down the dynamics. Although Marangoni effects are generally believed to be the cause for superspreading, the mechanism remains elusive, and merits further theoretical and experimental attention.

A less obvious way to intervene in the spreading dynamics is to change the bulk rheology of the fluid; this is mostly done by using polymeric additives. The dynamics of such non-Newtonian liquids is far less understood than their Newtonian counterpart; the main challenge is that the constitutive equation is in general non-linear (Rosenblat and Davis, 1985). For a non-Newtonian bulk rheology, most theoretical studies have used simple constitutive equations, focusing on shear-thinning behavior (Betelu and Fontelos, 2003, 2004; Gorodtsov, 1990; King, 2001a,b; Neogi and Ybarra, 2001; Rafaï *et al.*, 2004b; Starov *et al.*, 2003): the viscosity decreases with increasing velocity gradient in the fluid. Since the velocity gradient becomes large near the corner of the droplet, the viscosity becomes small there: shear-thinning was proposed to suppress the singularity at the contact line (Ansini and Giacomelli, 2002; Carré and Eustache, 1997, 2000; Carré and Woehl, 2002; Rafaï *et al.*, 2004b; Weidner and Schwartz, 1993).

Experimentally, the spreading of a shear-thinning fluid is found to be slightly slower than that of a Newtonian fluid: the power in the spreading law is found to be slightly smaller than 0.1, and decreases with increasing shear thinning (Rafaï *et al.*, 2004b). This agrees with detailed calculations of the spreading of power-law fluids, for which $\eta = a\dot{\gamma}^{-\alpha}$, where $\dot{\gamma}$ is the shear rate. Estimating the latter as $\dot{\gamma} \propto \dot{R}/(\theta_{ap}R)$, one finds (Betelu and Fontelos, 2004; Rafaï *et al.*, 2004b):

$$R = C\left(\gamma t^{1-\alpha}/a\right)^{1/(10-3\alpha)}. \qquad (99)$$

The first attempts to account for other non-Newtonian properties concluded that normal stress effects were unimportant (Neogi and Ybarra, 2001; Rosenblat and Davis, 1985). However, more recently is was shown that they do in fact matter, but that once more deviations from Tanner's law are small. The normal stress N_1 is related to the shear rate via the first normal stress coefficient Ψ_1: $N_1 = \Psi_1\dot{\gamma}^2$ (Larson, 1999). The normal stresses act in a similar way as the capillary pressure in driving the flow. Their contribution to the total pressure gradient can be estimated as $N_1 \sim \psi_1(\dot{R}/h)^2$, $\dot{R}$ being the contact line velocity and h the typical drop height. This leads to just a logarithmic correction to Tanner's law (Boudaoud, 2007; Rafaï *et al.*, 2004b):

$$R \approx V^{3/10}\left(\frac{\gamma t}{\eta}\right)^{1/10}\left(\ln\frac{\eta t}{10\psi_1}\right)^{-1/10}. \qquad (100)$$

For polymer solutions that exhibit normal stress effects but no shear thinning, fits to $R(t)$ indeed give spreading exponents slightly smaller than 1/10, consistent with a logarithmic correction (Rafaï *et al.*, 2004b). Thus in contrast to naive expectation, both shear thinning and normal stress effects tend to slow down the spreading of a drop. This can be understood qualitatively as follows. Both effects accelerate the flow near the contact line, and both effects do so more strongly as the shear rate is higher. Because the shear rate increases upon approaching the contact line, the parts closest to the corner will move faster, and the apparent contact angle decreases. Since the spreading velocity varies with the contact angle, the lowering of the contact angle decreases the driving force for spreading, and the contact line is slowed down, in agreement with the experimental observations.

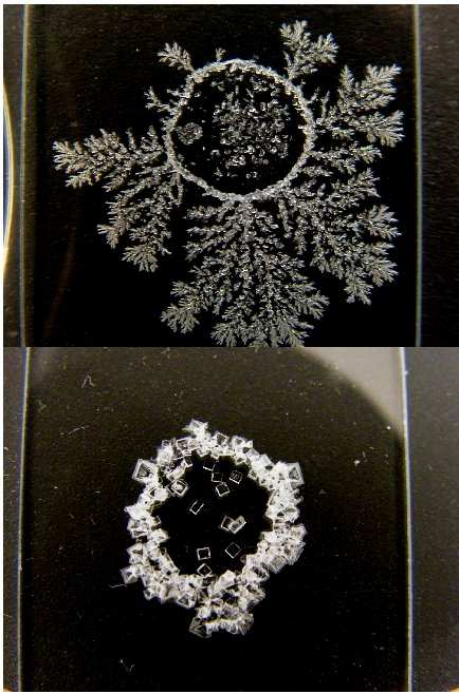

FIG. 44 Deposit from an evaporating droplet of two different salt solutions, top: Na_2SO_4, bottom: $NaCl$. This shows that the wetting properties of the salt crystals are important for determining where crystals form (Shahidzadeh *et al.*, 2008).

3. Evaporating drops

The seemingly simple problem of an evaporating droplet has attracted a great deal of attention over the past few years. The two situations that have been studied most are the "coffee drop" problem (Deegan *et al.*, 1997), in which a droplet is deposited on a rough substrate to which its contact line remains fully anchored during the evaporation, and droplets of completely wetting liquids deposited on a perfectly smooth surface (Cachile *et al.*, 2002a,b; Poulard *et al.*, 2003; Shahidzadeh-Bonn *et al.*, 2006). For the coffee stain problem , the reason that a dried-out drop of coffee leaves a circular mark on the table is that the evaporation drives a capillary flow which transports material from the center towards the edge, where it accumulates (Deegan *et al.*, 1997). This requires that the contact line remains pinned during the whole drying process. Subsequent research revealed that this is only one of the many patterns that may form during droplet drying. For very volatile liquids, for instance, a deposit may even form at the center of the drying drop (Hu and Larson, 2006) due to convection effects within the drop (Ristenpart *et al.*, 2007). Depending on the solute, a wide variety of different patterns may be obtained also (Deegan, 2000; Deegan *et al.*, 2000). Figure 44 shows an example of drying water droplets with different salts that crystallize during the drying; the crystals may either choose to form at the contact line ($NaCl$) or within the precursor film (Na_2S0_4), leading to very different deposits. Even periodic patterns can be obtained, and a great deal of research has been devoted recently to using drying droplets to obtain periodic nano-patterning using either molecules (Maheshwari *et al.*, 2008; van Hameren *et al.*, 2006), carbon nanotubes (Li *et al.*, 2006) or colloids (Lin *et al.*, 1999). It is not always clear what the mechanisms of formation for the different deposits are; for the periodic or quasi-periodic deposits a stick-slip motion of the contact line was proposed (Abkarian *et al.*, 2004; Maheshwari *et al.*, 2008; Rio *et al.*, 2006), but other mechanisms have been invoked also. This therefore remains an area for future research.

A theoretical understanding of evaporating drops is complicated by the fact that the form of the droplet during the evaporation is a priori unknown, and due to the large number of physical effects to be taken into account. For instance, the evaporation results in a decrease of the temperature within the droplet, which leads to both a heat flux from the substrate into the droplet, and to Marangoni effects (flows driven by surface tension gradients) if the temperature within the droplet is not uniform (Davis, 1987; Sultan *et al.*, 2004). More generally, hydrodynamic flows within the droplet have to be taken into account. The latter are responsible for the circular deposit formation when the contact line remains anchored. The surface to volume ratio being larger near the edge of the droplet, the evaporation leads to a flux of liquid from the center towards the edge. This flux brings along material that is deposited at the circular edge (Deegan *et al.*, 1997).

For the evaporation of a perfectly wetting liquid on a perfectly flat surface (e.g., droplets of water or hexane on mica), the effects of the anchoring of the contact line are small. Interestingly, the non-equilibrium contact angle θ_{ne} of a completely wetting but evaporating droplet can be nonzero. The evaporation can even lead to the dewetting of a liquid that completely wets the substrate in equilibrium (Elbaum and Lipson, 1994). It is not clear how to treat such a non-equilibrium situation, and the calculation of the contact angle of evaporating drops is a subject of debate (Bonn and Meunier, 1997; Bourges-Monnier and Shanahan, 1995). When depositing a drop which is perfectly wetting it first spreads on the surface. However, since the droplet evaporates at the same time, its radius starts to decrease shortly afterwards, to vanish at a time we denote by t_0 (Deegan *et al.*, 2000). Neglecting thermal and Marangoni effects, it is known that the evaporation rate is proportional to the perimeter of the droplet $dV/dt \propto -2\pi R$ (Deegan *et al.*, 2000). *Assuming* that θ_{ne} is constant and using $V \propto R^2 h \propto R^3 \theta_{ne}$ it follows that $R \propto (t - t_0)^{1/2}$ (Deegan *et al.*, 2000).

The experimental values for different simple liquids are indeed all close to an exponent of 1/2, in agreement with this simple argument. The experimental values do however deviate in a non-trivial way: the exponents found are slightly smaller than 1/2, the reason for which is still unclear (Cachile *et al.*, 2002a,b; Poulard *et al.*, 2003). Even more intriguingly, the value reported for water is

0.6 (Deegan, 2000; Shahidzadeh-Bonn *et al.*, 2006). Very recent experiments (Shahidzadeh-Bonn *et al.*, 2006) suggest that the difference might be due to the fact that the water vapor above the droplet is being convected away, because water vapor is lighter than air, contrary to the vapor of all other liquids used in the experiments. Because of the importance of the evaporation of water droplets for instance for industrial cooling applications and for the climate, this merits further investigation. Recent theory suggests that no simple similarity solution exist for the evaporating droplet problem, and so the experiments probe effective exponents (Poulard *et al.*, 2005).

IV. DISORDERED SOLID SURFACES

A. How to model a real solid surface?

The two most common heterogeneities that cause the contact angle hysteresis are chemical heterogeneities and roughness. In the first case, the surface is entirely characterized by the spreading coefficient $S(x, y)$ which now depends on the position (x, y) on the substrate, allowing one to define a local value of the contact angle. In the laboratory, systems with chemical disorder are often obtained by partially coating the surface of a highly wettable substrate such as glass by a low surface energy film, for instance a perfluorinated surfactant (Decker and Garoff, 1997) (see Johnson and Dettre (1993) for further references).

In such experiments, the treatment changes both the mean value of the wettability and the hysteresis of the substrate. In most cases, the disorder is poorly characterized since only the mean coverage of the substrate is known. In particular, the typical length scale of the disorder (if any such length scale exists) is unknown. Presumably, a better characterization will be available in the near future owing to the use of local microscopy techniques. For instance, AFM imaging of the very weak heterogeneities of silanized substrates has been used to successfully explain the shape of nanodroplets (Checco *et al.*, 2003).

To manufacture surfaces that are better characterized, model surfaces can be produced using photolithographic techniques. For example, the substrates used by Moulinet *et al.* (2002, 2004a) are made of random patches of chromium on glass (cf. Fig 9). These surfaces are however not perfectly flat since the chromium defects deposited on the glass have a thickness of the order of a few hundred Angstroms. However, their thickness is much smaller than their lateral size (a few microns), so that the effects of the chemical heterogeneity should largely dominate those due to the roughness. The use of such model substrates have permitted a precise characterization of the contact line roughness, as discussed below.

Independent of the origin and the length scale of the chemical heterogeneities, one anticipates that in simple cases the properties of the substrate can be described by a few parameters, namely the mean value of the spreading coefficient $\overline{S}$, the amplitude of the disorder $\Delta S \equiv \sqrt{(S-\overline{S})^2}$ and a correlation length ξ giving the characteristic length scale of the disorder. If the substrate is made of a surface with spreading coefficient S_0 which is covered by well-defined defects with spreading coefficient S_d, the natural parameters are rather the defect size d and the defect force $(S_d - S_0)d$, as will be discussed in detail in the next section. The important point here is that, once the local spreading coefficient $S(x, y)$ is known for all positions on the surface, the local force balance on the contact line can easily be written down as a local version of Young's law, provided of course the surface is flat. From this point of view, the second case of rough substrates is much more difficult to handle. A phenomenological attempt to understand how roughness affects wetting is contained in Wenzel's equation (44), discussed in section II.D.2. This relation for rough surfaces is similar to the Cassie-Baxter relation (13) for chemically heterogeneous substrates: it provides a prediction for the equilibrium state, which is usually out of reach, but does not tell us anything about the hysteresis.

In order to understand how the roughness can lead to hysteresis, let us consider the simplest geometry: a surface $z(y)$ with grooves parallel to the contact line (assumed along Oy). Applying Young's law leads to a local contact angle θ_{eq} between the liquid-vapor interface and the substrate. However, on the average, the contact angle θ between the liquid-vapor interface and the average surface is $\theta = \theta_{eq} - dz/dx$, where dz/dx is the local slope of the interface. This equation shows that the substrate is more or less wettable depending on the sign of dz/dx.

It was shown by Cox (1983) that indeed, to first order in the local slope, the roughness can be described in terms of a local spreading coefficient. However, for a large amplitude of the roughness, the situation is much more complicated and can lead to non-intuitive behavior of the contact angle. For instance, it has been observed that the contact angle hysteresis $\theta_a - \theta_r$ can be a non-monotonic function of the roughness (Ramos *et al.*, 2003); this was explained by the existence of air bubbles trapped between the liquid and the substrate. The encapsulation of air therefore provides us with a completely different way of intervening in the contact angle. It was shown recently that by a clever tuning of the surfaces, superhydrophobic surfaces with contact angles close to 180° for water can be created by trapping a significant amount of air between the liquid and the substrate (Bico *et al.*, 2001).

In what follows, we will discuss chemical and physical heterogeneities in the same manner. Since it is the simplest case to understand theoretically, we will restrict the discussion to the situation in which the inhomogeneous wetting properties of the substrate can be described by $S(x, y)$ or equivalently by a *local* equilibrium contact an-

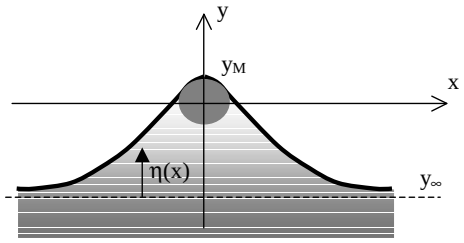

FIG. 45 A contact line pinned on a single defect

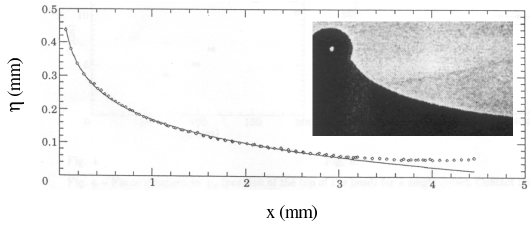

FIG. 46 Receding meniscus pinned on a defect. The experimental shape of the contact line (dots) is well fitted by (103) with $L = 2.4\,\mathrm{mm}$ (from Nadkarni and Garoff (1992)).

gle θ_{loc} defined by: $S(x,y) = \gamma(\cos\theta_{loc} - 1)$.

We will focus most of the discussion on macroscopic or mesoscopic defects ($d > 10\,\mathrm{nm}$). This is necessary if we want to describe the disorder of the substrate in terms of a local spreading coefficient. This restriction also enables us to neglect the thermal noise which is much smaller than the "quenched" noise due to the disorder. This is easily checked in experiments on patterned substrates, where the motion of the contact line is deterministic: when repeating experiments on the same substrate, the line always remains pinned on the same defects and therefore in the same configuration (Prevost *et al.*, 2002).

B. The single defect case

We first discuss the simplest situation of a single defect which permits to understand how hysteresis arises from the interplay of the defect pinning force and the contact line elasticity. A natural extension is the case of sufficiently dilute defects.

1. Pinning on a single defect

The pinning on a single defect has been discussed in an important paper by Joanny and de Gennes (1984). Consider a contact line whose average direction is along the x axis (cf.Fig. 45). Its distortion $\eta(x)$ with respect to its asymptotic position y_∞ is due to a defect of characteristic size d located at $x = 0, y = 0$. Because of the defect, the contact line is submitted to a total extra capillary force:

$$F_d = \int [S(x, \eta(x) + y_\infty) - S_0] dx, \qquad (101)$$

where S_0 is the spreading coefficient of the bare substrate, and θ_{eq} denotes the corresponding contact angle. The integral is dominated by the central region $x \sim d$: F_d depends mainly on the position y_M of the line in this region, hence y_M has to be determined as a function of y_∞. Note that the maximum value of F_d is on the order of $F_{max} = d(S_d - S_0)$ where S_d is the spreading coefficient on the defect.

The deformation of the meniscus induces an elastic restoring force $f_{el}(x)$ per unit length, where to first order in deformation,

$$f_{el}(x) = \frac{\gamma \sin^2\theta_{eq}}{\pi} \int \frac{\eta(x')}{(x-x')^2} dx' \qquad (102)$$

(we will use a lower case f for a force per unit length, and F for an actual force). This expression underlines the non-local character of the contact line elasticity, which results in the distortion of the whole meniscus. Of course, a small cutoff length scale ($\sim d$) is necessary to prevent the singularity that occurs for $x' \to x$. The deformation of the contact line extends up to a macroscopic cut-off length L, which is usually taken to be the capillary length ℓ_c for large enough drops.

It then follows that at equilibrium, the response $\eta(x)$ to the localized force F_d is:

$$\eta(x) = \frac{F_d}{\pi\gamma \sin^2\theta_{eq}} \ln(L/|x|). \qquad (103)$$

The logarithmic shape of the meniscus was confirmed experimentally, see Fig. 46 (Nadkarni and Garoff, 1992). The maximum deformation $\eta_M = y_M - y_\infty$ is reached for $x \sim d$ so that $\eta_M = \eta(d)$. Consequently the contact line behaves as a spring: $F_d = K\eta_M$, with a spring constant (the stiffness of the contact line) $K \equiv \pi\gamma \sin^2\theta_{eq}/\ln(L/d)$.

We are now in a position to determine y_M as a function of the position y_∞ far from the defect, given the pinning force $F_d(y_M)$ of the defect, which is determined by its shape. The force balance

$$K(y_M - y_\infty) = F_d(y_M) \qquad (104)$$

is best understood by considering the graph shown in Fig. 47. When the defect is very smooth, the equation has only a single root and the shape of the contact line is the same, not depending on whether the contact line is advancing or receding. Such defects are called "weak" in the language of random fields. For patterned substrates, $S(x,y)$ is discontinuous and the defects are strong ("mesa" defects in de Gennes' words). In this case, (104) has three roots, and the system displays contact angle hysteresis. In an advancing experiment, the line is initially at $y_\infty < 0$ and y_∞ increases. The position y_M of the center of the line is close to y_∞ until y_∞ reaches a position y_a where the center of the line jumps forward

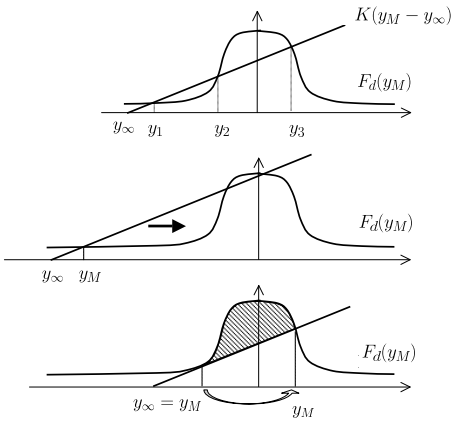

FIG. 47 Distortion of the contact line at equilibrium for a strong defect. Upper graph: for a given y_∞ there may be three equilibrium positions of the contact line, among which one (y_2) is unstable. Middle graph: for an advancing line far enough from the defect, $y_M \simeq y_\infty$. Lower graph: When $y_\infty = y_a$, y_M jumps forwards; the energy dissipated in the jump is the hatched area.

over the defect. In a receding experiment, a backwards jump occurs for a position $y_r < y_a$. Note that the maximum distortion y_r measured in a receding experiment on a wettable defect ($S_d = 0$) is:

$$y_r/d = \frac{1 - \cos\theta_e}{\pi \sin^2\theta_{eq}} \ln(L/d). \tag{105}$$

It follows that the maximum distortion is always at most of the order of the defect size.

The energy W_a dissipated in an advancing jump of the contact line is shown as the hatched area in Fig. 47; a similar construction can be done for the receding jump which dissipates W_r. For a strong defect, one finds:

$$W_a \sim W_r \sim [(S_d - S_0)d]^2/(\gamma \sin^2\theta_{eq}). \tag{106}$$

2. Dilute defects

Consider now a surface with a small but finite density n of defects. Strictly speaking, defects can only be considered as independent if the distance $1/nd$ between two defects along the line is larger than the capillary length ℓ_c over which the contact line is distorted by an isolated defect. This is a stringent condition, however the result that we shall derive below for the amplitude of the hysteresis agrees empirically with experiment up to coverage X of the order of 0.03 (Ramos *et al.*, 2003).

Far from the contact line, the liquid-vapor interface is flat and shows an apparent contact angle, which is θ_a for a line advancing at a vanishingly small velocity U, so the dissipated power per unit length is given by (15). For $U \gtrsim 0$, this energy is dissipated in the pinning and depinning events: $W = UnW_a$. The same reasoning for a receding meniscus leads to $H = n(W_a + W_r)$. Note

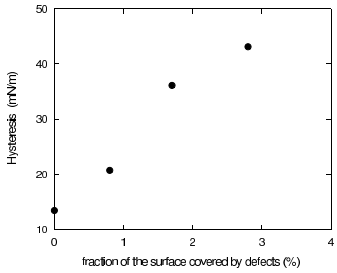

FIG. 48 Hysteresis as a function of the fraction X of the surface covered by defects (from Ramos *et al.* (2003)).

that the total energy dissipated in a forward-backward displacement Δy_∞ of the contact line is $H \times \Delta y_\infty$, which can be interpreted as the area of the force hysteresis cycle (see Fig. 10).

Using 106 leads to:

$$H \sim n[(S_d - S_0)d]^2/(\gamma \sin^2\theta_{eq}). \tag{107}$$

This model was tested recently by Ramos *et al.* (2003), using well controlled substrates with randomly positioned defects of a size on the order of 20 nanometers. For low concentrations of defects ($n < 10^{10} cm^{-2}$, i.e. a coverage smaller than 0.03), Ramos *et al.* (2003) find that H increases linearly with n. Moreover, the slope of H vs. n is consistent with the estimated pinning force on one defect. It is obvious in Fig. 48 that H does not vanish for $n = 0$; the same is true for the experimental data shown in Fig. 11. This illustrates how difficult it is to manufacture a true reference substrate with no hysteresis.

In addition, such pinning and depinning events generate a noise Δf in the force necessary to move the contact line at a given constant speed. For independent (non-interacting) defects, Δf is expected to scale as $n^{1/2} F_{max}$. Even if the size and strength of the defects are not known, the measurement of Δf thus allows to test the above expression for H: inserting the expression for Δf into (107) leads to $H \sim (\Delta f)^2/(\gamma \sin^2\theta_{eq})$. Of course, Δf can be measured only if the line does not probe too many defects at the same time so that the force is not averaged. An elegant way to circumvent this difficulty is to use thin fibers (Di Meglio and Quéré, 1990), which permits to check the dependence of H both on Δf and on θ_{eq}. The results of Di Meglio and Quéré (1990) agree with the theoretical estimates given above.

3. Dynamics

So far we have discussed mainly the hysteresis, or the value of the critical force f_c^+ necessary to unpin the line (for simplicity, we consider only an advancing contact line here). However, this does not answer the important question of what the mean velocity U of the contact line will be for a given applied force that is larger than f_c^+.

This problem was addressed by Raphaël and de Gennes (1989), who considered a line of length L advancing over

a substrate with dilute defects so that the line intersects only a single defect at a time. Assuming that the velocity is fixed, the variable that characterizes the dynamics is $\eta_M(t)$. The whole dynamics can consequently be expressed as an ordinary differential equation for η_M, which is the dynamical analog of (104). Neglecting inertia, this equation reads:

$$F_{dis}(\eta_M, t) = -K\eta_M + F_d(\eta_M - Ut). \qquad (108)$$

Raphaël and de Gennes (1989) argue that the dissipative force F_{dis} is due to viscous dissipation in the vicinity of the contact line, at a scale smaller than the size of the defects. This is reasonable when dealing with macroscopic defects. For example, using (74) with $W_m = 0$, one obtains $F_{dis} = \mu_0 d\eta_M/dt$ in a linear approximation. Moreover, a static expression for K is used in (108): it is assumed that the liquid-vapor interface responds instantaneously to changes in the shape of the contact line, consistent with dissipation being concentrated near it. Experimental time-resolved studies have shown that this assumption is valid for a water meniscus pinned by macroscopic defects ($\xi = 10\mu m$) (Moulinet *et al.*, 2004a). However, other studies have shown that this is no longer true for the special case of superfluid helium. The depinning velocity of the contact line is then of the same order of magnitude as capillary waves (Poujade *et al.*, 2002; Prevost *et al.*, 2002), a situation presumably similar to that of crack propagation in brittle solids (Schwarz and Fisher, 2001).

Even with these simplifications, (108) is difficult to solve because of the non-linear term $F_d(\eta_M - Ut)$. Once the solution $\eta_M(t)$ is known, the average force F applied to the contact line can be computed as the time average of $K\eta_M$. This gives $U \sim (F - F_c)^\beta$ with $\beta = 3/2$ and, surprisingly, $\beta = 1/2$ if the force is imposed instead of the velocity. Raphaël and de Gennes (1989) argue that β depends on the nature of the imposed parameter because the pinning occurs on a single defect so that the disorder is not averaged. Note that the same results for β were obtained by Joanny and Robbins (1990) in a different geometry, the dynamics of the contact line being also described by a single degree of freedom.

For the more frequently encountered case of interacting defects, the dynamics of the contact *line* cannot be reduced to the dynamics of a single *point*. So far, the predictions for the single defect problem have not been tested in experiments.

C. Substrates with interacting defects

We now consider substrates with a large number of defects which can act cooperatively to pin the contact line. We first describe the qualitative behavior of the contact line which has been studied in detail in a number of experiments (Decker and Garoff, 1997; Moulinet *et al.*, 2002, 2004a; Prevost *et al.*, 2002; Rolley *et al.*, 1998a; Schäffer and Wong, 2000).

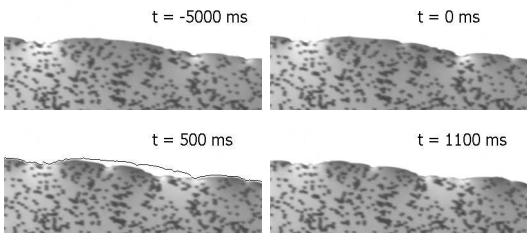

FIG. 49 Successive positions of the contact line. Almost nothing happens for $t < 0ms$, then an avalanche occurs which is nearly finished at $t = 500ms$.

When many defects are acting together, the contact line can be strongly distorted. Its distortion is governed by a balance between the contact line stiffness and the pinning forces. The distortion of the contact line can be characterized by the mean roughness W, which is defined as:

$$W^2(L) = \langle w^2 \rangle = \langle (\eta(x+L) - \eta(x))^2 \rangle \propto L^\zeta, \qquad (109)$$

where the average is performed along the line. It is the scaling of W with the line length L that has been the focus of great theoretical and experimental efforts. As usual for elastic interfaces (lines) in random media, one expects that W scales as L^ζ, where ζ is a universal roughness exponent (Barabasi and Stanley, 1995).

When the defects are macroscopic, the thermal noise is irrelevant: the line is trapped in a long-lived metastable state and does not move. When submitted to an increasing external force f, locally some parts of the contact line jump, but in general the contact line as a whole remains pinned until f exceeds the critical threshold f_c^+ above which the mean velocity U of the line is non-zero. Then, above the depinning threshold f_c^+, the motion of the contact line consists of a succession of slow drifts and fast avalanches, see Fig. 49. The measurement of the size distribution of the avalanches is a way to characterize the dynamics of the system.

Even simpler, one can measure the mean velocity U as a function of the applied force f. Above the threshold f_c^+, U is expected to scale like $(f - f_c^+)^\beta$; β is often called the velocity exponent. Using the vocabulary of phase transitions, the contact line undergoes a depinning transition at $f = f_c^+$ which is characterized by the critical exponents ζ and β. The U versus f characteristic resulting from an analogy with systems such as domain walls in ferromagnets is shown in Fig. 50.

Continuing the analogy with phase transitions, the roughness and velocity exponents are expected to depend only on the dimensionality of the system and on the range of the elastic interactions. For the contact line, we have seen that the elastic restoring force is non-local, and consequently the elastic interactions are of long range. This is in contrast to domain walls in thin magnetic films, for which the interactions are of short range. As a consequence, the domain walls behave as ordinary strings; in

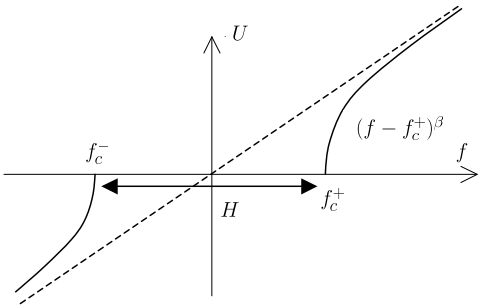

FIG. 50 Schematic of the velocity U as a function of f. The dashed curve corresponds to zero disorder.

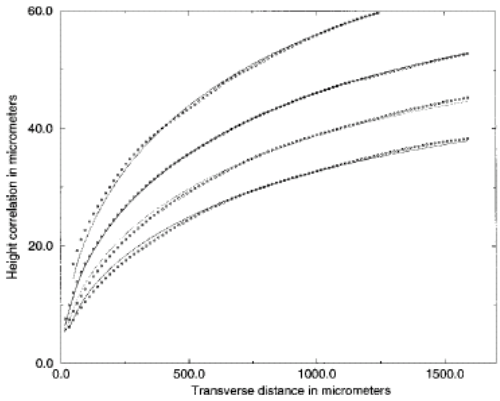

FIG. 51 Roughness $W(L)$ of the contact line plotted as a function of the scale L. Dots: measurements for a weakly disordered substrate for several values of L_D (Rolley *et al.*, 1998a). Lines: calculated scaling function (Hazareezing and Mézard, 1999).

this case, the predictions for critical exponents seem to agree with experiments (Lemerle *et al.*, 1998). Due to the long range of the interactions, measuring or computing ζ and β for the contact line problem turns out to be a difficult task and no general consensus has emerged yet as we shall see below.

1. The shape of the contact line at equilibrium

Before addressing the full problem of the dynamics of the contact line, let us discuss the roughness of the contact line when the defects are "weak". Early attempts to calculate ζ are due to Joanny and de Gennes (1984); Pomeau and Vannimenus (1984), and later Robbins and Joanny (1987). The latter use simple scaling arguments to minimize the total energy of the distorted line which is taken to be the sum of an elastic and a pinning contribution. For weak defects, metastability does arise from the collective behavior of the defects. Thus a new length scale L_D emerges, which is much larger than the correlation length ξ of the disorder. If the length L of the line is smaller than L_D, the disorder is too weak to pin the line, whose roughness remains smaller than ξ. However, if $L > L_D$, the disorder wins, the line is pinned and may become rough. The crossover length $L_D = \xi(\Delta S/\overline{S})^2$ (Robbins and Joanny, 1987) is called the Larkin length in the context of type II superconductors.

For $L > L_D$, Robbins and Joanny (1987) found the roughness exponent $\zeta = 1/3$. This value has been confirmed by a replica variational approach by Hazareezing and Mézard (1999), who also compute the entire scaling function $W(L)$, also taking gravity into account. The scaling function $W(L)$ has been measured with superfluid helium on a weakly disordered cesium surface (Rolley *et al.*, 1998a), finding good agreement with the theoretical predictions as shown in Fig. 51. However, it is not clear whether this solves the problem completely. Indeed the model predicts the scaling behavior *at equilibrium*, i.e. the scaling behavior of the minimum energy state of the line. On the other hand, the measured configurations of the line correspond to metastable configurations in which the line is trapped as long as the applied force is smaller than the depinning threshold. According to Hazareezing and Mézard (1999), the good agreement obtained by Rolley *et al.* (1998a) is presumably due to the fact that the large cutoff length ℓ_c is not much larger than L_D, so that there are only a few metastable states available for the contact line.

2. Hysteresis

The disorder leads to contact line pinning, which in turn provokes the hysteresis of the contact line. The precise value of the threshold is not universal: it depends on the shape and density of the defects, their chemical nature, etc. Predicting the critical depinning force F_c, i.e. the hysteresis, has attracted less attention from theoreticians than the quest for universal exponents, although from a practical point of view it is certainly a very important parameter .

For "weak" collective pinning Robbins and Joanny (1987) obtain

$$H \sim \Delta S^2/\gamma \sin^2\theta_{eq}. \tag{110}$$

This expression for H is identical to the one derived in the case of independent strong defects, (107). For a substrate covered by a density n of defects, this leads to $H \propto n$.

This result is not relevant for substrates with strong interacting defects, which is the case in well controlled experiments where patterned substrates are used. A numerical study of the hysteresis on a heterogenous substrate was performed by Crassous and Charlaix (1994). They recover the regime $H \propto n$ in the diluted limit of non interacting defects $n < 1/(d\ell_c)$. In the regime of collective pinning, H is found to scale like $n^{0.7}$. This value is consistent with the experimental data (Di Meglio, 1992), although both experimental and numerical data were restricted to a small range in n. Subsequent experiments with well-characterized substrates by Ramos *et al.* (2003)

found H to *decrease* at large n. This was interpreted as a consequence of an air bubble that remained trapped in the experiment when the surface becomes too hydrophobic. Therefore, there is clearly a need for further investigation of the hysteresis.

3. Predictions and measurement of the critical behavior

a. Equation of motion. The starting point for most theoretical and numerical work on interacting defects has been a localized version of (108), using (102), first proposed by Joanny and Robbins (1990). Neglecting inertia and thermal noise as before, a local force balance results in an equation for the position $\eta(x,t)$ of the contact line:

$$f_{diss} = f + (S(x,\eta(x)) - \overline{S}) + \frac{\gamma \sin^2\theta_{eq}}{\pi} \int dx' \frac{\eta(x')}{(x-x')^2}. \quad (111)$$

The force f_{diss} is usually evaluated from viscous dissipation localized in the vicinity of the contact line, on a length scale smaller than the one of the contact line distortions. Supposing that the fluctuations in S are not too large, the contact line is only weakly distorted and the local value of the contact angle is close to θ_{eq}. Then estimating the integral (74) as in (12) yields: $f_{diss} \approx -\alpha^{-1}(\partial\eta/dt)$, where $(\partial\eta/dt)$ is the local velocity. The effective mobility α is found to be $\alpha = \theta_{eq}/(3\eta \ln(\ell_c/\lambda))$.

On the r.h.s. of (111), f is the external force, and $(S(x,\eta(x)) - \overline{S})$ is a random noise due to the substrate disorder. It is usually assumed that the noise has short-range correlations, so that it can be described by its amplitude ΔS and its correlation length ξ. The last term on the r.h.s. is the elastic restoring force f_{el} given by (102). We stress that f_{el} has been derived using an expansion to first order in the deformation: it is thus a harmonic approximation to the restoring force on the contact line. The next non-zero term in the expansion (which turns out to be a third order term) was recently calculated by Golestanian and Raphaël (2001a).

This model is quite appealing since it provides us with a simple framework to understand the dynamics of the contact line. Only a few parameters are needed: (i) an effective mobility α, (ii) the disorder strength ΔS and the correlation length ξ and (iii) the parameter $\gamma \sin^2\theta_{eq}$ which controls the stiffness of the contact line. Except for the non-local form of the elastic restoring force, this model is similar to the phenomenological models used to describe the motion of elastic interfaces or lines moving through random media.

b. Critical behavior. The problem of the computation of the roughness and velocity exponents for the contact line triggered much theoretical and numerical work. Ertas and Kardar (1994) have studied the contact line dynamics by a functional renormalization group (fRG) technique. To one-loop order, they found $\beta = 7/9$ and $\zeta = 1/3$, i.e. ζ has the same value at threshold as at equilibrium. Following ideas put forward by Narayan and Fisher (1992), Ertas and Kardar (1994) subsequently argued that the roughness exponent equals 1/3 to all orders. However, it was shown later that extending Ertas and Kardar's RG calculation up to two-loop order leads to a different value of ζ than the equilibrium value. Notably, at the depinning threshold, $\zeta = 0.5 \pm 0.1$ and $\beta \simeq 0.4 \pm 0.2$ (Chauve *et al.*, 2001). This result is consistent with a numerical calculation by Rosso and Krauth (2002), based on an exact enumeration technique, which yields $\zeta = 0.39$.

A meaningful comparison between theory and experimental results for $W(L)$ is very challenging. Namely, the scaling $W \propto L^{\zeta}$ only holds for L larger than the typical length scale of the disorder ξ, and L smaller than the large-scale cutoff length $\ell_c \sim 1mm$. In addition, an optical measurement of $W(L)$ (which is the easiest to realize experimentally) requires ξ to be macroscopic. Using $(W/\xi) \sim (L/\xi)^{\zeta}$, one finds for $\xi = 1\mu m$, $\zeta = 0.39$ and $L = 1mm$ that $W = 15\mu m$. This is a small value, and one should consequently avoid the presence of large defects or large-scale heterogeneities which may have a dominant contribution to W when measuring the contact line roughness. The presence of such defects could explain the surprisingly high value for ζ obtained in some experiments (Decker and Garoff, 1997).

Careful experiments by Moulinet *et al.* (2002) on a glass substrate covered by micrometric size chromium defects have yielded $\zeta = 0.51 \pm 0.03$. This value was obtained initially from a simple analysis of the scaling of the *mean* width $W(L)$ of the contact line. The limitation of that method is that the scaling only holds for $\xi < L < \ell_c$, which is less than 3 decades in the experiments. A more precise characterization of the geometrical properties of the line can be achieved by measuring the full width distribution $\phi(w^2/W^2)$ of the contact line for a given value of L. The probability density ϕ is expected to be a universal function depending only on ζ (Rosso *et al.*, 2003). Moulinet *et al.* (2004b) have shown that indeed the experimental distribution is in excellent agreement with the predicted shape, provided that $\zeta = 0.50$ (see Fig. 52), which agrees with the value determined earlier. Thus, careful measurements are not consistent with the theoretical prediction $\zeta = 0.39$.

On the other hand, the velocity vs force characteristic $U(f)$ can be measured even if ξ is small. Thus, in principle, any measurement of $U(f)$ close to the depinning threshold f_c can yield the value of the critical velocity exponent β. A large number of experiments have indeed measured $U(f)$ in a partial wetting situation, using various techniques (see Schäffer and Wong (2000) for a short review). Surprisingly, the exponent β varies between 1 and 5 between different experiments. In addition, the value of β appears to be system-dependent and is in any case clearly inconsistent with the prediction of the fRG calculations.

However, for many of these experiments one may worry

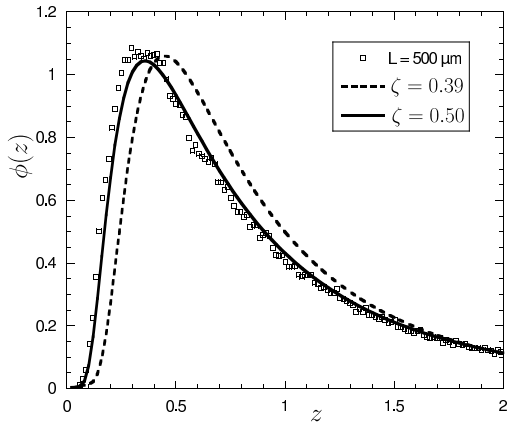

FIG. 52 Width distribution of a contact line $\phi(z)$, where $z = w^2/W^2$). Symbols: measured distribution for $L = 500\mu m$. Full/dashed line: scaling function for $\zeta = 0.50/\zeta = 0.39$.

whether the assumptions underlying (111) are justified, since the substrate is not well characterized. In most cases, the authors argue that the disorder is due to the roughness of the substrate. First, it is not obvious that the roughness has a short-range correlation characterized by a single scale ξ, which is a necessary condition for the model to apply. Second, even if the disorder is short range, it is not obvious that the correlation length ξ is large enough to neglect thermal fluctuations. Thus, it seems that using patterned substrates is the best way to determine β. However, experiments on such substrates have not been conclusive either, as pointed out by Moulinet *et al.* (2004a). The main reason is that the "bare" substrate without patterns already displays some intrinsic hysteresis and is presumably disordered at a microscopic scale. The dissipation of the contact line on the bare substrate can therefore not be described by a simple viscous term as assumed in (111). When adding macroscopic defects on the "bare" substrate, one observes an increase of the hysteresis (or a shift of the critical force), but the shape of $U(f)$ above the threshold is not changed much.

Hence one should be very careful when analyzing this characteristic, which depends in a complex way both on the pinning on macroscopic defects and on the dissipation at the microscopic scale. Using various disordered substrates, which can be prepared by changing the sample (Schäffer and Wong, 2000) or etching the surface (Kumar *et al.*, 1995), is not sufficient because the shape of $U(f)$ can be dominated by the dissipation at the microscopic scale. Measuring true critical behavior requires first to elaborate a nearly ideal substrate without hysteresis, and then to add some controlled disorder with a macroscopic correlation length ξ. In this respect, systems such as the one developed by Ramos *et al.* (2003) look promising.

c. Beyond the harmonic approximation. Up to now, the only reliable measurement of a critical exponent is the one for the roughness exponent $\zeta = 0.50$ (Moulinet *et al.*, 2002), while the theoretical prediction is $\zeta = 0.39$ (Rosso and Krauth, 2002). The reason for this disagreement could be the following. In the context of lines with standard short-range elasticity, it has been shown by Rosso and Krauth (2001) that a small non-harmonic correction to the elastic energy can lead to a strong change in the roughness exponent ζ. Indeed, very recent work by Le Doussal *et al.* (2006) shows that adding the first non-harmonic term to the contact line elastic restoring force leads to a value of ζ in better agreement with the experiments (Le Doussal *et al.*, 2006).

D. Thermal noise

Up to now, thermal fluctuations have been neglected, which is reasonable for macroscopic defects. More generally, thermal noise is negligible if k_BT is much smaller than the pinning energy E^*. The latter is related to the mean size of the activated jumps, which depends on the type of disorder.

For weak defects, i.e. collective pinning, the typical length L^* which is involved in a depinning event is of the order L_D at the threshold (Robbins and Joanny, 1987). As the applied force f decreases, L^* and E^* increase, in strong analogy with the size of the critical nucleus in homogeneous nucleation for first-order phase transitions. This leads to the "creep" regime (Feigel'man *et al.*, 1989), which gives for $f \ll f_c$:

$$U(f,T) \propto exp\left[-\left(\frac{f_c}{f}\right)^m \frac{T}{T_0}\right]. \qquad (112)$$

Such a dependence has been measured for magnetic domain walls, where m is found to be $1/4$ in agreement with the prediction (Lemerle *et al.*, 1998). Note that $m = 1$ for a contact line with long-range elastic interactions (Rolley *et al.*, 1998b).

We are mostly interested in the case of strong pinning, which occurs in most controlled experiments and practical situations. In this case, the pinning of the contact line occurs on a scale ξ and the typical pinning energy E^* is about $\xi^2 f_c$. With $f_c \simeq H/2 \sim 0.1\gamma$, one finds that thermal noise is negligible for many systems (e.g., water at room temperature but also superfluid helium at 1K) if $\xi \gg 1$nm. However, even if $E_* \gg k_BT$, activation is relevant when the applied force f is close to the depinning threshold f_c. Thus if E^* is taken as the potential V and ξ as the step length λ for the motion of a contact line in the description of section III.D.2, (78) becomes

$$U = \frac{\xi e^{-E^*/(k_BT)}}{\tau_0} \exp\left[f\xi^2/(2k_BT)\right]. \qquad (113)$$

Thus one expects a thermal rounding of the depinning transition(Middelton, 1992; Vandembroucq *et al.*, 2004),

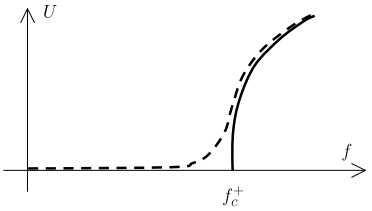

FIG. 53 Schematic of the velocity variation. At $T = 0$ (line), one expects a sharp depinning transition at $f = f_c$, which is blurred by thermal fluctuations at $T \neq 0$ (dashed line).

as depicted schematically in Fig. 53. Note that the prefactor of the exponential term is actually more complicated, due to the distribution of the energy barriers (Vandembroucq *et al.*, 2004). The thermal rounding of the depinning transition and an exponential variation of the velocity has been observed in various systems such as magnetic domain walls (Kirilyuk *et al.*, 1997), or solid friction (Baumberger *et al.*, 1999).

An activated motion of the contact line can be unambiguously observed if viscous dissipation is very small (Prevost *et al.*, 1999), as shown in Fig.31. Recent experiments with liquid hydrogen have also shown the same behavior (Rolley and Guthmann, 2007). By analyzing the $\ln U$ vs f plot in both experiments, the typical length scale of the disorder ξ is found to be of the order of 10 nm, and E^*/k_BT is in the range 100-1000. As a consequence, the rounding is observed only in a narrow range of force, typically a few percent of f_c. This is consistent with numerical results for charge density waves (Middelton, 1992). Therefore, in some special cases, thermally activated motion may indeed be observed.

However, even if the rounding is not observable in most systems, it may have some consequences for analyzing the depinning transition. In many experiments, the dependence $U(f)$ is measured over a limited range of f. As stressed by Schäffer and Wong (2000), experimental data fitted by a power law $U \propto (f - f_c)^\beta$ with $\beta \geq 2$ can also be fitted by an exponential law. So the surprising high value of β obtained in some experiments could be due to thermal activation. More generally, one should be careful about the analysis of the critical behavior if the typical length scale of the disorder is not known.

Besides the difficulty in analyzing the data in the presence of thermal noise, there is a more fundamental problem when using a substrate with mesoscopic disorder. If ξ is in the range 1-10 nanometers, it seems quite unreasonable to assume that the bulk viscous dissipation occurs at the contact line, on a scale smaller than the scale of the distortions of the contact line. The effective mobility introduced in (111) becomes questionable and one cannot avoid treating the coupling between the liquid flow and the motion of the contact line more quantitatively. This will lead to hydrodynamic coupling along the contact line, and make the problem very difficult.

In the depinning approach, there is a single physical mechanism and a single energy scale E^* which controls

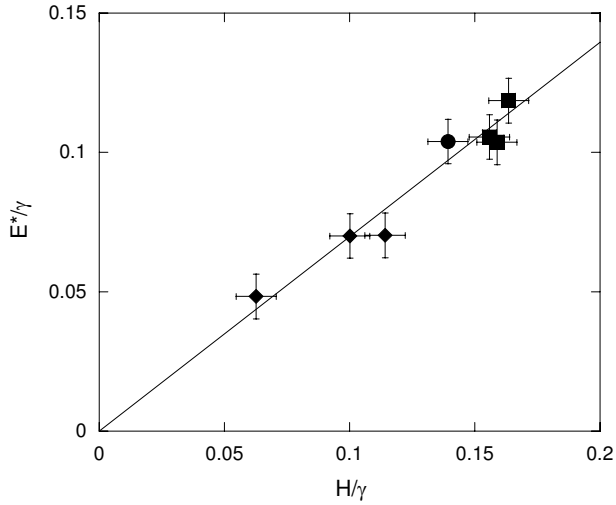

FIG. 54 Activation energy as a function of the hysteresis for liquid hydrogen on various disordered cesium substrates.

both the dynamics close to the threshold and the hysteresis H. Such a simple picture makes sense for simple systems such as cryogenic liquids on alkali substrates. or such substrates with a disorder scale of the order of 10 nm, Rolley *et al.* Rolley and Guthmann (2007) have shown that E^* is of the order of H (see fig. 54). On the other hand, in more ordinary systems such as water or alcohols on various polymeric materials, the molecular kinetic approach has been widely used to analyze experimental results (Blake, 1993; Hayes and Ralston, 1993).

In these analyses, no connection is made between the hysteresis and the energy V characterizing the activated dynamics. Hysteresis and dynamics are assumed to be controlled by two different mechanisms, so that it is not obvious to decide what sets the value of V. Recently, it was proposed that V/λ^2 is of the order of the work of adhesion $W_A = \gamma(1 + \cos\theta_{eq})$ (Blake and De Coninck, 2002). For systems with complex substrate-liquid interactions, the advance of the contact line could indeed be controlled by molecular processes, as in the original molecular kinetic theory.

For instance, studies of water on polyethylene therephtalate (PET) yield an activation length λ which is indeed microscopic (Hayes and Ralston, 1993), and V/λ^2 of the order of γ. On the other hand, the analysis in terms of a molecular-kinetic model leads to unreasonable values of λ and V in recent experiments by Petrov *et al.* (2003b). Using a range of simple liquids on amorphous teflon substrates Petrov et al. found an activation length λ of the order of 10 nm, much larger than a molecular length; also V does not scale like W_A. From their data, it is found that V/λ^2 is of the order of H. Thus the simple depinning approach seems to provide a better interpretation of this experiment.

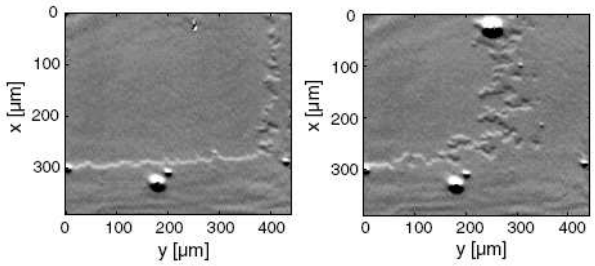

FIG. 55 Advancing thin film/thick film boundary (Helium film of thickness 50 nm on a cesium substrate at 1.87K).

E. Hot topics

1. Hysteresis again!

We still have a poor understanding of the hysteresis for random substrates as we have no theoretical nor experimental answer to such basic questions as: how does H depend on the density of defects or on the strength of the defects? Numerical studies as well as measurements on model substrates with macroscopic defects such as the ones employed by Ramos *et al.* (2003) would be highly desirable. However such studies cannot be directly relevant for much-used substrates such as polymeric materials; the latter often display some intrinsic hysteresis which is likely due to pinning at microscopic (nanometric) scales. In this case, H is rather controlled by the detailed properties of the substrate-fluid interaction, so a description in terms of a depinning transition is not likely to be relevant. More insight into the behavior of such systems could possibly be obtained by studying both the hysteresis and the activated dynamics of the contact line. It would be worth analyzing available data such as (Hayes and Ralston, 1993) or performing new experiments to determine whether H is related to the activation energy.

2. Prewetting transition on disordered substrates

So far, we have discussed what happens to a true contact line, that is the edge of a liquid drop in a partial wetting situation, when the solid substrate is heterogeneous. Slightly off the liquid-gas coexistence and on the prewetting line of the phase diagram, one may also observe a boundary between a thin film and a thick (mesoscopic) film. On a disordered substrate, this boundary is very distorted as shown in Fig. 55. Off coexistence, the local variations of the spreading coefficient are equivalent to a random field coupled to the surface film state (thin or thick), which is the order parameter. Thus, in principle, the system can be mapped onto a random field Ising model. The boundary is analogous to a domain wall in a ferromagnet with a true line tension (of order γ times the thickness of the thick film). The "Random-field Ising model" approach has been used to describe the hysteresis of the prewetting transition (Blossey *et al.*, 1998) on solid substrates as well as the activated motion of the boundary (Müller and Dupont-Roc, 2001). However, experimental results are still very sparse in this field.

References

Aarts, D. G. A. L., 2005, J. Phys. Chem. B **109**, 7407.

Aarts, D. G. A. L., R. P. A. Dullens, H. N. W. Lekkerkerker, D. Bonn, and R. J. van Roij, 2004a, J. Chem. Phys. **120**, 1973.

Aarts, D. G. A. L., and H. N. W. Lekkerkerker, 2004, J. Phys.: Condens. Matter **16**, S4231.

Aarts, D. G. A. L., M. Schmidt, and H. N. W. Lekkerkerker, 2004b, Science **304**, 847.

Aarts, D. G. A. L., J. H. van der Wiel, and H. N. W. Lekkerkerker, 2003, J. Phys.: Condens. Matter **15**, S245.

Abkarian, M., J. Nunes, and H. A. Stone, 2004, J. Am. Chem. Soc. **126**, 5978.

Abraham, D., A. Parry, and A. Wood, 2002a, Europhys. Lett. **60**, 106.

Abraham, D. B., R. Cuerno, and E. Moro, 2002b, Phys. Rev. Lett. **88**, 206101.

Abraham, D. B., and A. Maciolek, 2002, Phys. Rev. Lett. **89**, 286101.

Abraham, D. B., V. Mustonen, and A. Wood, 2003, Europhys. Lett. **63**, 408.

Abramowitz, M., and I. A. Stegun, 1968, *Handbook of Mathematical Functions* (Dover).

Ala-Nissila, T., S. Herminghaus, T. Hjelt, and P. Leiderer, 1996, Phys. Rev. Lett. **76**, 4003.

Alava, M., M. Dube, and M. Rost, 2004, Adv. Phys. **53**, 83.

Albano, E., A. D. Virgiliis, M. Müller, and K. Binder, 2003, J. Phys.: Condens. Matter **15**, 333.

Albrecht, A. O., and P. Leiderer, 1992, Phys. Rev. Lett. **68**, 3192.

Allen, M., and D. Tildesley, 1987, *Computer simulations of liquids* (Clarendon, New York).

Ansini, L., and L. Giacomelli, 2002, Nonlinearity **15**, 2147.

Arscott, S., M. Gaudet, M. Brinkmann, A. Ashcroft, and R. Blossey, 2006, J. Phys.: Condens. Matter **18**, S677.

Asakura, S., and F. Oosawa, 1954, J. Chem. Phys. **22**, 1255.

Asakura, S., and F. Oosawa, 1958, J. Pol. Sci. **33**, 183.

Aussere, D., A. M. Picard, and L. Léger, 1986, Phys. Rev. Lett. **57**, 2671.

Balibar, S., and S. Ishiguro, 2005, Pramana **64**, 743.

Barabasi, A.-L., and H. E. Stanley, 1995, *Fractal Concepts in Surface Growth* (Cambridge University Press, Cambridge).

Bartolo, D., F. Bouamrirene, E. A. Buguin, P. Silberzan, and S. Moulinet, 2006, Europhys. Lett. **74**, 299.

Bascom, W. D., R. Cottington, and C. Singleterry, 1964, in *Contact angle, wettability, and adhesion*, edited by F. M. Fowkes (Washington, DC), p. 355.

Bauer, C., and S. Dietrich, 1999a, Eur. Phys. J. B **10**, 767.

Bauer, C., and S. Dietrich, 1999b, Phys. Rev. E **60**, 6919.

Bauer, C., and S. Dietrich, 2000, Phys. Rev. E **61**, 1664.

Bauer, C., S. Dietrich, and A. Parry, 1999, Europhys. Lett. **47**, 474.

Baumberger, T., P. Berthoud, and C. Caroli, 1999, Phys. Rev. B **60**, 3928.

Bazhlekov, I. B., and A. K. Chesters, 1996, J. Fluid Mech. **329**, 137.

Beaglehole, D., 1989, J. Phys. Chem. **93**, 839.

Bechinger, C., D. Rudhardt, P. Leiderer, R. Roth, and S. Dietrich, 1999, Phys. Rev. Lett. **83**, 3960.
Becker, J., and G. Grün, 2005, J. Phys.: Condens.Matter **17**, S291.
Becker, J., G. Grün, R. Seemann, H. Mantz, K. Jacobs, K. R. Mecke, and R. Blossey, 2003, Nature Mat. **2**, 59.
Bekink, S., S. Karaborni, G. Verbist, and K. Esselink, 1996, J. Phys. Chem. **93**, 839.
Benney, D. J., 1966, J. Math. Phys. (N.Y.) **45**, 150.
Benney, D. J., and W. J. Timson, 1980, Stud. Appl. Maths. **63**, 93.
Benzi, R., L. Biferale, M. Sbragaglia, S. Succi, and F. Toschi, 2006, Phys. Rev. E **74**, 021509.
Bergeron, V., D. Bonn, J.-Y. Martin, and L. Vovelle, 2000, Nature **405**, 772.
Bertozzi, A. L., and M. P. Brenner, 1997, Phys. Fluids **9**, 530.
Bertozzi, A. L., A. Munch, X. Fanton, and A.-M. Cazabat, 1998, Phys. Rev. Lett. **81**, 5169.
Bertozzi, A. L., A. Munch, and M. Shearer, 1999, Physica D **134**, 431.
Bertrand, E., 2002, J. Petrol. Sci. Eng. **33**, 217.
Bertrand, E., D. Bonn, D. Broseta, H. Dobbs, J. O. Indekeu, J. Meunier, K. Ragil, and N. Shahidzadeh, 2002, J. Petrol. Sci. Eng. **33**, 217.
Bertrand, E., D. Bonn, H. Kellay, B. Binks, and J. Meunier, 2001, Europhys. Lett. **55**, 827.
Betelu, S. I., and M. A. Fontelos, 2003, Appl. Math. Lett. **16**, 1315.
Betelu, S. I., and M. A. Fontelos, 2004, Math. Computer Modelling **40**, 729.
Biance, A.-L., C. Clanet, and D. Quéré, 2003, Phys. Rev. E **69**, 016301.
Biben, T., P. Bladon, and D. Frenkel, 1996, J. Phys.: Condens. Matter **8**, 10799.
Bico, J., C. Marzolin, and D. Quéré, 1999, Europhys. Lett. **47**, 220.
Bico, J., C. Tordeux, and D. Quéré, 2001, Europhys. Lett. **55**, 214.
Bieker, T., and S. Dietrich, 1998, Physica A **252**, 85.
Bienia, M., M. Vallade, C. Quilliet, and F. Mugele, 2006, Europhysics Letters **74**, 103.
Biferale, L., R. Benzi, M. Sbragaglia, S. Succi, and F. Toschi, 2007, J. Computer-aided Mat. **14**, 447.
Binder, K., and D. P. Landau, 1988, Phys. Rev. B **37**, 1745.
Binder, K., D. P. Landau, and D. M. Kroll, 1986, Phys. Rev. Lett. **56**, 2272.
Binder, K., D. P. Landau, and S. Wansleben, 1989, Phys. Rev. B **40**, 6971.
Bischof, J., D. Scherer, S. Herminghaus, and P. Leiderer, 1996, Phys. Rev. Lett. **77**, 1536.
Blake, T. D., 1993, in *Wettability*, edited by J. Berg. (New York, Marcel Dekker), volume 49.
Blake, T. D., 2006, J. Colloid Inter. Sci. **299**, 1.
Blake, T. D., and J. De Coninck, 2002, Adv. Colloid Interface Sci. **96**, 21.
Blake, T. D., and J. M. Haynes, 1969, J. Colloid Interface Sci. **30**, 421.
Blake, T. D., and K. J. Ruschak, 1979, Nature **282**, 489.
Blake, T. D., and K. J. Ruschak, 1997, in *Liquid film coating*, edited by S. F. Kistler and P. M. Schweizer (London, Chapman and Hall).
Blatter, G., M. V. Feigelman, V. B. Geshkenbein, A. I. Larkin, and V. M. Vinokur, 1994, Rev. Mod. Phys. **66**, 1125.
Blossey, R., 2003, Nature Mater. **2**, 301.
Blossey, R., T. Kinoshita, and J. Dupont-Roc, 1998, Physica A **248**, 247.
Bonn, D., E. Bertrand, N. Shahidzadeh, K. Ragil, H. T. Dobbs, A. I. Posazhennikova, D. Broseta, J. Meunier, and J. O. Indekeu, 2001, J. Phys.: Condens. Matter **13**, 4903.
Bonn, D., H. Kellay, and G. H. Wegdam, 1992, Phys. Rev. Lett. **69**, 1975.
Bonn, D., and J. Meunier, 1997, Europhys. Lett. **39**, 341.
Bonn, D., and D. Ross, 2001, Rep. Progr. Phys. **64**, 1085.
Borgas, M. S., and J. B. Grotberg, 1988, J. Fluid Mech. **193**, 151.
Borgs, C., J. De Coninck, R. Kotecky, and M. Zinque, 1995, Phys. Rev. Lett. **74**, 2292.
Boudaoud, A., 2007, Eur. Phys. J. **22**, 107.
Boulter, C. J., 1997, Phys. Rev. Lett. **79**, 1897.
Bourges-Monnier, C., and M. E. R. Shanahan, 1995, Langmuir **11**, 2820.
Brader, J., R. Evans, and M. Schmidt, 2003, Mol. Phys. **101**, 3349.
Brenner, M. P., and A. L. Bertozzi, 1993, Phys. Rev. Lett. **71**, 593.
Brézin, E., B. I. Halperin, and S. Leibler, 1983a, J. Physique (Paris) **44**, 775.
Brézin, E., B. I. Halperin, and S. Leibler, 1983b, Phys. Rev. Lett. **50**, 1387.
Briant, A. J., A. J. Wagner, and J. M. Yeomans, 2004, Phys. Rev. E **69**, 031602.
Briant, A. J., and J. M. Yeomans, 2004, Phys. Rev. E **69**, 031603.
Brinkmann, M., and R. Lipowsky, 2002, J. Appl. Phys. **92**, 4296.
Brochard-Wyart, F., and J. Daillant, 1990, Can. J. Phys. **68**, 1084.
Brochard-Wyart, F., and P.-G. de Gennes, 1992, Adv. Colloid Interface Sci. **9**, 1.
Brochard-Wyart, F., J. M. di Meglio, D. Quéré, and P.-G. de Gennes, 1991, Langmuir **7**, 335.
Bruch, W., M. W. Cole, and E. Zaremba, 1997, *Physical Adsorption: Forces and Phenomena* (Clarendon: New York).
de Bruijn, R. A., 1993, Chem. Eng. Sci. **48**, 277.
Bruschi, L., A. Carlin, and G. Mistura, 2001, J. Chem. Phys. **115**, 6200.
Bruschi, L., A. Carlin, and G. Mistura, 2002, Phys. Rev. Lett. **89**, 166101.
Bruschi, L., A. Carlin, A. Parry, and G. Mistura, 2003a, Phys. Rev. E **68**, 021606.
Bruschi, L., E. Carlin, and G. Mistura, 2003b, J. Phys.: Condens. Matter **15**, S315.
Bruschi, L., G. Fois, G. Mistura, M. Tormen, V. Garbin, E. di Fabrizio, A. Gerardino, and M. Natali, 2006, J. Chem. Phys. **125**, 144709.
Bryk, P., R. Roth, K. Mecke, and S. Dietrich, 2003a, Phys. Rev. E **68**, 031602.
Bryk, P., R. Roth, M. Schoen, and S. Dietrich, 2003b, Europhys. Lett. **63**, 233.
Brzoska, J. B., N. Shahidzadeh, and F. Rondelez, 1992, Nature **360**, 719.
Burlatsky, S. F., G. Oshanin, A.-M. Cazabat, and M. Moreau, 1996, Phys. Rev. Lett. **76**, 86.
Burley, R., and B. S. Kennedy, 1976a, Chem. Eng. Sci. **31**, 901.
Burley, R., and B. S. Kennedy, 1976b, Brit. Polym. J. **8**, 140.
Burley, R., and B. S. Kennedy, 1978, in *Wetting, Spreading and Adhesion*, edited by J. F. Padday (Academic Press,

London).
Cachile, M., O. Benichou, and A.-M. Cazabat, 2002a, Langmuir **18**, 8070.
Cachile, M., O. Benichou, and A.-M. Cazabat, 2002b, Langmuir **18**, 7985.
Cachile, M., M. Schneemilch, A. Hamraoui, and A.-M. Cazabat, 2002c, J. Colloid Interf. Sci. **96**, 59.
Cahn, J. W., 1977, J. Chem. Phys. **66**, 3667.
Cahn, J. W., 2000, Physica A **279**, 195.
Carey, B. S., L. E. Scriven, and H. T. Davis, 1978, AIChE Journal **24**, 10761080.
Carré, A., and F. Eustache, 1997, C. R. Acad. Sci. Paris **325**, 709.
Carré, A., and F. Eustache, 2000, Langmuir **16**, 2936.
Carré, A., and P. Woehl, 2002, Langmuir **18**, 3600.
Cassie, A. B. D., 1952, Discuss. Faraday Soc. **75**, 5041.
Cazabat, A.-M., and M. A. Cohen-Stuart, 1986, J. Phys. Chem. **90**, 5845.
Cazabat, A.-M., S. Gerdes, M. P. Valignat, and S. Villette, 1997, Interf. Sci. **5**, 129.
Cazabat, A.-M., F. Heslot, P. Carles, and S. M. Troian, 1992, Colloid Interface Sci. **39**, 61.
Cazabat, A.-M., F. Heslot, S. M. Troian, and P. Carles, 1991, Nature **346**, 824.
Chauve, P., P. Le Doussal, and K. J. Wiese, 2001, Phys. Rev. Lett. **86**, 1785.
Checco, A., Y. Cai, O. Gang, and B. Ocko, 2006, Ultramicroscopy **106**, 703.
Checco, A., P. Guenoun, and J. Daillant, 2003, Phys. Rev. Lett. **91**, 186101.
Chen, H.-Y., D. Jasnow, and J. Vinals, 2000, Phys. Rev. Lett. **85**, 1686.
Chen, J.-D., 1988, J. Colloid Interf. Sci. **122**, 60.
Chen, J.-D., and N. Wada, 1989, Phys. Rev. Lett. **62**, 3050.
Chen, Q., E. Ramé, and S. Garoff, 1995, Phys. Fluids **7**, 2631.
Chen, Q., E. Ramé, and S. Garoff, 1997, J. Fluid Mech. **337**, 49.
Chen, X., E. Rame, and S. Garoff, 2004, Phys. Fluids **16**, 287.
Cheng, E., and M. Cole, 1990, Phys. Rev. B **41**, 9650.
Cheng, E., M. W. Cole, J. Dupont-Roc, and W. F. Saam, 1993, Rev. Mod. Phys. **65**, 557.
Cheng, E., M. W. Cole, W. F. Saam, and J. Treiner, 1991, Phys. Rev. Lett. **67**, 1007.
Cho, J.-H. J., B. M. Law, and F. Rieutord, 2004, Phys. Rev. Lett. **92**, 166102.
Cohen, I., H. Li, J. Hougland, M. Mrksich, and S. R. Nagel, 2001, Science **292**, 265.
Cottin-Bizonne, C., J.-L. Barrat, L. Boquet, and E. Charlaix, 2003, Nature Mater. **2**, 237.
Cottin-Bizonne, C., B. Cross, A. Steinberger, and E. Charlaix, 2005, Phys. Rev. Lett. **94**, 056102.
Courrech du Pont, S., and J. Eggers, 2006, Phys. Rev. Lett. **96**, 034501.
Cox, R. G., 1983, J. Fluid Mech. **131**, 1.
Cox, R. G., 1986, J. Fluid Mech. **168**, 169.
Cox, R. G., 1998, J. Fluid Mech. **347**, 249.
Crassous, J., and E. Charlaix, 1994, Europhys. Lett. **28**, 415.
Damman, P., N. Baudelet, and G. Reiter, 2003, Phys. Rev. Lett. **91**, 216101.
Davidovitch, B., E. Moro, and H. A. Stone, 2005, Phys. Rev. Lett. **95**, 244505.
Davis, J. M., and S. M. Troian, 2003a, Phys. Rev. E **67**, 016308.
Davis, J. M., and S. M. Troian, 2003b, Phys. Fluids **15**, 1344.
Davis, S. H., 1987, Annu. Rev. Fluid Mech. **19**, 403.
de Bruyn, J. R., 1992, Phys. Rev. A **46**, R4500.
De Coninck, J., S. Hoorelbeke, M. P. Valignat, and A.-M. Cazabat, 1993, Phys. Rev. E **48**, 4549.
De Coninck, J., J. Ruiz, and S. Miracle-Sole, 2002, Phys. Rev. E **65**, 036139.
de Feijter, J. A., 1988, in *Thin liquid films*, edited by I. B. Ivanov (Marcel Dekker, New York), pp. 1–47.
de Gennes, P.-G., 1981, J. Phys. Lett. **42**, L377.
de Gennes, P.-G., 1985, Rev. Mod. Phys. **57**, 827.
de Gennes, P.-G., 1986, Coll. Pol. Sci. **264**, 463.
de Gennes, P.-G., F. Brochart-Wyart, and D. Quéré, 2003, *Capillarity and Wetting Phenomena: Drops, Bubbles, Pearls, Waves* (Springer).
de Gennes, P.-G., and A.-M. Cazabat, 1990, C. R. Acad. Sci. Paris, Serie **310**, 1601.
de Gennes, P.-G., X. Hua, and P. Levinson, 1990, J. Fluid Mech. **212**, 55.
de Laplace, P. S., 1805, *Mechanique Celeste Supplement au X Libre* (Courier: Paris).
Decker, E. L., and S. Garoff, 1997, Langmuir **13**, 6321.
Deegan, R. D., 2000, Phys. Rev. E **61**, 475.
Deegan, R. D., O. Bakajin, T. F. Dupont, G. Huber, S. R. Nagel, and T. A. Witten, 1997, Nature **389**, 827.
Deegan, R. D., O. Bakajin, T. F. Dupont, G. Huber, S. R. Nagel, and T. A. Witten, 2000, Phys. Rev. E **62**, 756.
Delon, G., 2007, *Thesis*, Ph.D. thesis, Université Paris VI.
Delon, G., M. Fermigier, J. H. Snoeijer, and B. Andreotti, 2007, J. Fluid Mech., submitted .
Deneka, C. W., G. Kar, and T. O. Mensah, 1988, Method of coating optical waveguide fiber, US Patent no.= 4792347.
Deryaguin, B. V., 1940, Acta physico-chimica USSR **12**, 181.
Deryaguin, B. V., 1943, Acta physico-chimica USSR **20**, 349.
Deryaguin, B. V., and S. M. Levi, 1964, *Film Coating Theory* (Focal, London).
Di Meglio, J.-M., 1992, Europhys. Lett. **17**, 607.
Di Meglio, J.-M., and D. Quéré, 1990, Europhys. Lett. **11**, 163.
Dickman, R., P. Attard, and V. Simonian, 1997, J. Chem. Phys. **107**, 205.
Dietrich, S., 1988, in *Phase Transitions and Critical Phenomena*, edited by C. Domb and J. L. Lebowitz (London: Academic), volume 12, pp. 1–218.
Dietrich, S., 1999, in *New approaches to problems in liquid state theory (NATO ASI series C vol 529)*, edited by C. Caccamo, J.-P. Hansen, and G. Stell (Kluwer, Dordrecht), p. 197.
Dietrich, S., and M. Napiórkowski, 1991, Physica A **177**, 437.
Dietrich, S., M. N. Popescu, and M. Rauscher, 2005, J. Phys.: Condens. Matter **17**, S577.
Dietrich, S., and M. Schick, 1985, Phys. Rev. B **31**, 4718.
Dijkstra, M., R. van Roij, and R. Evans, 1999, Phys. Rev. Lett. **82**, 117.
Dijkstra, M., and R. van Roij, 2002, Phys. Rev. Lett. **89**, 208303.
Drazin, 1992, *Nonlinear systems* (Cambridge).
Duez, C., C. Ybert, C. Clanet, and L. Bocquet, 2007, Nat. Phys. **3**, 180.
Duffy, B. R., and S. K. Wilson, 1997, Appl. Math. Lett. **63**, 63.
Duft, D., T. Achtzehn, R. Müller, B. A. Huber, and T. Leisner, 2003, Nature **421**, 128.
Durian, D. J., and C. Franck, 1987, Phys. Rev. Lett. **59**, 555.
Dussan V., E. B., 1979, Ann. Rev. Fluid Mech. **11**, 371.

Dussan V., E. B., and R. T.-P. Chow, 1979, J. Fluid Mech. **137**, 1.
Dussan V., E. B., E. Ramé, and S. Garoff, 1991, J. Fluid Mech. **230**, 97.
Dzyaloshinskii, I., E. M. Lifshitz, and L. P. Pitaevskii, 1961, Adv. Phys. **10**, 165.
Ebner, C., and W. F. Saam, 1977, Phys. Rev. Lett. **38**, 1486.
Ebner, C., and W. F. Saam, 1987, Phys. Rev. Lett. **58**, 587.
Eggers, J., 1997, Rev. Mod. Phys. **69**, 865.
Eggers, J., 2001, Phys. Rev. Lett. **86**, 4290.
Eggers, J., 2002, Phys. Rev. Lett. **89**, 084502.
Eggers, J., 2004a, Phys. Rev. Lett. **93**, 094502.
Eggers, J., 2004b, Phys. Fluids **16**, 3491.
Eggers, J., 2005a, Phys. Rev. E **72**, 061605.
Eggers, J., 2005b, Phys. Fluids **17**, 082106.
Eggers, J., and H. A. Stone, 2004, J. Fluid Mech. **505**, 309.
Ehrhard, P., 1993, J. Fluid Mech. **257**, 463.
Ehrhard, P., and S. H. Davis, 1991, J. Fluid Mech. **229**, 365.
Elbaum, M., and S. G. Lipson, 1994, Phys. Rev. Letters **72**(22), 3562.
Eres, M. H., L. W. Schwartz, and R. V. Roy, 2000, Phys. Fluids **12**, 1278.
Ertas, D., and M. Kardar, 1994, Phys. Rev. E **49**, R2532.
Esztermann, A., M. Heni, H. Löwen, J. Klier, M. Sohaili, and P. Leiderer, 2002, Phys. Rev. Lett. **88**, 055702.
Esztermann, A., and H. Löwen, 2005, J. Phys.: Condens. Matter **17**, S429.
Evans, R., 1990, in *Liquids at Interfaces, Les Houches Session XLVIII*, edited by J. Charvolin, J.-F. Joanny, and J. Zinn-Justin (Amsterdam: Elsevier), pp. 1–98.
Evans, R., and U. Marini Bettolo Marconi, 1985, Chem. Phys. Lett. **114**, 415.
Eyring, H. J., 1941, *The Theory of Rate Processes* (McGraw-Hill, New York).
Feigel'man, M. V., V. B. Geshkenbein, A. I. Larkin, and V. M. Vinokur, 1989, Phys. Rev. Lett. **63**, 2303.
Fenistein, D., D. Bonn, S. Rafaï, G. H. Wegdam, J. Meunier, M. Telo da Gama, and A. O. Parry, 2002, Phys. Rev. Lett. **89**, 096101.
Ferguson, A., 1929, J. Sci. Instrum. **6**, 163.
Fermigier, M., and P. Jenffer, 1991a, Ann. Physique **13**, 37.
Fermigier, M., and P. Jenffer, 1991b, J. Coll. Int. Sci. **146**, 226.
Fetzer, R., K. Jacobs, A. Münch, B. Wagner, and T. P. Witelski, 2005, Phys. Rev. Lett. **95**, 127801.
Findenegg, G. H., and R. Löring, 1984, J. Chem. Phys. **81**, 3270.
Finlow, D. E., P. R. Kota, and A. Bose, 1996, Phys. Fluids **8**, 302.
Fisher, D. S., and D. A. Huse, 1985, Phys. Rev. B **32**, 247.
Fisher, M. E., 1986, J. Chem. Soc. Faraday Trans. II **82**, 1569.
Fisher, M. E., and A. J. Jin, 1992, Phys. Rev. Lett. **69**, 792.
Fontelos, M. A., and U. Kindelán, 2008, unpublished .
Fox, H. W., and W. A. Zisman, 1950, J. Colloid. Sci. **5**, 514.
Fraysse, N., and G. M. Homsy, 1994, Phys. Fluids **6**, 6.
Fuchs, M., and K. S. J. Schweizer, 2002, Phys.: Condens. Matter **14**, R239.
Fukuto, M., Y. F. Yano, and P. S. Pershan, 2005, Phys. Rev. Lett. **94**, 135702.
Gang, O., K. Alvine, M. Fukuto, P. Pershan, C. Black, and B. Ocko, 2005, Phys. Rev. Lett. **95**, 217801.
Garcia, R., and M. H. W. Chan, 1999, Phys. Rev. Lett. **83**, 1187.
Garcia, R., and M. H. W. Chan, 2002, Phys. Rev. Lett. **88**, 086101.
Garnier, N., R. O. Grigoriev, and F. Schatz, 2003, Phys. Rev. Lett. **91**, 054501.
Gau, H., S. Herminghaus, P. Lenz, and R. Lipowsky, 1999, Science **283**, 46.
de Gennes, P.-G., 1983, C. R. Acad. Sc. Paris **297:II**, 9.
Geoghegan, M., and G. Krausch, 2003, Prog. Polym. Sci. **28**, 261.
Getta, T., and S. Dietrich, 1998, Phys. Rev. E **57**, 655.
Gittes, F. T., and M. Schick, 1984, Phys. Rev. B **30**, 209.
Gogotsi, Y., J. A. Libera, C. Guvenc-Yazicioglu, and C. M. Megaridis, 2001, Appl. Phys. Lett. **79**, 1021.
Golestanian, R., and E. Raphaël, 2001a, Phys. Rev. E **64**, 031601.
Golestanian, R., and E. Raphaël, 2001b, Europhys. Lett. **55**, 228.
Golestanian, R., and E. Raphaël, 2003, Phys. Rev. E **67**, 031603.
Gompper, G., and D. M. Kroll, 1988a, Europhys. Lett. **5**, 49.
Gompper, G., and D. M. Kroll, 1988b, Phys. Rev. B **37**, 3821.
Gorodtsov, V. A., 1990, J. Engrg. Phys. **57**, 879.
Götzelmann, B., R. Evans, and S. Dietrich, 1998, Phys. Rev. E **57**, 6785.
Götzelmann, B., R. Roth, S. Dietrich, M. Dijkstra, and R. Evans, 1999, Europhys. Lett. **47**, 398.
Greenall, M., A. Parry, and J. Romero-Enrique, 2004, J. Phys.: Condens. Matter **16**, 2515.
Greenspan, H. P., 1978, J. Fluid Mech. **84**, 125.
Grigoriev, R. O., 2003, Phys. Fluids **15**, 1363.
Grigoriev, R. O., 2005, Physica D **209**, 105.
Grün, G., 2004, Comm. Partial Diff. Eqs. **29**, 1697.
Grün, G., K. R. Mecke, and M. Rauscher, 2006, J. Stat. Phys. **122**, 1261.
Gutoff, E. B., and C. E. Kendrick, 1982, AIChE J. **28**, 459.
Hadjiconstantinou, N. G., 1999a, Phys. Rev. E **59**, 2475.
Hadjiconstantinou, N. G., 1999b, J. Comp. Phys. **154**, 245.
Hadjiconstantinou, N. G., 2003, J. Fluid Mech. **497**, 123.
Hadjiconstantinou, N. G., and A. T. Patera, 1997, Int. J. Modern Phys. C **8**, 967.
Halpin-Healy, T., and E. Brézin, 1987, Phys. Rev. Lett. **58**, 1220.
Hamaker, H. C., 1937, Physica **4**, 1058.
Hanke, A., E. Eisenriegler, and S. Dietrich, 1999, Phys. Rev. E **59**, 6853.
Hansen, R. J., and T. Y. Toong, 1971, J. Colloid Interf. Sci **36**, 410.
Hardy, W. P., 1919, Philos. Mag. **38**, 49.
Harnau, L., F. Penna, and S. Dietrich, 2004, Phys. Rev. E **70**, 021505.
Hauge, E., 1992, Phys. Rev. A **46**, 4994.
Hayes, R. A., and J. Ralston, 1993, J. Colloid Int. Sc. **159**, 429.
Hazareezing, A., and M. Mézard, 1999, Phys. Rev. E **60**, 1269.
Helfrich, W., 1973, Z. Naturforsch. **28**, 693.
Helfrich, W., 1978, Z. Naturforsch. A **33**, 305.
Helfrich, W., and R.-M. Servuss, 1984, Nuovo Cimento D **3**, 137.
Henderson, J., 2004a, J. Chem. Phys. **120**, 1535.
Henderson, J., 2004b, Phys. Rev. E **69**, 061613.
Henderson, J., 2006, J. Phys. Cond. Matt. **18**, V11.
Hennequin, Y., D. G. A. L. Aarts, J. O. Indekeu, H. N. W. Lekkerkerker, and D. Bonn, 2008, Phys. Rev. Lett. **100**, 178305.
Henrich, B., C. Cupelli, M. Santer, and M. Moseler, 2008,

unpublished .
Herminghaus, S., R. Seemann, and K. Jacobs, 2002, Phys. Rev. Lett. **89**, 056101.
Hertlein, C., L. Helden, A. Gambassi, S. Dietrich, and C. Bechinger, 2008, Nature **451**, 136.
Hervet, H., and P.-G. de Gennes, 1984, C. R. Acad. Sc. Paris, Serie II **299**, 499.
Heslot, F., A.-M. Cazabat, and P. Levinson, 1989a, Phys. Rev. Lett. **62**, 1286.
Heslot, F., N. Fraysse, and A.-M. Cazabat, 1989b, Nature **338**, 640.
Hill, R. A., 1998, Curr. Opin. Coll. Interf. Sci. **3**, 247.
Hjelt, T., S. Herminghaus, T. Ala-Nissila, , and S. C. Ying, 1998, Phys. Rev. E **57**, 1864.
Hocking, L. M., 1976, J. Fluid Mech. **76**, 801.
Hocking, L. M., 1977, J. Fluid Mech. **79**, 209.
Hocking, L. M., 1981, Q. J. Appl. Math. **34**, 37.
Hocking, L. M., 1983, Q. J. Appl. Math. **36**, 55.
Hocking, L. M., 1992, J. Fluid Mech. **239**, 671.
Hocking, L. M., 1993, Phys. Fluids A **5**, 793.
Hocking, L. M., 1994, Phys. Fluids **6**, 3224.
Hocking, L. M., 2001, Euro. J. Appl. Math. **12**, 195.
Hoffman, R. L., 1975, J. Coll. Interface Sci. **50**, 228.
Hohenberg, P. C., and B. I. Halperin, 1977, Rev. Mod. Phys. **49**, 435.
Hoogerbrugge, P. J., and J. M. V. A. Koelman, 1992, Europhys. Lett. **19**, 155.
Hu, H., and R. G. Larson, 2006, J. Phys. Chem. B **110**, 7090.
Huh, C., and L. E. Scriven, 1971, J. Coll. Int. Sci. **35**, 85.
Huppert, H. E., 1982a, Nature **300**, 427.
Huppert, H. E., 1982b, J. Fluid Mech. **121**, 43.
Huse, D. A., 1984, Phys. Rev. B **29**, 6985.
Indekeu, J. O., 1991, Physica Scripta **T35**, 31.
Indekeu, J. O., 1994, Int. J. Mod. Phys. B **8**, 309.
Indekeu, J. O., K. Ragil, D. Bonn, D. Broseta, and J. Meunier, 1999a, J. Stat. Phys. **95**, 1009.
Indekeu, J. O., K. Ragil, D. Broseta, D. Bonn, and J. Meunier, 1999b, in *New approaches to Problems in Liquid State Theory*, edited by C. Caccamo, J.-P. Hansen, and G. Stell (Kluwer Academic Publishers), pp. 337–344.
Inverarity, G., 1969a, Brit. Polym. J. **1**, 254.
Inverarity, G., 1969b, Ph.D. Thesis, Univ. of Manchester .
Ishino, C., K. Okumura, and D. Quéré, 2004, Europhys. Lett. **68**, 419.
Israelachvili, J., 1992, *Intermolecular and Surface Forces* (Academic Press: London).
Israelachvili, J. N., 1986, J. Colloid Interf. Sci. **110**, 263.
Iwamoto, C., and S. Tanaka, 2002, Acta Mater **50**, 749.
J. C. Berg, e., 1993, *Wettability* (Marcel Dekker, New York).
Jackson, J. D., 1975, *Classical Electrodynamics* (Wiley).
Jacobs, K., K. R. Mecke, and S. Herminghaus, 1998, Langmuir **14**, 965.
Jacqmin, D., 2000, J. Fluid Mech. **402**, 57.
Jacqmin, D., 2002, J. Fluid Mech. **455**, 347.
Jensen, O. E., and J. B. Grotberg, 1992, J. Fluid Mech. **240**, 259.
Jeong, J.-T., and H. K. Moffatt, 1992, J. Fluid Mech. **241**, 1.
Jerret, J. M., and J. R. de Bruyn, 1992, Phys. Fluids A **4**, 234.
Joanny, J.-F., and P.-G. de Gennes, 1984, C. R. Acad. Sc. Paris, Serie II **299**, 605.
Joanny, J.-F., and P.-G. de Gennes, 1984, J. Chem. Phys. **81**, 552.
Joanny, J.-F., L. Leibler, and P.-G. de Gennes, 1979, J. Polym. Sci.: Polym. **17**, 1073.
Joanny, J.-F., and M. O. Robbins, 1990, J. Chem. Phys. **92**, 3206.
Jochem, C. M. G., and J. W. C. van der Ligt, 1987, Method of and arrangement for coating a fibre, US Patent No. 4704307.
Johnson, and Dettre, 1993, in *Wettability*, edited by J. C. Berg (Marcel Dekker, New York), pp. 1–74.
Johnson, M. F. G., R. A. Schluter, M. J. Miksis, and S. G.Bankoff, 1999, J. Fluid Mech. **394**, 339.
de Jonghe, V., and D. Chatain, 1995, Acta. Metall. Mater. **43**, 1505.
Joseph, D. D., J. Nelson, M. Renardy, and Y. Renardy, 1991, J. Fluid Mech. **223**, 383.
Kabza, K. G., J. E. Gestwicki, and J. L. J. McGrath, 2000, J. Chem. Educ. **77**, 63.
Kafka, F. Y., and V. Dussan, 1979, J. Fluid Mech. **95**, 539.
Kahlweit, M., R. Strey, and G. Busse, 1993, Phys. Rev. E **47**, 4197.
Kalliadasis, S., 2000, J. Fluid Mech. **413**, 355.
Kardar, M., and R. Golestanian, 1999, Rev. Mod. Phys. **71**, 1233.
Kataoka, D. E., and S. M. Troian, 1997, J. Colloid Interf. Sci. **192**, 350.
Kataoka, D. E., and S. M. Troian, 1998, J. Colloid Interf. Sci. **203**, 335.
Kavehpour, H. P., B. Ovryn, and G. H. McKinley, 2002, Coll. Surf. A **206**, 409.
Kavehpour, H. P., B. Ovryn, and G. H. McKinley, 2003, Phys. Rev. Lett. **91**, 196104.
Kayser, R. F., M. R. Moldover, and J. W. Schmidt, 1986, J. Chem. Soc. Faraday Trans. II **82**, 1701.
Kerle, T., J. Klein, and K. Binder, 1996, Phys. Rev. Lett. **77**, 1318.
Kerle, T., J. Klein, and K. Binder, 1999, Eur. Phys. J. B **7**, 401.
King, J. R., 2001a, in *Free Surface Flows* (Kluwer, Dordrecht), pp. 153–160.
King, J. R., 2001b, in *Free Surface Flows* (Kluwer, Dordrecht), pp. 7–18.
Kirilyuk, A., J. Ferré, V. Grolier, J.-P. Jamet, and D. Renard, 1997, Journal of Magnetism and Magnetic Materials **171**, 45.
Kistler, S., 1993, in *Wettability*, edited by J. C. Berg (Marcel Dekker, New York), pp. 311–429.
Klier, J., P. Stefanyi, and A. F. G. Wyatt, 1995, Phys. Rev. Lett. **75**, 3709.
Koch, W., S. Dietrich, and M. Napiórkowski, 1995, Phys. Rev. E **51**, 3300.
Kondic, L., 2003, SIAM Review **45**, 95.
Kondic, L., and A. L. Bertozzi, 1999, Phys. Fluids **11**, 3560.
Koplik, J., J. R. Banavar, and J. F. Willemsen, 1989, Phys. Fluids A **1**, 781.
Krech, M., 1994, *The Casimir effect in critical systems* (World Scientific, Singapore).
Krech, M., and S. Dietrich, 1991, Phys. Rev. Lett. **66**, 345.
Krim, J., J. G. Dash, and J. Suzanne, 1984, Phys. Rev. Lett. **52**, 640.
Kumar, S., D. H. Reich, and M. O. Robbins, 1995, Phys. Rev. E **52**, R5776.
Kusumaatmaja, H., and J. M. Yeomans, 2007, Langmuir **23**, 6019.
Lacey, A. A., 1982, Stud. Appl. Math. **67**, 217.
Landau, L. D., and B. V. Levich, 1942, Acta physico-chimica

USSR **17**, 42.
Landau, L. D., and E. M. Lifshitz, 1984, *Fluid Mechanics* (Pergamon: Oxford).
Larson, R. G., 1999, *The structure and rheology of complex fluids* (Oxford University Press).
Lauga, E., M. P. Brenner, and H. A. Stone, 2008, in *Springer Handbook of Experimental Fluid Mechnaics*, edited by C. Tropea, J. F. Foss, and A. Yarin (Springer), p. chapter 19.
Law, B. M., 1991, Phys. Rev. Lett. **67**, 1555.
Le Doussal, P., K. J. Wiese, E. Raphaël, and R. Golestanian, 2006, Phys. Rev. Lett. **96**, 015702.
Le Grand, N., A. Daerr, and L. Limat, 2005, J. Fluid Mech. **541**, 293.
Léger, L., M. Erman, A. M. Guinet-Picard, D. Ausserre, and C. Strazielle, 1988, Phys. Rev. Lett. **60**, 2390.
Léger, L., and J.-F. Joanny, 1992, Rep. Prog. Phys. **55**, 431.
Leizerson, I., and S. G. Lipson, 2003, Appl. Phys. Lett. **83**, 260.
Leizerson, I., S. G. Lipson, and A. V. Lyushnin, 2003, Nature **422**, 395.
Lekkerkerker, H. N. W., W. C. K. Poon, P. N. Pusey, A. Stroobants, and P. B. Warren, 1992, Europhys. Lett. **20**, 559.
Lemerle, S., J. Ferré, C. Chappert, V. Mathet, T. Giamarchi, and P. Le Doussal, 1998, Phys. Rev. Lett. **80**, 849.
Lenz, P., and R. Lipowsky, 1998, Phys. Rev. Lett. **80**, 1920.
Levinson, P., A.-M. Cazabat, M. A. Cohen-Stuart, F. Heslot, and S. Nicolet, 1988, Revue Phys. Appl. **23**, 1009.
Li, Q. W., Y. T. Zhu, I. A. Kinloch, and A. H. Windle, 2006, J.Phys.Chem B **110**, 13926.
Likos, C. N., 2001, Phys. Rep. **348**, 267.
Limat, L., and H. A. Stone, 2003, Europhys. Lett. **65**, 365.
Lin, X. M., G. M. Wang, C. M. Sorensen, and K. J. Klabunde, 1999, J.Phys.Chem B **103**, 5488.
Lipowsky, R., 1984, Phys. Rev. Lett. **52**, 1429.
Lipowsky, R., 2001, Current Opinion in Colloid and Interface Science **6**, 40.
Lipowsky, R., M. Brinkmann, R. Dimova, T. Franke, J. Kierfeld, and X. Zhang, 2005a, J. Phys.: Condens. Matter **17**, S537.
Lipowsky, R., M. Brinkmann, R. Dimova, C. Haluska, J. Kierfeld, and J. Shillcock, 2005b, J. Phys.: Condens. Matter **17**, S2885.
Lipowsky, R., and M. E. Fisher, 1987, Phys. Rev. B **36**, 2126.
Lipowsky, R., D. M. Kroll, and R. K. P. Zia, 1983, Phys. Rev. B **27**, R4499.
Lipowsky, R., P. Lenz, and P. Swain, 2000, Colloids and Surfaces A **161**, 3.
Lippmann, G., 1875, Ann. Chim. Phys. **5**, 494.
Lopez, J., C. A. Miller, and E. Ruckenstein, 1976, J. Colloid Interface Sci. **56**, 460.
Lorenceau, E., D. Quéré, and J. Eggers, 2004, Phys. Rev. Lett **93**, 254501.
Lorenceau, E., F. Restagno, and D. Quéré, 2003, Phys. Rev. Lett. **90**, 184501.
Mahadevan, L., and Y. Pomeau, 1999, Phys. Fluids **11**, 2449.
Maheshwari, S., L. Zhang, Y. Zhu, and H.-C. Chang, 2008, Phys. Rev. Lett. **100**, 044503.
Mao, Y., M. Cates, and H. Lekkerkerker, 1995, Physica A **222**, 10.
Marsh, J. A., S. Garoff, and E. Dussan V., 1993, Phys. Rev. Lett. **70**, 2778.
Matar, O. K., and S. M. Troian, 1999, Phys. Fluids **11**, 3232.
McHale, G., M. I. Newton, S. M. Rowan, and M. Banerjee, 1995, J. Phys. D: Appl. Phys. **28**, 1925.
Mechkov, S., G. Oshanin, M. Rauscher, M. Brinkmann, A. M. Cazabat, and S. Dietrich, 2007, Europhys. Lett. **80**, 66002.
Mecke, K., and S. Dietrich, 1999, Phys. Rev. E **59**, 6766.
Mecke, K. R., and M. Rauscher, 2005, J. Phys.: Condensed Matter **17**, S3515.
Melo, F., J.-F. Joanny, and S. Fauve, 1989, Phys. Rev. Lett. **63**, 1958.
Middelton, A., 1992, Phys. Rev. B **45**, R9465.
Milchev, A., M. Mueller, K. Binder, and D. Landau, 2003a, Phys. Rev. Lett. **90**, 136101.
Milchev, A., M. Müller, K. Binder, and D. Landau, 2003b, Phys. Rev. E **68**, 031601.
Mitlin, V. S., 1993, J. Colloid Interface Sci. **156**, 491.
Moldover, M. R., 1985, Phys. Rev. A **31**, 1022.
Moldover, M. R., and J. W. Cahn, 1980, Science **207**, 1073.
de la Mora, J. F., and I. G. Loscertales, 1994, J. Fluid Mech. **260**, 155.
Mora, S., J. Daillant, K. Mecke, D. Luzet, A. Braslau, M. Alba, and B. Struth, 2003, Phys. Rev. Lett. **90**, 216101.
Moseler, M., 2007, private communication.
Moseler, M., and U. Landman, 2000, Science **289**, 1165.
Moulinet, S., C. Guthmann, and E. Rolley, 2002, Eur. Phys. J. E **8**, 437.
Moulinet, S., C. Guthmann, and E. Rolley, 2004a, Eur. Phys. J. B **37**, 127.
Moulinet, S., A. Rosso, W. Krauth, and E. Rolley, 2004b, Phys. Rev. E **69**, 035103(R).
Mugele, F., and J.-C. Baret, 2005, J. Phys.: Condens. Matter **17**, R705.
Mugele, F., and J. Buehrle, 2007, J. Phys.: Condens. Matter **19**, 375112.
Mugele, F., A. Klingner, J. Buehrle, D. Steinhauser, and S. Herminghaus, 2005, J. Phys.: Condens. Matter **17**, 559.
Müller, M., and K. Binder, 2005, J. Phys.: Condens. Matter **17**, S333.
Müller, X., and J. Dupont-Roc, 2001, Europhys. Lett. **54**, 533.
Münch, A., B. Wagner, M. Rauscher, and R. Blossey, 2006, Eur. Phys. J. E **20**, 365.
Münch, A., B. Wagner, and T. P. Witelski, 2005, J. Engin. Math. **53**, 359.
Nacher, P. J., and J. Dupont-Roc, 1991, Phys. Rev. Lett. **67**, 2966.
Nadkarni, G. D., and S. Garoff, 1992, Europhys. Lett. **20**, 523.
Nakajami, A., K. Hashimoto, T. Watanabe, K. Takai, G. Yamouchi, and A. Fujishima, 2000, Langmuir **16**, 7044.
Nakanishi, H., and M. E. Fisher, 1982, Phys. Rev. Lett. **49**, 1565.
Napiórkowski, M., and S. Dietrich, 1993, Phys. Rev. E **47**, 1836.
Napiórkowski, M., W. Koch, and S. Dietrich, 1992, Phys. Rev. A **45**, 5760.
Narayan, O., and D. S. Fisher, 1992, Phys. Rev. B **46**, 11520.
Navier, C. L., 1827, Mem. Acad. R. Sci. France **6**, 389.
Neogi, P., and R. M. Ybarra, 2001, J. Chem. Phys. **115**, 7811.
O'Connell, S. T., and P. A. Thompson, 1995, Phys. Rev. E **52**, R5792.
Ogarev, V. A., T. N. Timonina, V. V. Arslanov, and A. A. Trapeznikov, 1974, J. Adhesion **6**, 337.
Onda, T., N. Shibuichi, N. Satoh, and K. Tsuji, 1996, Langmuir **12**, 2125.

Oron, A., S. H. Davis, and S. G. Bankoff, 1997, Rev. Mod. Phys. **69**, 931.

Pandit, R., M. Schick, and M. Wortis, 1982, Phys. Rev. B **26**, 5112.

Parry, A., M. Greenall, and J. Romero-Enrique, 2003, Phys. Rev. Lett. **90**, 046101.

Parry, A., M. Greenall, and A. Wood, 2002, J. Phys.: Condens. Matter **14**, 1169.

Parry, A., C. Rascón, and A. Wood, 2000, Phys. Rev. Lett. **85**, 345.

Parry, A., A. Wood, E. Carlon, and A. Drzewiński, 2001a, Phys. Rev. Lett. **87**, 196103.

Parry, A. O., 1996, J. Phys. Cond. Matt. **8**, 10761.

Parry, A. O., C. Rascón, N. R. Bernardino, and J. M. Romero-Enrique, 2006, J. Phys. Cond. Matt. **18**, 6433.

Parry, A. O., J. M. Romero-Enrique, and A. Lazarides, 2004, Phys. Rev. Lett. **93**, 086104.

Parry, A. O., A. J. Wood, and C. Rascón, 2001b, Journal of Physics: Condensed Matter **13**, 4591.

Pattle, R. E., 1959, Q. J. Mech. Appl. Math. **12**, 407.

Petrov, J. G., J. Ralston, M. Schneemilch, and R. A. Haynes, 2003a, J. Phys. Chem. **107**, 1634.

Petrov, J. G., J. Ralston, M. Schneemilch, and R. A. Haynes, 2003b, Langmuir **19**, 2795.

Petrov, J. G., and R. V. Sedev, 1985, Colloids Surfaces **13**, 313.

Pismen, L. M., and Y. Pomeau, 2000, Phys. Rev. E **62**, 2480.

Pismen, L. M., and Y. Pomeau, 2004, Phys. Fluids **16**, 2604.

Pismen, L. M., and U. Thiele, 2006, Phys. Fluids **18**, 042104.

Podgorski, T., J. M. Flesselles, and L. Limat, 2001, Phys. Rev. Lett. **87**, 036102(1).

Pomeau, Y., 1986, J. Colloid Interface Sci. **113**, 5.

Pomeau, Y., 2000, C.R. Acad. Sci. Paris **328**, 411.

Pomeau, Y., 2002, C.R. Mecanique **330**, 207.

Pomeau, Y., and J. Vannimenus, 1984, J. Colloid Int. Sc. **104**, 477.

Poon, W., 2002, J. Phys.: Condens. Matter **14**, R589.

Popescu, M. N., and S. Dietrich, 2004, Phys. Rev. E **69**, 061602.

Poujade, M., C. Guthmann, and E. Rolley, 2002, Europhys. Lett. **59**, 862.

Poulard, C., O. Benichou, and A.-M. Cazabat, 2003, Langmuir **19**, 8828.

Poulard, C., G. Guena, A.-M. Cazabat, A. Boudaoud, and M. Ben Amar, 2005, Langmuir **21**, 8226.

Prevost, A., E. Rolley, and C. Guthmann, 1999, Phys. Rev. Lett. **83**, 348.

Prevost, A., E. Rolley, and C. Guthmann, 2002, Phys. Rev. B **65**, 064517.

Qian, T., X.-P. Wang, and P. Sheng, 2003, Phys. Rev. E **68**, 016306.

Qian, T., X.-P. Wang, and P. Sheng, 2004, Phys. Rev. Lett. **93**, 094501.

Qian, T., X.-P. Wang, and P. Sheng, 2006, J. Fluid Mech. **564**, 333.

Quéré, D., 1991, C. R. Acad. Sci. Paris, Serie II **313**, 313.

Quéré, D., 2005, Rep. Prog. Phys. **68**, 2495.

Quilliet, C., and B. Berge, 2001, Curr. Op. Colloid Interface Sci. **6**, 34.

Rafaï, S., D. Bonn, E. Bertrand, J. Meunier, V. C. Weiss, and J. O. Indekeu, 2004a, Phys. Rev. Lett. **92**, 245701.

Rafaï, S., D. Bonn, and A. Boudaoud, 2004b, J. Fluid Mech. **513**, 77.

Rafaï, S., D. Bonn, and J. Meunier, 2007, Physica A **386**, 31.

Rafaï, S., D. Sarker, V. Bergeron, J. Meunier, and D. Bonn, 2002, Langmuir **18**, 10486.

Ragil, K., D. Bonn, D. Broseta, and J. Meunier, 1996a, J. Chem. Phys. **105**, 5160.

Ragil, K., J. Meunier, D. Broseta, J. O. Indekeu, and D. Bonn, 1996b, Phys. Rev. Lett. **77**, 1532.

Ramé, E., 2002, in *Encyclopedia of Surface and Colloid Science* (New York, Marcel Dekker), pp. 3602–3618.

Ramos, S. M. M., E. Charlaix, A. Benyagoub, and M. Toulemonde, 2003, Phys. Rev. E **67**, 031604.

Raphaël, E., and P.-G. de Gennes, 1989, J. Chem. Phys. **90**, 7577.

Rascón, C., and A. Parry, 2005, Phys. Rev. Lett. **94**, 096103.

Rascón, C., and A. O. Parry, 2000a, J. Chem. Phys. **112**, 5175.

Rascón, C., and A. O. Parry, 2000b, Nature **407**, 986.

Rauscher, M., A. Münch, B. Wagner, and R. Blossey, 2005, Eur. Phys. J. E **17**, 373.

Redon, C., F. Brochard-Wyart, and F. Rondolez, 1991, Phys. Rev. Lett. **66**, 715.

Rejmer, K., S. Dietrich, and M. Napiórkowski, 1999, Phys. Rev. E **60**, 4027.

Ren, W., and W. E, 2007, Phys. Fluids **19**, 022101.

Renardy, M., Y. Renardy, and J. Li, 2001, J. Comput. Phys. **171**, 243.

Rio, E., A. Daerr, B. Andreotti, and L. Limat, 2005, Phys. Rev. Lett. **94**, 024503.

Rio, E., A. Daerr, F. Lequeux, and L. Limat, 2006, Langmuir **22**, 3186.

Ristenpart, W. D., P. G. Kim, C. Domingues, J. Wan, and H. A. Stone, 2007, Phys. Rev. Lett. **99**, 234502.

Robbins, M. O., and J.-F. Joanny, 1987, Europhys. Lett. **3**, 729.

Rolley, E., and C. Guthmann, 1997, J. Low Temp. Phys. **108**, 1.

Rolley, E., and C. Guthmann, 2007, Phys. Rev. Lett. **98**, 166105.

Rolley, E., C. Guthmann, R. Gombrowicz, and V. Repain, 1998a, Phys. Rev. Lett. **80**, 2865.

Rolley, E., A. Prevost, and C. Guthmann, 1998b, J. Low Temp. Phys. **113**, 787.

Romero-Enrique, J., and A. Parry, 2005, Europhys. Lett. **72**, 1004.

Rosenblat, S., and S. H. Davis, 1985, in *Frontiers in Fluid Mechanics* (Springer), pp. 171–183.

Ross, D., D. Bonn, and J. Meunier, 1999, Nature **400**, 737.

Ross, D., D. Bonn, and J. Meunier, 2001a, J. Chem. Phys. **114**, 2784.

Ross, D., D. Bonn, A. I. Posazhennikova, J. O. Indekeu, and J. Meunier, 2001b, Phys. Rev. Lett. **87**, 176103.

Ross, D., P. Taborek, and J. E. Rutledge, 1998, J. Low Temp. Phys. **111**, 1.

Rosso, A., and W. Krauth, 2001, Phys. Rev. Lett. **87**, 187002.

Rosso, A., and W. Krauth, 2002, Phys. Rev. E **65**, 025101(R).

Rosso, A., W. Krauth, P. Le Doussal, J. Vannimenus, and K. J. Wiese, 2003, Phys. Rev. E **68**, 036128.

Roth, R., R. Evans, and S. Dietrich, 2000, Phys. Rev. E **62**, 5360.

Rowlinson, J. S., and B. Widom, 1982, *Molecular Theory of Capillarity* (Oxford: Clarendon).

Ruckenstain, E., and R. K. Jain, 1974, J. Chem. Soc. Faraday Trans. II **70**, 132.

Ruijter, M. J., T. D. Blake, and J. De Coninck, 1999, Langmuir **15**, 7836.

Rutledge, J. E., and P. Taborek, 1992, Phys. Rev. Lett. **69**, 937.
Saam, W. F., and V. B. Shenoy, 1995, J. Low. Temp. Phys. **101**, 225.
Sabisky, E. S., and C. H. Anderson, 1973, Phys. Rev. A **7**, 790.
Safran, S. A., 2003, *Statistical thermodynamics of surfaces, interfaces, and membranes* (Westview Press).
Samid-Merzel, N., S. G. Lipson, and D. S. Tannhauser, 1998, Phys. Rev. E **57**, 2906.
Saulnier, F., E. Raphaël, and P.-G. de Gennes, 2002a, Phys. Rev. E **66**, 061607.
Saulnier, F., E. Raphaël, and P.-G. de Gennes, 2002b, Phys. Rev. Lett. **88**, 196101.
Schäffer, E., and P. Z. Wong, 2000, Phys. Rev. E **61**, 5257.
Schawrtz, L. W., D. Roux, and J. J. Cooper-White, 2005, Physica D **209**, 236.
Schick, M., 1990, in *Liquids at Interfaces, Les Houches Session XLVIII*, edited by J. Charvolin, J.-F. Joanny, and J. Zinn-Justin (Amsterdam: Elsevier), pp. 415–497.
Schimmele, L., M. Napiórkowski, and S. Dietrich, 2007, J. Chem. Phys. **127**, 164715.
Schmidt, J. W., and M. R. Moldover, 1986, J. Chem. Phys **84**, 4564.
Schwartz, L. W., and S. Garoff, 1985, Langmuir **1**, 219.
Schwarz, J. M., and D. Fisher, 2001, Phys. Rev. Lett. **87**, 096107.
Schweika, W., H. Reichert, W. Babik, O. Klein, and S. Engemann, 2004, Phys. Rev. B **70**, 041401(R).
Sedev, R. V., and J. G. Petrov, 1991, Colloids and Surfaces **53**, 147.
Sedev, R. V., and J. G. Petrov, 1992, Colloids and Surfaces **62**, 141.
Seebergh, J. E., and J. C. Berg, 1992, Chem. Engin. Sci. **47**, 4468.
Seemann, R., M. Brinkmann, E. Kramer, F. Lange, and R. Lipowsky, 2005a, PNAS **102**, 1848.
Seemann, R., S. Herminghaus, and K. Jacobs, 2001a, Phys. Rev. Lett. **86**, 5534.
Seemann, R., S. Herminghaus, and K. Jacobs, 2001b, J. Phys. Condens. Mat. **13**, 4925.
Seemann, R., S. Herminghaus, C. Neto, S. Schlagowski, D. Podzimek, R. Konrad, H. Mantz, and K. Jacobs, 2005b, J. Phys.-Condes. Matter **17**, S267.
Seppecher, P., 1996, Int. J. Engng. Sci. **34**, 977.
Seyrat, E., and R. A. Hayes, 2001, J. Appl. Phys. **90**, 1383.
Shahidzadeh, N., E. Bertrand, J.-P. Dauplait, J.-C. Borgotti, and D. Bonn, 2003, Transp. Porous Media **52**, 213.
Shahidzadeh, N., D. Bonn, K. Ragil, D. Broseta, and J. Meunier, 1998, Phys. Rev. Lett. **80**, 3992.
Shahidzadeh, N., S. Rafai, D. Bonn, and G. Wegdam, 2008, to be published .
Shahidzadeh-Bonn, N., S. Rafaï, A. Azouni, and D. Bonn, 2006, J. Fluid Mech. **549**, 307.
Sharma, A., 1993, Langmuir **9**, 861.
Sharma, A., and A. T. Jameel, 1993, J. Colloid Interf. Sci. **161**, 190.
Shen, C., and D. W. Ruth, 1998, Phys. Fluids **10**, 789.
Shenoy, V. B., and W. F. Saam, 1995, Phys. Rev. Lett. **75**, 4086.
Shibuichi, S., T. Onda, N. Satoh, and K. Tsujii, 1996, J. Phys. Chem. **100**, 19512.
Silberzan, P., L. Léger, D. Ausserre, and J. J. Benattar, 1991, Langmuir **7**, 1647.
Silve, N., and E. Dussan V., 1985, Phys. Fluids **28**, 5.
Simpkins, P. G., and V. J. Kuck, 2003, J. Col. Interf. Sci. **263**, 562.
Snoeijer, J., N. Le Grand, L. Limat, H. A. Stone, and J. Eggers, 2007, Phys. Fluids **19**, 042104.
Snoeijer, J. H., 2006, Phys. Fluids **18**, 021701.
Snoeijer, J. H., G. Delon, B. Andreotti, and M. Fermigier, 2006, Phys. Rev. Lett. **96**, 174504.
Snoeijer, J. H., E. Rio, N. Le Grand, and L. Limat, 2005, Phys. Fluids **17**, 072101.
Sohaili, M., J. Klier, and P. Leiderer, 2005, J. Phys.: Condens. Matter **17**, S415.
Somalinga, S., and A. Bose, 2000, Phys. Fluids **12**, 499.
Spaid, M. A., and G. M. Homsy, 1996, Phys. Fluids **8**, 460.
Spelt, P. D. M., 2005, J. Comput. Phys. **207**, 389.
Sprenger, M., F. Schlesener, and S. Dietrich, 2005, Phys. Rev. E **71**, 056125.
Starov, V. M., A. N. Tyatyushkin, M. G. Velarde, and S. A. Zhdanov, 2003, J. Coll. Int. Sci. **257**, 284.
Starov, V. M., M. G. Velarde, and C. J. Radke, 2007, *Wettability* (CRC Press, Boca Raton).
Stewart, M. C., and R. Evans, 2005, Phys. Rev. E **71**, 011602.
Stone, H. A., L. Limat, S. K. Wilson, J. M. Flesselles, and T. Podgorski, 2002, C. R. Physique **3**, 103.
Ström, G., M. Fredriksson, P. Stenius, and B. Radoev, 1990a, J. Colloid Interf. Sci. **134**, 117.
Ström, G., M. Fredriksson, P. Stenius, and B. Radoev, 1990b, J. Colloid Interf. Sci. **134**, 107.
Sullivan, D. E., and M. M. Telo da Gama, 1986, in *Fluid interfacial Phenomena*, edited by C. Croxton (New York: Wiley), pp. 45–134.
Sultan, E., A. Boudaoud, and M. Ben Amar, 2004, J. Engin. Math. **50**, 209.
Sur, J., A. L. Bertozzi, and R. P. Behringer, 2003, Phys. Rev. Lett. **90**, 126105.
Swain, P., and R. Lipowsky, 1998, Langmuir **14**, 6772.
Swain, P., and R. Lipowsky, 2000, Europhys. Lett. **49**, 203.
Tabeling, P., 2004, *Microfluidics* (EDP Sciences: Paris).
Tanner, L. H., 1979, J. Phys. D: Appl. Phys. **12**, 1473.
Tasinkevych, M., and S. Dietrich, 2006, Phys. Rev. Lett. **97**, 106102.
Tasinkevych, M., and S. Dietrich, 2007, Eur. Phys. J. E **23**, 117.
Taylor, G. I., 1934, Proc. Roy. Soc. London A **146**, 501.
Teletzke, G. F., H. T. Davis, and L. E. Scriven, 1988, Revue Phys. Appl. **23**, 989.
Thiele, U., 2003, Eur. Phys. J. E **12**, 409.
Thiele, U., and E. Knobloch, 2003, Phys. Fluids **15**, 892.
Thiele, U., K. Neuffer, M. Bestehorn, Y. Pomeau, and M. G. Velarde, 2002, Colloid Surf. A **206**, 87.
Thompson, P. A., and M. O. Robbins, 1989, Phys. Rev. Lett. **63**, 766.
Thompson, P. A., and S. M. Troian, 1997, Nature **389**, 360.
Trejo, L. M., J. Garcia, C. Varea, and A. Robledo, 1988, Europhys. Lett. **7**, 537.
Troian, S., X. Wu, and S. A. Safran, 1989a, Phys. Rev. Lett. **62**, 1496.
Troian, S. M., E. Herbolzheimer, S. A. Safran, and J.-F. Joanny, 1989b, Europhys. Lett. **10**, 25.
Tuinier, R., J. Rieger, and C. G. de Kruif, 2003, Adv. Coll. Interface Sci. **103**, 1.
Valignat, M. P., N. Fraysse, A.-M. Cazabat, F. Heslot, and P. Levinson, 1993, Thin Solid Films **234**, 475.
van Hameren, R., P. Schon, A. M. van Buul, J. Hoogboom,

S. V. Lazarenko, J. W. Gerritsen, H. Engelkamp, P. C. M. Christianen, H. A. Heus, J. C. Maan, T. Rasing, S. Speller, *et al.*, 2006, Science **314**, 1433.
Vandembroucq, D., R. Skoe, and S. Roux, 2004, Phys. Rev. E **70**, 051101.
Vilmin, T., and E. Raphaël, 2005, Europhys. Lett. **72**, 781.
Vilmin, T., E. Raphaël, P. Damman, S. Sclavons, S. Gabriele, M. Hamieh, and G. Reiter, 2006, Europhys. Lett. **73**, 906.
Voinov, O. V., 1976, Fluid Dynamics **11**, 714.
Voinov, O. V., 1977, J. Appl. Mech. Tech. Phys. **18**, 216.
Voinov, O. V., 1995, J. Multiphase Flow **21**, 801.
Voinov, O. V., 2000a, J. Colloid Interf. Sci. **226**, 5.
Voinov, O. V., 2000b, J. Colloid Interf. Sci. **226**, 22.
Voinov, O. V., 2002, in *Encyclopedia of Surface and Colloid Science* (New York, Marcel Dekker), pp. 1546–1559.
Vrij, A., 1966, Discuss. Faraday Soc. **42**, 23.
Vrij, A., 1976, Pure Appl. Chem. **48**, 471.
Warner, M. R. E., R. V. Craster, and O. K. Matar, 2004, J. Fluid Mech. **510**, 169.
Wayner, P. C., 1993, Langmuir **9**, 294.
Webb III, E. B., G. S. Grest, and D. R. Heine, 2003, Phys. Rev. Lett. **91**, 236102.
Weidner, D. E., and L. W. Schwartz, 1993, Phys. Fluids **6**, 3535.
Weiss, V. C., E. Bertrand, S. Rafaï, J. O. Indekeu, and D. Bonn, 2007, J. Chem. Phys., submitted .
Weiss, V. C., and J. O. Indekeu, 2003, J. Chem. Phys. **118**, 10741.
Wenzel, R. N., 1936, Ind. Engin. Chem. **28**, 988.
Werner, A., M. Müller, F. Schmid, and K. Binder, 1999, J. Chem. Phys. **110**, 1221.
Wessels, P. P. F., M. Schmidt, and H. Löwen, 2004, J. Phys.: Condens. Matter **16**, S4169.
Wijting, W. K., N. A. M. Besseling, and M. A. C. Stuart, 2003a, Phys. Rev. Lett. **90**, 196101.
Wijting, W. K., N. A. M. Besseling, and M. A. C. Stuart, 2003b, J. Phys. Chem. B **107**, 10565.
Wu, S., 1982, in *Polymer Interfaces and Adhesion* (Marcel Dekker, New York), pp. 279–329.
Yang, S., H. Tan, D. Yan, E. Nies, and A. Shi, 2007, Phys. Rev. E **75**, 061803.
Young, T., 1805, Phil. Trans. R. Soc. London **95**, 65.
Zapperi, S., P. Cizeau, G. Durin, and H. E. Stanley, 1998, Phys. Rev. B **58**, 6353.
Ziegler, J., J. H. Snoeijer, B. Andreotti, M. Fermigier, and J. Eggers, 2007, unpublished .